

Sediments in sea ice drive the Canada Basin surface Mn maximum: insights from an Arctic Mn ocean model

Birgit Rogalla^{1,1,1}, Susan E. Allen^{1,1,1}, Manuel Colombo^{1,1,1}, Paul G. Myers^{2,2,2}, and Kristin J. Orians^{1,1,1}

¹University of British Columbia

²University of Alberta

November 30, 2022

Abstract

Biogeochemical cycles in the Arctic Ocean are sensitive to the transport of materials from continental shelves into central basins by sea ice. However, it is difficult to assess the net effect of this supply mechanism due to the spatial heterogeneity of sea ice content. Manganese (Mn) is a micronutrient and tracer which integrates source fluctuations in space and time. The Arctic Ocean surface Mn maximum is attributed to freshwater, but studies struggle to distinguish sea ice and river contributions. Informed by observations from 2009 IPY and 2015 Canadian GEOTRACES cruises, we developed a three-dimensional dissolved Mn model within a 1/12 degree coupled ocean-ice model centered on the Canada Basin and the Canadian Arctic Archipelago (CAA). Simulations from 2002-2019 indicate that annually, 93% of Mn contributed to the Canada Basin upper ocean is released by sea ice, while rivers, although locally significant, contribute only 2%. Downstream, sea ice provides 34% of Mn transported from Parry Channel into Baffin Bay. While rivers are often considered the main source of Mn, our findings suggest that in the Canada Basin they are less important than sea ice. However, within the shelf-dominated CAA, both rivers and sediment resuspension are important. Climate induced disruption of the transpolar drift may reduce the Canada Basin Mn maximum and supply downstream. Other nutrient elements found in sediments, such as Fe, may be similarly affected. These results highlight the vulnerability of the biogeochemical supply mechanisms in the Arctic Ocean and the subpolar seas to climatic changes.

Sediments in sea ice drive the Canada Basin surface Mn maximum: insights from an Arctic Mn ocean model

B. Rogalla¹, S. E. Allen¹, M. Colombo¹, P. G. Myers², K. J. Orians¹

¹Department of Earth, Ocean, and Atmospheric Sciences, University of British Columbia, Vancouver,
British Columbia V6T1Z4, Canada

²Department of Earth and Atmospheric Sciences, University of Alberta, 1-26 ESB, Edmonton, Alberta
T6G2E3, Canada

Key Points:

- We present an ocean model of Mn in the Canadian Arctic that captures observed spatial variation
- Non-local sediments transported by sea ice are a key source of micronutrients such as Mn to the Canada Basin
- Rivers are most important for Mn in coastal regions of the Canadian Arctic

Abstract

Biogeochemical cycles in the Arctic Ocean are sensitive to the transport of materials from continental shelves into central basins by sea ice. However, it is difficult to assess the net effect of this supply mechanism due to the spatial heterogeneity of sea ice content. Manganese (Mn) is a micronutrient and tracer which integrates source fluctuations in space and time. The Arctic Ocean surface Mn maximum is attributed to freshwater, but studies struggle to distinguish sea ice and river contributions. Informed by observations from 2009 IPY and 2015 Canadian GEOTRACES cruises, we developed a three-dimensional dissolved Mn model within a 1/12 degree coupled ocean-ice model centered on the Canada Basin and the Canadian Arctic Archipelago (CAA). Simulations from 2002-2019 indicate that annually, 87-93% of Mn contributed to the Canada Basin upper ocean is released by sea ice, while rivers, although locally significant, contribute only 2.2-8.5%. Downstream, sea ice provides 34% of Mn transported from Parry Channel into Baffin Bay. While rivers are often considered the main source of Mn, our findings suggest that in the Canada Basin they are less important than sea ice. However, within the shelf-dominated CAA, both rivers and sediment resuspension are important. Climate induced disruption of the transpolar drift may reduce the Canada Basin Mn maximum and supply downstream. Other micronutrients found in sediments, such as Fe, may be similarly affected. These results highlight the vulnerability of the biogeochemical supply mechanisms in the Arctic Ocean and the subpolar seas to climatic changes.

Plain Language Summary

Autumn storms on the Siberian side of the Arctic Ocean churn up sediment that freezes into sea ice. The prevailing ocean currents and winds push this sea ice across the Arctic Ocean towards the Canada Basin, where it melts and releases the sediment into the ocean. Sediment contains manganese and other nutrient elements that help support plankton and life. Using our manganese ocean model, 87-93% of Mn in the Canada Basin comes from “dirty” sea ice from 2002 to 2019, while rivers supply 2.2-8.5%. As a result of climate change, less dirty sea ice may make it across the Arctic Ocean, which could reduce this supply system of manganese and other similar micronutrients. This change also has potential impacts downstream: water from the Canada Basin travels through the shallow Canadian Arctic Archipelago into Baffin Bay and eventually the North Atlantic. We found that about 34% of Mn transported along this route comes from “dirty”

sea ice. In the Canadian Arctic Archipelago, other sources contribute as well: tides churn up sediments from the ocean floor and many rivers flow into the channels. Our study highlights ways in which climate change may impact the nutrient supply systems in the Arctic Ocean.

1 Introduction

As the sea ice regime in the Arctic Ocean transitions from multi-year ice to predominantly first-year ice with overall reductions in sea ice extent, thickness and altered drift patterns (Stroeve et al., 2012; Stroeve & Notz, 2018; Spreen et al., 2011; Kwok et al., 2013), biogeochemical cycles and primary productivity are impacted through changes to the sea ice supply mechanism. The Arctic Ocean continental shelves connect land and ocean through the transfer of river runoff and sea ice from near-shore regions to the central basins (Charette et al., 2016). Reductions in sea ice export from the shelves weakens the long range transport of ice-rafted matter (Krumpen et al., 2019), including sediments (Dethleff et al., 2000; Darby et al., 2011), nutrients and trace metals (Tovar-Sánchez et al., 2010; Measures, 1999), pollutants (Pfirman et al., 1995; Peeken et al., 2018) and climate-relevant gases (Damm et al., 2018), to the surface ocean in regions far away from boundary sources. It is challenging to quantify the contribution of materials supplied by sea ice with observations alone due to the high spatial and temporal variability in the amount of sediment in sea ice and because it is difficult to distinguish it from additional contributions to the surface ocean such as river runoff. However, it is clear that changes to the physical processes in the Arctic Ocean will have impacts on the biogeochemical cycles and primary productivity of the basins themselves, as well as downstream in sub-polar seas (Drinkwater & Harding, 2001; Greene & Pershing, 2007).

Continental shelves cover half of the area of the Arctic Ocean (Jakobsson, 2002) and their shallow depths facilitate the incorporation of suspended matter into sea ice as it forms (Kempema et al., 1989). The narrow and deeper North American shelves are not as important for basin-wide sea ice sediment transport as the wide Siberian shelves (Eicken et al., 2005). In the Siberian shelf regions, fast ice builds up near shore in the fall, coinciding with storm-related resuspension events, forming sediment-rich sea ice (Nürnberg et al., 1994). The transpolar drift transports this sea ice, as well as some ice from the Chukchi Sea, towards the North Pole and the anticyclonic Beaufort Gyre redirects a portion into the Canada Basin (T. Martin & Gerdes, 2007). This passage takes sev-

eral years, during which the ice undergoes cycles of melting, freezing and deformation. The materials released by melt alter the geochemical signature of the underlying water (Pfirman et al., 1995). Several studies indicate an increase in sea ice exchange caused by faster ice drift speeds (Spreen et al., 2011; Kwok et al., 2013; Newton et al., 2017; Kipp et al., 2018); however a recent study indicates a disruption in long range sea ice transport due to the melt of first-year ice before it is incorporated into the transpolar drift (Krumpen et al., 2019). Reductions in long range sea ice transport can impact the supply of freshwater and nutrients to the surface ocean at the end of the transpolar drift namely: Fram Strait, and indirectly the Canada Basin, the Canadian Arctic Archipelago (CAA), and the subpolar North Atlantic. In order to establish the importance of sediment from sea ice for biogeochemical cycles in the indirectly impacted regions of the Canada Basin and the Canadian Arctic Archipelago, we developed a model of dissolved manganese (Mn).

Mn is a reactive trace element and an important micronutrient which shares many sources with iron (Fe) in the Arctic Ocean (Brand et al., 1983; Bruland et al., 1991; Jensen et al., 2020). Mn has a scavenged-type profile with high concentrations near sources and low background concentrations. This contrast makes it a convenient source tracer. Over the Arctic Ocean shelves, sediment resuspension contributes Mn to the lower water column (Evans & Nishioka, 2018; Colombo et al., 2020). Pacific water from the Bering Strait and Chukchi Sea is a source of Mn to the halocline of the Arctic Ocean (Jensen et al., 2020; Colombo et al., 2020). Mn is typically highest at the surface where atmospheric deposition, river runoff and ice melt contribute, and where photo-reduction of Mn is enhanced and bacterially-mediated Mn oxidation is inhibited (Sunda & Huntsman, 1994). In the Arctic Ocean, this surface maximum is attributed to freshwater sources (Campbell & Yeats, 1982; Yeats & Westerlund, 1991; Middag et al., 2011b; Cid et al., 2012; Kondo et al., 2016; Colombo et al., 2020). Observational studies have identified the origin of this freshwater as river discharge (Campbell & Yeats, 1982; Yeats & Westerlund, 1991; Evans & Nishioka, 2018), sea ice meltwater (Measures, 1999; S. Wang et al., 2014, for Fe), or a combination of both (Middag et al., 2011b; Cid et al., 2012; Kondo et al., 2016; Colombo et al., 2020). Mn concentrations in rivers are significantly higher than in the ocean (Colombo et al., 2019). Similarly, trace metals and nutrients in sea ice occur in concentrations in excess of those in the ocean (Campbell & Yeats, 1982; Hölemann et al., 1999; Granskog et al., 2003; Krachler et al., 2005; Aguilar-Islas et al., 2008; Tovar-

Sánchez et al., 2010; Kondo et al., 2016; Evans & Nishioka, 2018). The relative importance of river runoff and sea ice depends in part on the distance from the source and the modification of input to the ocean (Fichot et al., 2013). The Canada Basin is distant from land sources, while the narrow and shallow systems of channels that make up the CAA are in close contact with the land-ocean interface and are more directly impacted by boundary processes such as river discharge and sedimentary inputs (Colombo et al., 2021). We will investigate the hypothesis that sediments transported by sea ice are an important source of Mn in the Canada Basin, as suggested for reactive trace metals by Measures (1999).

In order to distinguish the individual importance of external Mn sources within the Canada Basin and the CAA, model studies are needed. Past studies have used tracers such as terrestrial dissolved organic matter to trace river runoff on the scale of months to years (Fichot et al., 2013; Mann et al., 2016) and the oxygen isotope ratio (Yamamoto-Kawai et al., 2009) to distinguish the meteoric and sea ice melt contributions to freshwater in the Canada Basin. Mn is an interesting complementary tracer: it can trace both the impact of river runoff and sediments in sea ice, and incorporates information about chemical transformation such as redox conditions and removal over time, thereby helping inform freshwater influence on biogeochemical cycling. Mn is also an essential micronutrient and integrates processes that fluctuate on short time scales. As a result, Mn helps address one of the main limitations of the study of sediment entrainment and export events by sea ice: that they are episodic and localized in nature (Eicken et al., 2005). Similarly, while sediment resuspension occurs intermittently, Mn integrates the effect of this component on the lower water column. After establishing the contributions of the Mn sources, we use Mn as a tool to study the general role of sea ice transport for biogeochemical cycles.

In this paper, we present a model of Mn in the Canadian Arctic Archipelago and the Canada Basin, informed by in situ observations collected during the 2009 IPY GEOTRACES cruise (Sim, 2018) and the 2015 Canadian GEOTRACES cruises (Colombo et al., 2020). Our work builds on the comprehensive first global model of Mn in the ocean (Van Hulten et al., 2017) and previous smaller scale models of Mn in the North Pacific Ocean (Johnson et al., 1996) and near hydrothermal vents (Lavelle et al., 1992). We incorporate new parameterizations for sediment resuspension, release of shelf sediments in sea ice, and fluvial contributions, to capture the drivers of Mn distributions in the Cana-

dian Arctic. With this model, we show that the long range transport of sediments by sea ice from the Siberian shelves drives the surface Mn maximum in the Canada Basin while rivers are important in coastal regions. Using these results, we discuss implications of future sea ice melt on Mn and Fe nutrient budgets in the Canada Basin and downstream in the Canadian Arctic Archipelago and Baffin Bay.

2 Methods

2.1 Coupled Ocean-Ice Model

For our simulations, we use ocean and ice dynamics calculated by the Arctic and Northern Hemispheric Atlantic (ANHA12) configuration (Hu et al., 2018) of the Nucleus for European Modelling of the Ocean (NEMO) version 3.4 (Madec, 2008). The ANHA12 configuration has a nominal horizontal resolution of $1/12^\circ$ which resolves freshwater fluxes associated with coastal currents in the CAA, as well as eddies (Bacon et al., 2014; Chelton et al., 1998). The position of the grid’s artificial pole in Northern Canada increases the resolution in the CAA to about 2-3 km (Fig. 1). In the vertical, there are 50 depth levels ranging from 1 m thickness at the surface to 454 m near the bottom. The bottom bathymetry is represented using partial steps.

The ANHA12 domain has two open boundaries: one in Bering Strait and the other at 20°S in the Atlantic Ocean. These boundaries are forced with Global Ocean Reanalyses and Simulations data (Masina et al., 2017). The ocean surface is forced with hourly atmospheric data from the Canadian Meteorological Centre’s global deterministic prediction system (Smith et al., 2014) and the rivers are forced with monthly runoff climatology with enhanced Greenland melt runoff (Dai et al., 2009; Bamber et al., 2012). The river forcing from 2010 is repeated for the following years (Hu et al., 2019).

The sea ice in ANHA12 is represented using the dynamic and thermodynamic Louvain-la-Neuve (LIM2) sea ice model with an elastic-viscous-plastic ice rheology (Fichefet & Maqueda, 1997; Bouillon et al., 2009). An evaluation of LIM2 in the ANHA12 configuration is provided by Hu et al. (2018). The general spatial distribution of ice thickness within the Canada Basin and the CAA is captured well. However, sea ice concentration and thickness are overestimated in the Canada Basin, likely because of underestimated melt (Grivault et al., 2018; Hu et al., 2019). In the northern CAA, the model has very thick sea ice (> 4 m), the central CAA has intermediate thickness ice (2.5-3 m), and there

is thin (< 2 m) ice in the eastern and southern channels of the CAA. The ANHA12 simulations are limited by the lack of a land-fast ice parameterization, resulting in ice velocities that are higher than observed in Parry Channel, impacting the winter transport (Grivault et al., 2018). In addition, tides are not included and as a result, the polynyas which form due to tidally enhanced mixing are not well reproduced (Hughes et al., 2018).

The advection and diffusion of tracers are calculated within NEMO by the TOP engine (Gent et al., 1995; Lévy et al., 2001). Tracer advection is calculated with the Total Variance Dissipation (TVD) scheme (Zalesak, 1979) and we use the Flow Relaxation Scheme (FRS) for the tracer boundary conditions. The vertical diffusion of tracers is calculated from the Turbulent Kinetic Energy closure scheme within ANHA12 and the horizontal eddy diffusivity parameter is set to $50.0 \text{ m}^2 \text{ s}^{-1}$.

2.2 Model of Mn in the Canadian Arctic

The Mn model runs offline in NEMO version 3.6 using five day averaged dynamics fields from the ANHA12 reference run from January 2002 to December 2019 (Hu et al., 2018). The Mn model consists of two main sets of computations: the advection and diffusion of tracers calculated by the NEMO-TOP engine (Gent et al., 1995; Lévy et al., 2001), and the source and sink contributions. The source and sink parameterizations were developed guided by observations from the 2015 Canadian GEOTRACES cruises (Colombo et al., 2020) and inspired by the first global model of Mn (Van Hulten et al., 2017). In order to reduce the computational cost, we calculate the model on a sub-domain of ANHA12, centered on the CAA (Fig. 1). Note that since we run offline, the physics originates from the full domain.

The known sources and sinks of Mn in the ocean are: rivers, hydrothermal vents, sediment diffusion, sediment resuspension, reversible scavenging, sinking, uptake and remineralization, atmospheric dust deposition, and flux from ice (Middag et al., 2011b; Balzer, 1982; Klinkhammer & Bender, 1980; Evans & Nishioka, 2018). From this list, we incorporate the processes that are important for dissolved Mn in the Arctic (summarized in Fig. 2 and Eqn. 1 and 2). We directly model dissolved Mn(II), dMn, and oxidised Mn(IV), oMn, for reversible scavenging (similar to Van Hulten et al., 2017, Eqn. 2). We do not directly trace lithogenic particles containing Mn, i.e. particle-bound Mn (pMn), but we incorporate their indirect effect through dissolution. We did not incorporate hydrother-

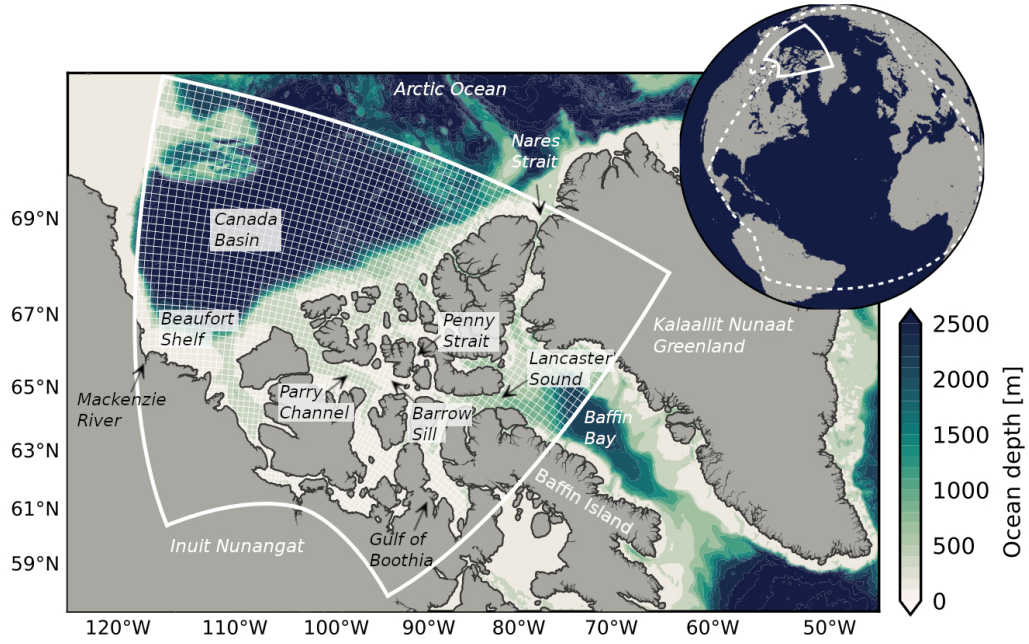


Figure 1. The Mn model domain is centered on the Canadian Arctic Archipelago with highest horizontal resolution in the south (about 3 km). The nominal horizontal resolution of the grid is $1/12^\circ$; the thin white grid depicts one in every ten ocean grid points. The solid white line shows the Mn model domain extent, while the dashed white line in the inset globe delineates the domain of the Arctic and Northern Hemispheric Atlantic configuration (Hu et al., 2018) of the ocean-ice model.

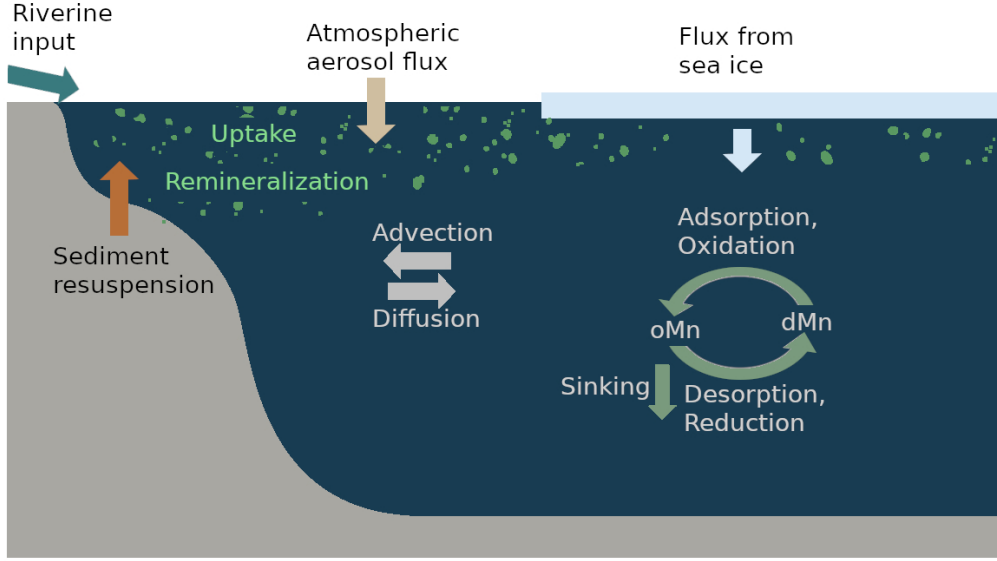


Figure 2. Summary of the processes that affect dissolved Mn (dMn) and oxidised Mn (oMn) concentrations in the Canadian Arctic Archipelago and the Canada Basin.

mal vents as a source of Mn in the Arctic, since the influence of the Gakkel Ridge is restricted to Nansen and Amundsen Basins due to scavenging nearby the source (Lavelle et al., 1992; Middag et al., 2011b). We also do not include sediment diffusion (reductive dissolution) because observations have indicated that these processes are not significant for Mn in the CAA (Colombo et al., 2020). The Mn model equations are:

$$\frac{\partial dMn}{\partial t} = S_{river} + S_{sediment} + S_{atm} + S_{ice} + S_{sed\ ice} + S_{bio} + R_{scav} + \text{advection} + \text{diffusion} \quad (1)$$

$$\frac{\partial oMn}{\partial t} = -R_{scav} - R_{sink} + \text{advection} + \text{diffusion} \quad (2)$$

which include the contribution of rivers (S_{river}), sediment resuspension or non-reductive dissolution ($S_{sediment}$), atmospheric dust deposition (S_{atm}), dust flux from ice (S_{ice}), sediment released by ice ($S_{sed\ ice}$), biological uptake and remineralization (S_{bio}), the reversible scavenging terms (R_{scav}), and sinking (R_{sink}). The details of the parameterizations are described in the following sections and the parameter values used for the runs are listed in Table 1.

The model was initialized with output from the global Mn model (Van Hulten et al., 2017) and concentrations are held constant at the sub-domain boundaries. At these boundaries, the ratio of dissolved to oxidised Mn from the global model were not rep-

Table 1. Constants and parameter values used in the Mn model runs.

Parameter	Description	Value	Source
α_0	Fractional solubility of Mn at 4°C	0.65	Fishwick et al. (2018)
$f_{Mn\ crust}$	Mn fraction in Earth’s crust	527 ppm	Wedepohl (1995)
$f_{Mn\ sed}$	Mn fraction in marine sediment	270 ppm	Macdonald and Gobeil (2012)
m	Molar mass of Mn	54.938 g mol ⁻¹	—
$R_{Mn:N}$	Extended Redfield ratio Mn:N	1.6 : 23,000	Kuss and Kremling (1999)
k_d	Reduction and desorption rate	$4.7 \cdot 10^{-7} \text{ s}^{-1}$	Bruland et al. (1994)
	Photo-enhanced reduction rate	$2.7 \cdot 10^{-5} \text{ s}^{-1}$	Sunda and Huntsman (1994)
k_p	Oxidation and adsorption rate	$7.0 \cdot 10^{-7} \text{ s}^{-1}$	This study ^a
s_{ox}	Sinking rate	0.6 m day ⁻¹	Roy-Barman (2009) / This study
C	Tidal erosion tuning constant	$2.1 \cdot 10^{-6}$	This study
γ	Solubility tuning constant	0.065	This study
R / SPM	River characteristic content		This study ^b
	- Glacial	164 nM / 261 mg L ⁻¹	
	- Continental	30 nM / 12 mg L ⁻¹	
	- Other	2 nM / 4 mg L ⁻¹	

^aUsing data from Colombo et al. (2020, 2022).^bUsing data from Colombo et al. (2019); Brown et al. (2020).

representative (oxidised Mn was too low) and resulted in unusual scavenging behavior. Instead, we used dissolved and oxidised Mn concentrations in a band just inside the domain (where the model had established normal scavenging behavior) from a test model run at the end of spin up for the boundary conditions. We conducted sensitivity experiments of the western and northern boundary conditions with enhanced concentrations to delineate the influence of Pacific water and the transpolar drift on the Canada Basin (Text S1, Fig. S1-4).

2.2.1 Riverine Source

River discharge contributes Mn to the shelf seas and into the Arctic Ocean (Middag et al., 2011a). Dissolved Mn is contributed directly in its dissolved form and indirectly through the dissolution from particle-bound Mn. The contribution of riverine Mn depends on the river discharge, Q , and the concentration in the rivers. These concentrations vary based on properties of the river’s catchment basin: glacial rivers are strongly enriched in dissolved Mn, continental rivers are somewhat enriched, and in all other rivers, Mn is not significantly enriched (Colombo et al., 2019). At each time step, the rivers contribute dissolved Mn following:

$$S_{river} = \frac{\overbrace{Q}^{\text{dissolved Mn}}}{\rho_0 \Delta z_{surface}} R_{class} + \beta \frac{\overbrace{Q}^{\text{particle origin dissolved Mn}}}{\rho_0 \Delta z_{surface}} \frac{SPM_{class} \cdot \alpha_0 \cdot f_{Mn, crust}}{m} \quad (3)$$

where ρ_0 is the density of the river water, $\Delta z_{surface}$ is the surface grid box thickness, β is a factor which ranges from 0-1 in our experiments (not tuned, but tested in the upper bound river experiment), $f_{Mn, crust}$ is the crustal abundance of Mn, m is the molar mass of Mn, and α_0 is the fractional solubility of Mn. We use an average value for the fractional solubility (65%) measured in seawater at 4°C, since this lower temperature better reflects the CAA (Fishwick et al., 2018). This fractional solubility falls within the range measured in samples across the world (Fishwick et al., 2018). Each river is assigned a class with an associated characteristic trace metal concentration, R_{class} , and suspended particulate matter content, SPM_{class} , based on catchment basin properties: glacial, continental, and other (Fig. 3 and Table 1). The Mn concentrations and SPM content associated with the classes are determined from rivers sampled in the CAA (Colombo et al., 2019; Brown et al., 2020).

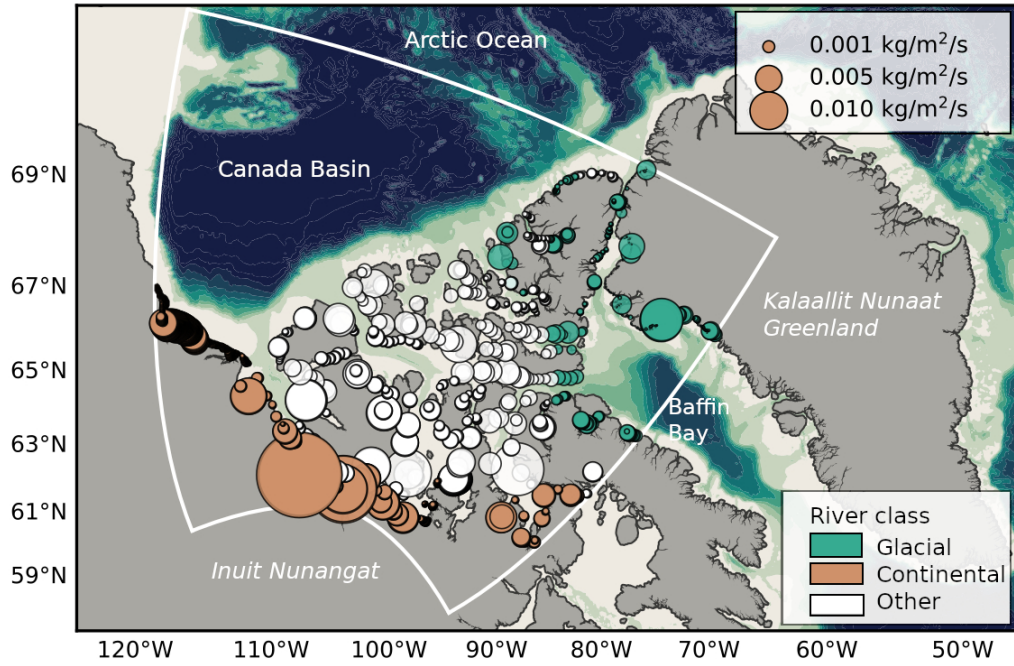


Figure 3. Model rivers were classified based on their drainage basin properties: glacial (green), continental (orange), or other (white). The points on this map are the locations of the river water input in the model and their sizes are proportional to the river discharge in September, 2015 (forcing is repeated from year 2010). Note that the river freshwater flux is remapped to prevent negative model salinities, hence some large rivers are represented as single point sources, while others such as the Mackenzie River consist of multiple point sources along the coastline (Hu et al., 2019).

2.2.2 Atmospheric Aerosol Flux and Release from Sea Ice

Atmospheric aerosols contribute Mn to the ocean through direct deposition to surface waters, Φ_{atm} , or through the deposition onto sea ice and the subsequent release during melt, Φ_{ice} . We parameterized these particulate contributions to dMn as:

$$S_{atm\ or\ ice} = \frac{\alpha_0 \cdot f_{Mn\ crust}}{m \cdot \Delta z_{surface}} \cdot \Phi_{atm\ or\ ice} \quad (4)$$

The atmospheric and sea ice flux terms are derived from monthly Community Earth System Model (CESM) results. The combined monthly dry and wet atmospheric deposition fluxes originate from historical (1920-2005) and future (2006-2080) runs of the Community Atmosphere Model with Chemistry (CAM-Chem) downloaded from the Climate Data Gateway (CESM1 CAM5 BGC Large Ensemble Atmosphere Post Processed Data; Tilmes et al., 2016). We estimate tracer fluxes from ice using the monthly Community Ice Code ensemble results (CICE; Holland et al., 2012; Kay et al., 2015). These ensemble run sets have a horizontal atmospheric resolution of $0.9 \times 2.5^\circ$ and ocean/ice resolution of $1.6 \times 2.5^\circ$ which we linearly interpolated to the ANHA12 grid. We do not tune any of the parameters in this process.

2.2.3 Sediment Resuspension over the Continental Shelf

Dissolved Mn increases near the ocean floor in the Canadian Arctic by sediment resuspension (non-reductive dissolution; Colombo et al., 2020). While reductive dissolution is important over the Chukchi Shelf regions (Vieira et al., 2019), we did not include sediment diffusion as reducing conditions in the sediments are not prevalent in the CAA (Colombo et al., 2021; Lehmann et al., 2022). Sediment resuspension occurs intermittently; Mn integrates the resuspension events and thereby provides a cumulative view of its prevalence. We incorporated the contribution from sediment resuspension to dMn as a continuous process:

$$S_{sediment} = \Phi_{erosion} \cdot \frac{\alpha \cdot f_{Mn\ sed}}{m \cdot \Delta z_{bottom}} \quad (5)$$

where $f_{Mn\ sed}$ is the fraction of Mn in the particle phase in marine sediments. This fraction is likely to be lower than measured in the continental crust, i.e. Wedepohl (1995), since it's undergone some amount of chemical transformation. We used the Mn fraction estimated by Macdonald and Gobeil (2012) from sediments in cores on the shelf and slopes surrounding the Canada Basin. In Eqn. 5, $\Phi_{erosion}$ is the "erosion ability" (see Fig. S5

for the forcing field). This term incorporates the spatial differences in dynamics within the CAA. West of Barrow Sill, the system has lower mixing rates (Hughes et al., 2018) and tidal speeds (Epstein, 2018), than the region east of Barrow Sill and around the central sills area. These differences impact the sediment resuspension rates, apparent in the much stronger near-bottom increases of observed dMn in the eastern CAA (Colombo et al., 2020). We estimate the ability of sediment to be eroded with the barotropic tidal speed, U_{tidal} , and a tuning constant, C :

$$\Phi_{erosion} = C \cdot U_{tidal}^2 \quad (6)$$

The barotropic tidal speeds are from the MOG2D-G model (Carrère & Lyard, 2003) and are significantly higher in the eastern CAA, compared to the western CAA (Epstein, 2018). Locations where the tidal speeds are less than 1 cm s^{-1} are masked, since they are below a critical threshold for motion for particles greater than 0.1 mm, i.e. sand. In areas where resuspension occurs frequently, the easily accessible Mn on particles has already been removed, resulting in a lower solubility. We reduce the fractional solubility in Eqn. 5 at high tidal speeds according to:

$$\alpha = \alpha_0 \cdot \frac{\gamma(1 - e^{-U_{tidal}^2/\gamma})}{U_{tidal}^2} \quad (7)$$

where γ is a tuning parameter. At small tidal speeds, Eqn. 7 approaches α_0 while at tidal speeds greater than 0.1 m s^{-1} , fractional solubility decreases and the overall resuspension rate approaches a constant $\alpha_0 \gamma C$ (Fig. S6). The tuning parameters were estimated based on model behaviour in several tuning runs (see Section 2.3).

2.2.4 Sediment Entrained in Sea Ice and Subsequent Melt

Sediment entrained in sea ice has been identified as an important source of reactive trace metals such as aluminum and iron in the ocean, and thus may also be important for Mn (Measures, 1999). In order to parameterize this contribution to dMn, we couple the Mn contained in sediments in sea ice and the sea ice melt rate, I_{melt} :

$$S_{sed \text{ ice}} = \frac{\alpha_0 \cdot f_{Mn \text{ sed}}}{m \cdot \Delta z_{surface}} \cdot S_p \cdot I_{melt} \quad (8)$$

where S_p is the sediment content in sea ice at each grid point. The sediment content is spatially variable, and depends on the amount of sediment that was incorporated during ice formation on the shelves and on sea ice transport. Mn from the sediments dissolves with fractional solubility, α_0 , and subsequently undergoes redox cycling and sinking as elsewhere within the water column. Sea ice also contains dissolved Mn, however

this component drains out with the brine during early melt (Domena, 2017), and is likely removed within the first melt season. Hence, we did not consider the dissolved Mn in sea ice brine fraction in our model.

Through particle tracking experiments with Ocean Parcels (Lange & Van Sebille, 2017), we estimated the contribution of sea ice formed over the Siberian shelves during the stormy fall months (September-December) to the ice in the Canada Basin (Fig. 4). We released parcels every month over the course of a year and traced them backwards for three years (the average sea ice age in the Canada Basin and the northwestern CAA based on satellite information). Almost 40% of the sea ice tracks in the northwestern CAA and Canada Basin region originated from the Siberian shelves via the transpolar drift during the fall months, when strong sediment resuspension events coincide with sea ice formation. The rest of the tracks transit this region during other times of year, circulate within the central Canada Basin during the three years of tracking, or originate from the outer Siberian shelf or Chukchi Sea. The results of the particle tracking experiments were interpolated and smoothed to create a forcing field which incorporates the spatial variation in sediment content in sea ice (Fig. S7). In addition, we assumed a low background value of shelf sediments in sea ice in the CAA. We multiply this forcing field by a tuned constant, 0.85 kg m^{-3} , which reflects the sediment content of the ice if it were fully formed over the Siberian shelf in the fall, i.e. the proportion of Siberian tracks was one.

2.2.5 Uptake and Remineralization

Dissolved Mn is taken up by phytoplankton in the euphotic zone and is subsequently remineralized below the euphotic zone. We can quantify this particulate contribution to dMn by pairing the addition and removal of Mn to the uptake and remineralization of nitrate:

$$S_{bio} = R_{Mn:N} \cdot \Delta N \quad (9)$$

where $R_{Mn:N}$ is the extended Redfield ratio for Mn to nitrogen based on observations in the North Atlantic (23,000 N : 1.6 Mn; Kuss & Kremling, 1999), and ΔN is the month-to-month change in nitrate concentration during the summer months (April-August) from 2002-2015 derived from the Canadian Ocean Ecosystem Model (CanOE; Hayashida et al., 2019). The North Atlantic nutrient balance is strongly influenced by Arctic Ocean

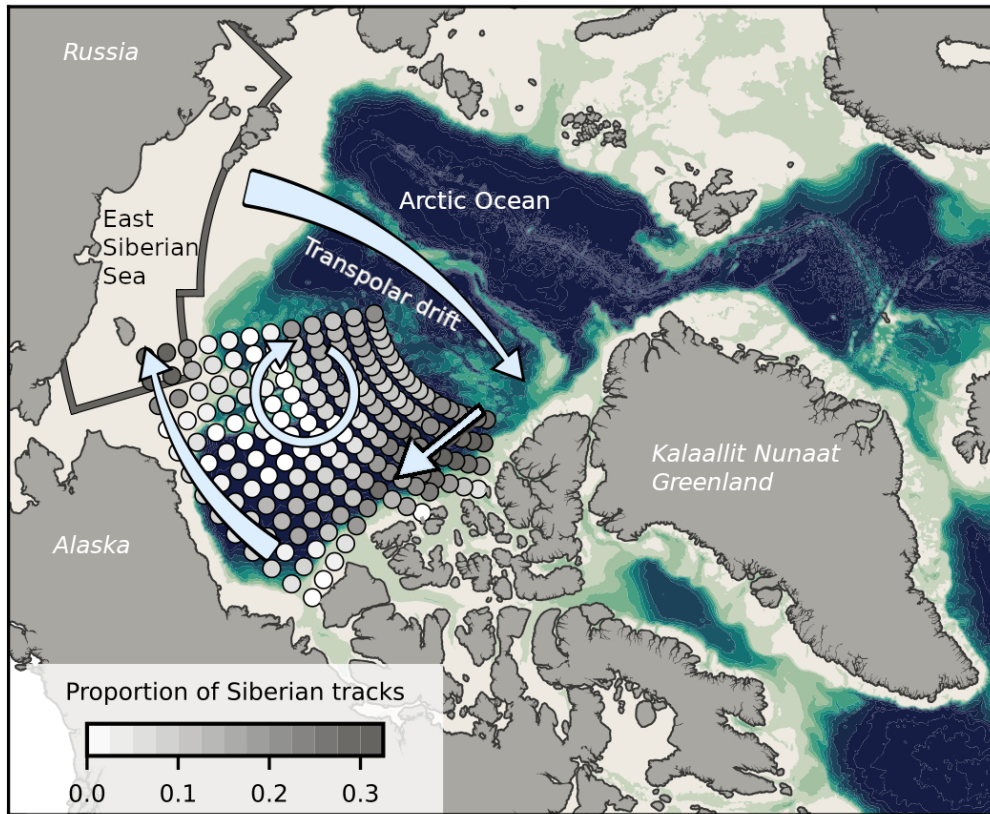


Figure 4. Sediment rich sea ice, produced over the Siberian shelves (East Siberian Sea; region definition outlined in gray) in the fall, is transported across the Arctic Ocean via the transpolar drift. From there it is found predominantly along the outer edges of the Beaufort Gyre; the largest contribution occurs in the northeastern CAA. Ice motion patterns are indicated with light blue arrows. For locations in the Canada Basin, the proportion of parcels traced back to the Siberian shelves (region defined with the brown outline) in the fall months are shown.

outflow (Yamamoto-Kawai et al., 2006) and may thus be representative of the CAA. The Mn:N ratio could be lower in the Arctic Ocean, in which case we slightly underestimate uptake and remineralization. We assume that the month-to-month change in nitrate is zero during seasons with low biological activity to avoid confusing the replenishment of nitrate via mixing with remineralization at the surface. We did not tune the uptake and remineralization.

2.2.6 Reversible Scavenging and Sinking

Dissolved Mn oxidizes forming larger aggregates and adsorbs to particle surfaces. dMn is regenerated by the reduction of oxidised Mn and desorption from particles. Since we do not directly model particle-bound Mn, but rather incorporate its effect on dMn through dissolution from the source components, we calculate the reversible scavenging based on the dissolved and oxidised Mn concentrations (Van Hulst et al., 2017):

$$R_{scav} = -k_p \cdot [dMn] + k_d \cdot [oMn] \quad (10)$$

where k_p is the adsorption and oxidation rate, and k_d is the desorption and reduction rate (see Text S2 for the full derivation). The R_{scav} term appears with opposing signs in the dMn and oMn equations (Eqn. 1 and 2). We estimate the rate constant k_p from observations of dissolved and particulate Mn in the Canadian Arctic (Colombo et al., 2020, 2022). As this estimate is based on field data, the rate intrinsically incorporates the impact of abiotic and microbially enhanced oxidation. Assuming steady state, the ratio of the scavenging rates is equal to the ratio of dissolved to particulate Mn concentrations. This assumption reduces the available observations to those far away from sources and sinks, i.e. deep stations in Baffin Bay and the Canada Basin (Fig. S8). The ratio of scavenging rates, k_p/k_d , is estimated as 1.47 ± 0.25 and with a k_d of $4.7 \cdot 10^{-7} \text{ s}^{-1}$ (Bruland et al., 1994), k_p is estimated as $7.0 \cdot 10^{-7} \text{ s}^{-1}$ (Fig. S9). The reduction rate, k_d , increases from the base rate up to $2.7 \cdot 10^{-5} \text{ s}^{-1}$ in the euphotic zone (photo-enhanced reduction; Sunda & Huntsman, 1994), proportional to the solar flux that penetrates into the ocean at the surface, limited by the ice cover (from ANHA12). We estimate the euphotic zone depth as 70 m in the Canada Basin with a gradual transition to 50 m in the CAA (Fig. S10) based on estimates by Bhatia et al. (2021) and Laney et al. (2017); the euphotic zone depth estimate does not account for sea ice cover. The scavenging rates in the model do not depend on the dissolved oxygen concentration since Arctic waters are generally well oxygenated.

The oxidised Mn aggregates sink, R_{sink} , and are removed through burial as in Van Hulten et al. (2017):

$$R_{sink} = s_{ox} \frac{\partial[oMn]}{\partial z} \quad (11)$$

where s_{ox} is the sinking rate. The sinking rate was based on the estimate by Roy-Barman (2009) of 0.4 m d^{-1} in the interior of the Arctic Ocean and then increased to 0.6 m d^{-1} based on an evaluation of modelled background oMn concentrations in the Canada Basin far away from sources and sinks.

2.3 Tuning

Of the parameters in our model (Table 1), we tuned the oMn sinking rate, sediment resuspension rate, sediment solubility parameter, and the sediment content in sea ice (in that order). Below, we describe our choice of criteria and approaches for tuning these parameters, and compare the parameter values with observations.

The sinking rate sets the background oMn (and through reduction, dMn) concentrations in regions far away from sources such as deep parts of the Canada Basin. We initialized the sinking rate in our model as 0.4 m d^{-1} based on a sinking rate derived by Roy-Barman (2009) from modelled and measured ^{230}Th profiles in the interior of the Arctic Ocean. With a sinking rate of 0.4 m d^{-1} , the deep oMn concentrations in the Canada Basin in the model were overestimated. An increased sinking rate of 0.6 m d^{-1} gave reasonable background oMn concentrations. The global model of Mn uses a sinking rate of 1 m d^{-1} up to 10 m d^{-1} to account for loss near hydrothermal vents (Van Hulten et al., 2017).

Our sediment resuspension parameterization incorporates two tuned parameters: the tidal erosion rate constant, C , and solubility parameter, γ . The tidal erosion rate controls the background (below about 100 m) and near-bottom dMn concentrations in shelf areas, so in our domain predominantly the CAA. With observed dMn profiles in the CAA, we assessed the tidal erosion constant that best represented dMn in the lower water column with multiple test model runs. The solubility parameter limits the sediment resuspension rate in shelf regions with high tidal speeds, and the most appropriate value was estimated mainly based on comparing modelled dMn with observations at stations CAA6 and CAA9 (characterized by strong tidal speeds). The resultant sediment resuspension rates in our model range from 0 to $2808 \text{ g m}^{-2} \text{ yr}^{-1}$ (median of re-

gions with resuspension is $58 \text{ g m}^{-2} \text{ yr}^{-1}$). Particulate material collected in sediment traps over the Beaufort Shelf from spring 1987 to 1988 contained total dry weight particle fluxes associated with terrigenous input ranging from 10 to $80 \text{ g m}^{-2} \text{ yr}^{-1}$ (O'Brien et al., 2006). The largest particle fluxes occurred during the summer and fall. Our median tuned sediment resuspension rate falls within this range.

We tuned the sediment content in sea ice last, as it is the most important parameter in our study. This parameter affects the surface dMn concentrations primarily in the Canada Basin where sea ice contains a significant proportion of non-local sediments (Fig. 4). We assessed the representation of surface dMn concentrations at stations in the Canada Basin after a few years of spin up using several values of the sediment content in ice parameter. The chosen sediment content in sea ice in the Canada Basin in our model ranges from 0 to 267 g m^{-3} (median is 28 g m^{-3} ; average is 64 g m^{-3}). In observations, the sediment load ranges by several orders of magnitude depending on the location sampled, the type of ice, and is highly variable year-to-year (see Table S1 for a non-comprehensive list of observed sediment content). In the Beaufort Sea, the observed sediment content in ice cores ranged from 31 to 593 g m^{-3} with an average of 157 g m^{-3} (Reimnitz et al., 1993). Our tuned ice sediment content is smaller, but of a similar order of magnitude.

2.4 Experimental Design

Three numerical experiments were performed with the Mn model, running from 2002 to 2019: the reference and “clean” sea ice cases, and a sensitivity experiment for the rivers. An additional experiment was performed from 2002 to 2015 to assess the magnitude of the impact of biological uptake and remineralization. The reference run includes all model components except uptake and remineralization, and uses a lower bound estimate of the river contributions (no particle-bound Mn, $\beta = 0$ in Eqn. 3). The clean sea ice case is the same as the reference run, except that the sea ice does not contain sediment (i.e. $S_{sed\ ice} = 0$). In order to bound the riverine influence, we perform a sensitivity experiment with a distinctly upper bound riverine estimate ($\beta = 1$ in Eqn. 3), compared to the lower bound estimate from the reference run. The treatment of riverine Mn introduces uncertainties in the model due to the complex estuarine cycling and the influence of particulate matter on dissolved Mn concentrations. In the “upper bound”

river experiment, we include the contribution from riverine sediments on the Mn concentrations in addition to the dissolved Mn.

Each experiment is spun up by repeating the year 2002 three times, before starting the full run. The run is considered spun up when the year-to-year change in Mn profiles is minimal (Fig. S11). Analysis was performed using Python 3 (<https://anaconda.com>) within Jupyter Notebooks with the NumPy, Pandas, SciPy, Matplotlib, Seaborn, scikit-learn, and cmocean packages (Pedregosa et al., 2011; Hunter, 2007; Kluyver et al., 2016; Oliphant, 2006; The Pandas development team, 2020; Thyng et al., 2016; Virtanen et al., 2020; Waskom & the Seaborn development team, 2020).

3 Results

Mn profiles throughout our domain are typical for a scavenged type element: concentrations are higher near sources with a low and homogeneous background (Fig. 5). The background concentrations are controlled by scavenging, sinking, advection and mixing, and the resultant redistribution of materials throughout the water column, while the surface Mn maximum is a result of the contributions from river runoff, sea ice melt, dust deposition, photoreduction, and sediment that is resuspended directly into the polar mixed layer. Sediment resuspension leads to near-bottom increases in some regions.

3.1 Model Evaluation

We evaluate the Mn model by comparing simulated dissolved Mn concentrations in August-September 2009 and 2015 from the reference experiment with measurements collected by the IPY and Canadian GEOTRACES cruises during those time periods (Sim, 2018; Colombo et al., 2020, Fig. 5-9). We also show mean polar mixed layer dMn concentrations alongside observations from the 2015 US GEOTRACES GN01 section (Fig. 9a; Jensen et al., 2020; GEOTRACES Intermediate Data Product Group, 2021). We do not focus on particulate Mn as it is only incorporated into the model to estimate the scavenging of dMn. Nevertheless, modelled oMn displays the observed variability in the upper 100 m in the CAA in 2015 well (Fig. S12). Overall, our intention is not to replicate the observations, but to incorporate all the processes that control Mn distributions and to capture observed spatial variation. The observations were not used in initial conditions or boundary conditions to allow for an independent evaluation.

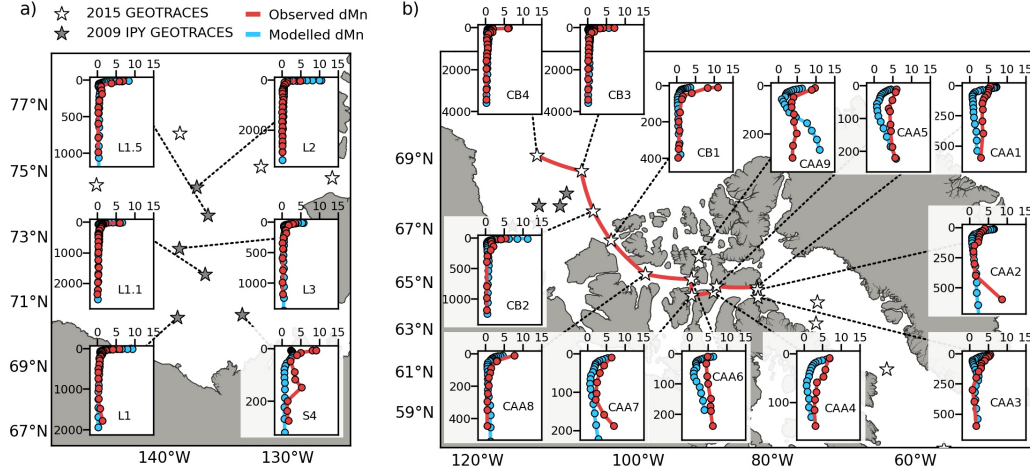


Figure 5. Simulated dissolved Mn profiles (blue) from the reference run compared to observed concentrations (red) from the (a) 2009 IPY GEOTRACES cruise on the Beaufort Shelf and (b) the 2015 Canadian GEOTRACES cruises in the Canadian Arctic Archipelago. Profiles are labelled with station names and their locations are marked with gray (2009 stations) and white (2015 stations) stars. Simulated concentrations were averaged over the time periods of the cruise observations, i.e. August-September. Note that the profile depth (vertical) scales vary.

The model captures the regional variation of Mn concentrations along a transect from the deeper Canada Basin into the shallow CAA (Fig. 6). Observed surface concentrations range from 5-10 nM in the Canada Basin and on the Beaufort Shelf, up to 10-11 nM at CB1, CAA8, and CAA9, and around 5 nM in the rest of the CAA (Fig. 5 and 6). The representation of the Canada Basin and the Beaufort shelf surface is variable and dependent on the specific patterns of sea ice melt and the Pacific Water inflow. Overall, the model does well in the southern Canada Basin and on the Beaufort Shelf (Fig. 9a). In the central Canada Basin, modelled concentrations are lower than observed; a reflection of the lower sediment content in the model sea ice forcing in this portion of the Canada Basin (Fig. S7). Along the western domain boundary and on the Beaufort Shelf, inflow of Pacific Water increases Mn concentrations in the model and observations (Fig. 9a, S2). Surface concentrations are overestimated at L2, L1, and CB2 and underestimated at S4 on the Beaufort shelf, and at stations CB4, CB1, and CAA8 in the western CAA which receive outflow from the Canada Basin (Fig. 5). Within the CAA, surface concentrations are overestimated at stations CAA1 and CAA2 in Lancaster Sound where waters from Baffin Bay recirculate, while on the south side of the Channel at CAA3, the model cap-

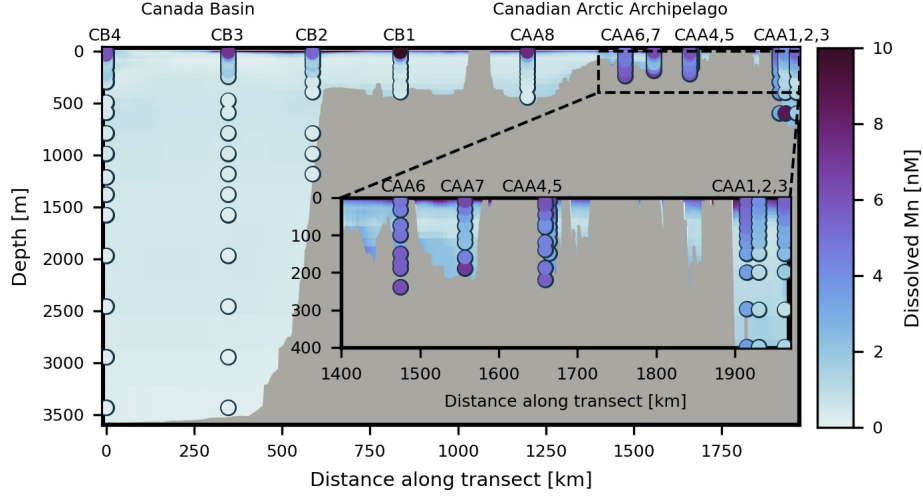


Figure 6. A transect of dissolved Mn concentrations from the Canada Basin through Parry Channel in the Canadian Arctic Archipelago to Baffin Bay (path is shown in red in Fig. 5b). The background shading corresponds to simulated dMn averaged over the sampling time period (August-September, 2015) and the circles indicate observed dMn concentrations from the 2015 GEOTRACES cruises. The inset expands on the Parry Channel region east of Barrow Sill.

tures the surface concentrations (Fig. 5). Background concentrations in the model and observations are low (0-2 nM) in the Canada Basin (0-900 km along the transect in Fig. 6) and increase (to 1-4 nM) as the waters travel through the shelf areas of the CAA.

Within Parry Channel, background concentrations west of Barrow Sill are around 1-2 nM, similar to the Canada Basin, while in the eastern CAA they increase to 3-5 nM with near-bottom maxima (appear as a slight bend in the modelled Mn profiles in Fig. 5 and Fig. 6). Background concentrations in shallow regions are set by the sediment re-suspension rate which increases concentrations up to where the surface stratification limits vertical mixing, while within the polar mixed layer concentrations are set by surface sources. At depths of 40-100 m in the CAA, just below the polar mixed layer, the model underestimates Mn. Within this depth range, Mn is remineralized, acting as a source that is not considered in the reference experiment. In the biological experiment, we estimate that remineralization accounts for up to 0.3 nM (Fig. S19 and Text S3). At 100-200 m depth in the Canada Basin and on the Beaufort shelf, observed Mn concentrations are slightly higher than the background concentrations. This increase is associated

with the winter Bering Sea Water and is not captured by the model, as it was not represented in the model’s western boundary condition.

The net effect of sediment resuspension is well-represented in the background concentrations, however there are a couple of unusual modelled near-bottom Mn profiles (Fig. 5). At station CAA9 in Penny Strait, the Mn model overestimates background and bottom concentrations by 5 nM. At this station, strong mixing results in constant, “vertical” observed Mn profiles (Hughes et al., 2018). Sediment resuspension, based on tidal stress, dominates as a source of Mn to this region. However, this version of the physical model does not incorporate tides. Hence, we add Mn at the bottom, proportional to the strength of tidal stress, without redistributing it due to tidal mixing. At stations CAA2 and CAA7, on the south side of Parry Channel, observed Mn concentrations increase up to 10 nM near the ocean bottom. These peaks in the observations are attributed to sediment resuspension (Colombo et al., 2020), although the specific mechanism for the strong peak is unclear. The model does not reproduce these local extreme increases, which likely vary on much smaller spatial scales than our parameterizations can resolve. An increase in Mn over the 40 m above the bottom is reproduced by the model at stations CAA2, CAA4, CAA5 and CAA7.

While the model is limited in its representation of regions with strongly variable resuspension rates, it performs well within a range of environments: from deep regions in the Canada Basin to shallow areas in the CAA. The model is configured to ask questions about the drivers of Mn variability. It is important to keep in mind that our parameterizations are limited by the spatial and temporal resolution of available information; small scale variations are unlikely to be captured by the model.

3.2 Importance of Sediment in Sea Ice

In order to evaluate the importance of sea ice and rivers on the representation of Mn in the upper water column (above 50 m), we compare the results of the “clean” sea ice and upper bound river experiments with the reference experiment (Fig. 7). For all experiments, the representation of surface concentrations has a broad spread. The “clean” sea ice experiment underestimates concentrations in the upper water column by several nM (Fig. 7a) and its mean underestimates concentrations by 4 nM. The mean of the reference run, with sediment in sea ice, falls within 1 nM of observed concentrations. The

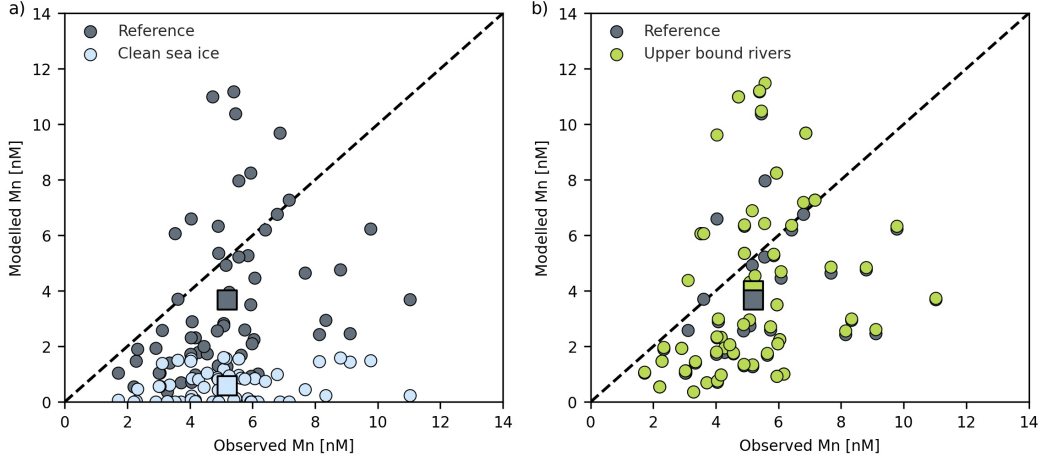


Figure 7. Nearest-depth modelled dMn concentrations compared with observations for depths shallower than 50 m for 2009 IPY and 2015 Canadian GEOTRACES cruises. Square markers indicate the averages of the experiments and observations. (a) The modelled dMn concentrations at the evaluation stations most closely resemble the observations in the reference experiment with sediment in sea ice compared to the “clean” sea ice experiment. Both of these experiments use the lower bound river estimate. (b) The lower and upper bound river experiments, which include sediment within the sea ice, indicate that additional contribution from riverine particulate matter has a relatively small impact.

upper bound river experiment slightly increases the surface concentrations relative to the reference experiment, particularly in the eastern CAA (Fig. 7b). Estimates for stations in the Canada Basin are unaffected by the addition of particulate matter in rivers.

We expect substantial vertical gradients in concentrations in the surface layer in the Arctic Ocean as a result of the strong stratification. It is difficult to assess the uppermost modelled concentrations as the shallowest observations are collected at around 10 m below the surface, while the shallowest model estimate is at 0.5 m depth. However, the Mn-salinity relationship in the model is similar to the observations for the experiment with sediment in sea ice (Fig. S13). In the “clean” sea ice experiment, the model significantly underestimates the low-salinity Mn endmember.

3.3 Contributions from External Sources of Mn

To assess the relative contributions of each of the external Mn sources, we calculated the annual contribution and flux from these model components in the reference experiment. Our estimate is for the upper 55 m of the water column as we are most interested in the surface layer. An estimate of the full water column differs by including the effects of resuspension in regions deeper than 55 m, thus increasing the importance of resuspension (Table S2). We include estimates from the upper bound river experiment, which does not account for any removal of particulate or dissolved Mn in estuaries, as ranges in the text. We did not include the contributions from (photo)reduction and remineralization as sources of dMn in these calculations since they are part of the internal cycling of Mn. In order to identify regional differences, we separated the domain into the Canada Basin and the Canadian Arctic Archipelago (details in Fig. S14) and subdivided the CAA into west and east along 100°W. Overall, the Canada Basin is more isolated and receives a lower annual contribution of Mn than the CAA: 238-254 versus 370-530 $\mu\text{mol m}^{-2} \text{ yr}^{-1}$ (Table 2).

In our model, the dominant source of Mn in the Canada Basin is the release of sediment by sea ice melt (Table 2); it accounts for 87-93% of the average yearly addition of Mn. The amount of melt fluctuates interannually, similar to sea ice area changes observed with satellite data. Nevertheless, from 2002 to 2019, sea ice melt is consistently the largest contributor of Mn in our model in the Canada Basin. Sediment resuspension contributes about 4.4-4.7% in the Canada Basin, mainly over the Beaufort shelf, and river discharge, predominantly from the Mackenzie River, contributes 2.2-8.5%. Atmospheric dust deposited onto the ocean surface, or released during sea ice melt, is not a significant source of Mn anywhere in the domain.

In the CAA, sediment resuspension contributes 40-58% of the annual external addition of Mn to the water column (Table 2). Sediment released by sea ice accounts for 26-37% of Mn; a combination of relatively “clean” sea ice with high melt rates. The river contributions cover a broader range from 5.0-34% in the CAA, compared to 2.2-8.5% in the Canada Basin. Since the total annual Mn addition is greater in the CAA, rivers contribute significantly more dMn to the CAA. Although the Canada Basin receives runoff from the Mackenzie River, the CAA has many rivers of a range of sizes that drain into it, including glacial rivers with high characteristic Mn concentrations.

Table 2. External source contributions to the upper water column of the Canada Basin and the Canadian Arctic Archipelago.^a

	Canada Basin		Canadian Arctic Archipelago	
Component contribution	$\mu\text{mol m}^{-2} \text{ yr}^{-1}$	%	$\mu\text{mol m}^{-2} \text{ yr}^{-1}$	%
River discharge	5.3 (22)	2.2 (8.5)	19 (178)	5.0 (34)
Sediment resuspension	11	4.7 (4.4)	213	58 (40)
Sediment from sea ice	221	93 (87)	138	37 (26)
Dust released by sea ice	0.2	0.1	0.3	0.1
Direct dust deposition	0.0	0.0	0.0	0.0
Total	238 (254)	100	370 (530)	100

^aCalculated as the spatial average annual dissolved Mn contributed by external model source components to the upper 55 m of the water column ($\mu\text{mol m}^{-2} \text{ yr}^{-1}$) in the reference experiment, averaged over the years 2002-2019, separated by region (Fig. S14). Sediment release by sea ice is the only component that varies significantly year-to-year. Estimates from the upper bound river experiment are indicated in parentheses.

Table 3. External source contributions to the upper water column of the western and eastern Canadian Arctic Archipelago.^a

	Western CAA		Eastern CAA	
Component contribution	$\mu\text{mol m}^{-2} \text{ yr}^{-1}$	%	$\mu\text{mol m}^{-2} \text{ yr}^{-1}$	%
River discharge	6.5 (28)	2.2 (8.7)	27 (289)	6.5 (42)
Sediment resuspension	155	52 (49)	256	61 (37)
Sediment from sea ice	136	46 (43)	140	33 (20)
Dust released by sea ice	0.3	0.1	0.3	0.1
Direct dust deposition	0.0	0.0	0.0	0.0
Total	297 (318)	100	424 (686)	100

^aSame as Table 2, except the Canadian Arctic Archipelago (CAA) was subdivided into western and eastern halves along 100°W (near Barrow Sill).

Within the CAA, there is a significant difference in dynamical regime west and east of the approximately 120 m deep Barrow Sill (Table 3; Hughes et al., 2017; Colombo et al., 2020, 2021; Q. Wang et al., 2012). The overall contribution of Mn to the water column in the eastern CAA is 424-686 $\mu\text{mol m}^{-2} \text{yr}^{-1}$, compared to 297-318 $\mu\text{mol m}^{-2} \text{yr}^{-1}$ in the west. The main contributor to this difference is the 1.6 times stronger sediment resuspension in the eastern CAA. In addition, rivers contribute more strongly to the eastern CAA relative to the western CAA, 6.5-42% versus 2.2-8.7%, with a broader range in the estimate of their role in the eastern CAA. The eastern CAA receives contributions from the high Mn content glacial rivers that drain Greenland, Ellesmere Island, and Baffin Island.

Throughout our domain, Mn concentrations are highest in the summer months as a result of seasonally fluctuating components (Fig. 8a). Sea ice melt is largest in July, while the river runoff peak occurs during the freshet in May-June. Due to the large supply of dissolved Mn in the summer months and the increased solar flux, (photo)reduction and oxidation are stronger from July through September. For the month of September, we identified which component on average controls Mn for each horizontal grid cell over the full time series (Fig. 8b). Note that this figure shows where the model adds the contribution from a component; where the Mn ends up depends on the advection and diffusion of the tracer as well.

Within the Canada Basin and portions of the western CAA (the Amundsen Gulf and western Parry Channel), sea ice melt controls the simulated Mn concentrations (Fig. 8b). In the interior of the Beaufort Gyre region, far away from sources and with relatively “clean” sea ice, none of the components contribute significantly. Over the Beaufort Shelf, the Mackenzie River is a regionally important source of Mn; generally river runoff is a significant source at river mouths. In the shallower shelf regions, such as the Beaufort Shelf and the CAA, sediment resuspension is prevalent.

The magnitudes of annual Mn fluxes from sources in this Arctic Model (AM; Table 2) are comparable to those in the first global model of Mn by Van Hulten et al. (2017) (VH). In VH, dust contributes 0-2 $\mu\text{mol m}^{-2} \text{yr}^{-1}$ in the Arctic Ocean, whereas in AM it ranged from 0-0.3 $\mu\text{mol m}^{-2} \text{yr}^{-1}$ (combining direct dust deposition from the atmosphere and indirect release from ice). AM riverine fluxes were 5.3-22 $\mu\text{mol m}^{-2} \text{yr}^{-1}$ in the Canada Basin and 19-178 $\mu\text{mol m}^{-2} \text{yr}^{-1}$ in the CAA; higher than the VH estimate

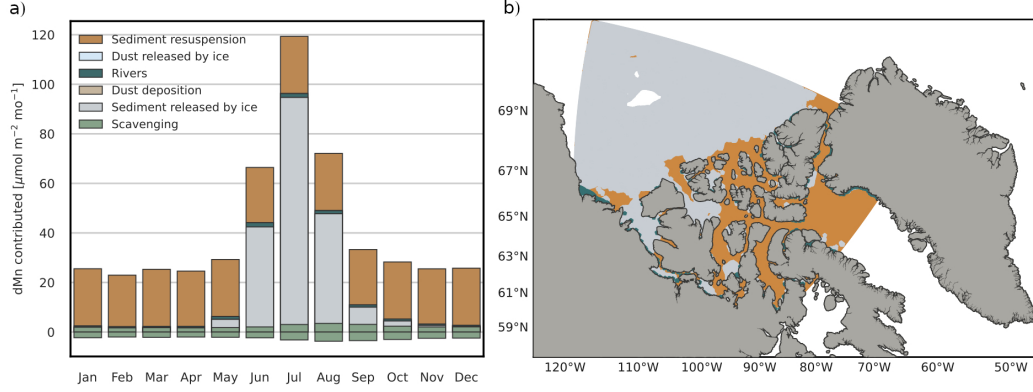


Figure 8. Sediment released by sea ice dominates Mn contributions in the Canada Basin and peaks in July, while sediment resuspension is prevalent over shelf areas including the Canadian Arctic Archipelago. (a) Climatology of the seasonal cycle of Mn contributions for the full water column. The oxidation (removal) and reduction (addition) of Mn through scavenging are calculated as the average through the water column. Sediment resuspension is added at the bottom grid cell, while all other sources act directly on the ocean surface. The contributions from dust deposition and release from ice are too small to appear. (b) Most important Mn contributors to the water column in September based on climatology. At each grid cell, the color represents the most important model forcing component. Places within the model domain where the net contributions are smaller than $0.5 \mu\text{mol m}^{-2} \text{mo}^{-1}$ are white (i.e. in the Canada Basin).

of $0\text{--}2\ \mu\text{mol m}^{-2}\ \text{yr}^{-1}$. This range likely reflects a combination of the high Mn content of rivers in the Arctic (Colombo et al., 2019) and alternate treatment of rivers; VH assumes a relation between Fe and Mn content, while AM uses observations specific to the Arctic rivers and their catchment basins. In VH, the flux of Mn from bottom sediments in the Arctic Ocean was $5\text{--}75\ \mu\text{mol m}^{-2}\ \text{yr}^{-1}$; AM has $11\text{--}213\ \mu\text{mol m}^{-2}\ \text{yr}^{-1}$. The difference in the upper limit of the range likely reflects the distinctive processes considered by the models: the global model considers sediment diffusion for the flux from sediments, whereas AM considers sediment resuspension because it is more important in the CAA (Colombo et al., 2020). It is also challenging to resolve the large continental shelf regions in the Canadian Arctic in a global model. Lastly, on a global scale, hydrothermal input of Mn at spreading ridges is important (Van Hulten et al., 2017), however we did not include this contribution because the spreading ridges in the Arctic are far away from the AM domain.

3.4 Simulated Surficial Mn During the Summer and the Polar Night

The most significant seasonal and interannual changes in Mn concentrations occur in the polar mixed layer, defined here as the upper 35 m of the water column. For the following characterizations of the simulated concentrations, we will focus on this layer. The upper few meters of the ocean have a strong gradient in Mn concentrations (simulated profile in Fig. S15). It is not possible to measure this layer with conventional methods from a large ship. As such, we exclude the surface 3 m in the results presented here (see Fig. S16 for the surface Mn field) to allow for more direct comparison with existing observations.

During summer months, surface Mn concentrations in the Canada Basin mirror the areas of strong sea ice melt and higher sediment content, forming a seasonal Mn maximum (Fig. 9a, S7). Nearby the western and northern Canada Basin domain boundaries, Pacific Water and transpolar drift water can increase Mn concentrations (Fig. 9a, S2, S4). The highest modelled Mn values are found along the outer edges of the Beaufort Gyre (up to 14 nM). Although rivers contribute only a few percent annually to Mn in the Canada Basin (Table 2), over the continental shelf, plumes of higher Mn concentrations extend along coastlines in the summer, starting during the spring freshet (Fig. 9a and Fig. 8b). The plume from the Mackenzie River, the largest river in our domain, extends eastward along the shelf in August, 2015. Glacial drainage is apparent in surface

Mn concentrations in a number of coastal regions (Fig. 9a). Along the coast of Greenland, high concentration Mn runoff drains the ice sheet and a number of plumes extend from Nares Strait. In the northern CAA, higher surface concentrations result from a combination of sea ice melt and glacial runoff (Fig. 8b). Mn from the Pacific water inflow via the western model boundary influences the Beaufort Shelf but does not significantly affect surface concentrations in the Parry Channel (Text S1, Fig. S2).

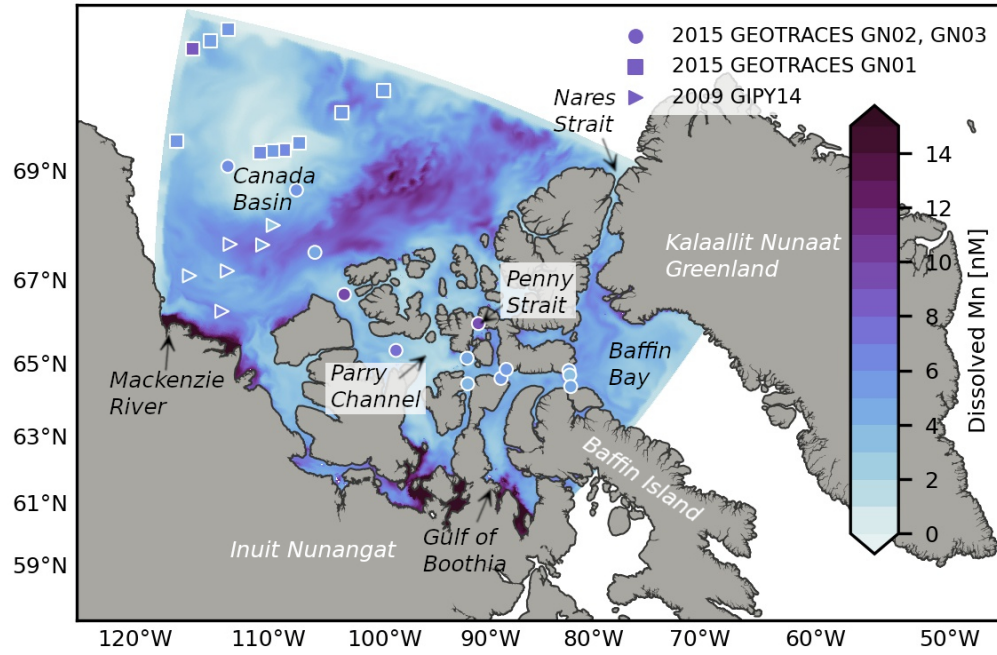
Mn concentrations exhibit spatial variability within the CAA (Fig. 9). In west-central CAA, concentrations are low (2-6 nM) and homogeneous. Southern regions, including the Gulf of Boothia, have some of the highest concentrations (8-14+ nM) and flow into the Parry Channel east of Barrow Sill. In this section of central and eastern Parry Channel (and Penny Strait), intermediate concentrations (4-8 nM) are present. In Lancaster Sound, the outflow from Parry Channel follows the southern half of the channel while waters from Baffin Bay (5-8 nM) recirculate along the northern half of Lancaster Sound. Baffin Bay is characterized by lower interior surface concentrations and higher bands associated with Nares Strait and Lancaster Sound outflow.

During the Polar Night, fewer sources contribute Mn (Fig. 8a) and there is less spatial contrast in surface concentrations (Fig. 9b). Surface concentrations typically range from 1-5 nM, while in the summer they ranged up to 14 nM. The surface Mn maximum is seasonal; by winter, scavenging has removed the relic of summer surface source signatures. Regions where Mn is most impacted by sediment resuspension (Fig. 8b), such as the Gulf of Boothia, still have high concentrations in the winter as this component does not vary seasonally.

4 Discussion

In the Arctic Ocean, maximum Mn concentrations occur near the surface in the polar mixed layer and are attributed to freshwater sources such as river discharge and sea ice melt (Campbell & Yeats, 1982; Yeats & Westerlund, 1991; Middag et al., 2011b; Cid et al., 2012; Kondo et al., 2016; Colombo et al., 2020). We present a regional model of Mn in the Canadian Arctic that captures the spatial variability and magnitude of observed concentrations. With results from three Mn model experiments (reference, “clean” sea ice, and upper bound river), we identified the dominance of non-local sediment released by sea ice in the Canada Basin, while rivers had a more regional importance. These

a) August



b) January

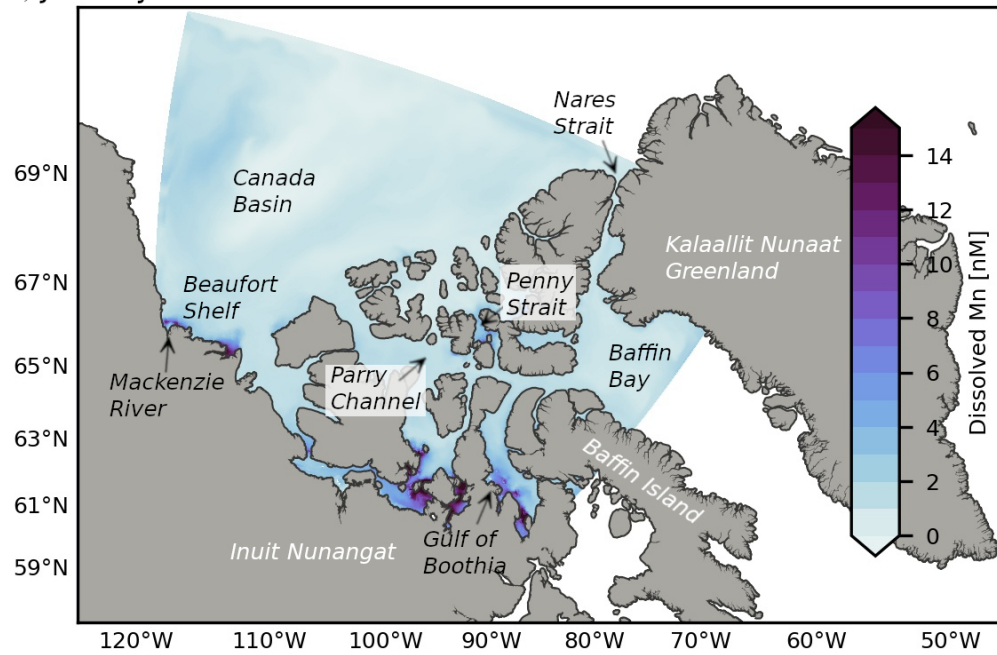


Figure 9. Simulated monthly Mn concentrations in the Polar Mixed Layer, excluding the surface three meters to allow for direct comparison with observations (surface fields in Fig. S16). (a) August, 2015. Markers indicate Polar Mixed Layer dissolved Mn observations from the 2009 GIPY14 and 2015 GEOTRACES GN01, GN02, and GN03 cruises. In the summer, sea ice melt and sediment resuspension dominate the Mn concentrations in the Canada Basin and the Canadian Arctic Archipelago, while freshwater sources such as the Mackenzie River and Greenland meltwater are important regionally. (b) January, 2015. During the Polar night, simulated Mn concentrations are homogeneous and low, however, sediment resuspension continues to drive higher concentrations in the south-central CAA.

findings suggest that future changes to sea ice transport across the Arctic Ocean may have a significant impact on the supply of Mn and other micronutrients to the Canada Basin and downstream to the CAA.

4.1 Ice-rafted Sediments are the Predominant Source of Mn in the Canada Basin

With our model, we found that 87-93% of Mn in the Canada Basin is supplied by sediment from sea ice and 26-37% in the CAA (Table 2). Sediments released by sea ice melt dominate the Mn concentrations in the polar mixed layer during the summer months (Fig. 9a), while in the winter, sea ice blocks the direct surface input of Mn and a lower, more homogeneous distribution results (Fig. 9b). Sediment transport and release by sea ice is the main source of Mn (and likely other similar nutrients) within the Canada Basin, and plays a role within the CAA as well. The majority of sea ice in the interior of the Canada Basin originates from the Siberian shelf regions and traverses the Arctic Ocean via the transpolar drift (Darby, 2003; Eicken et al., 2005; T. Martin & Gerdes, 2007). It spends several years in transit, during which it undergoes freeze-thaw cycles and loses some sediment. The Chukchi Sea may also contribute sea ice to the Canada Basin via the transpolar drift (T. Martin & Gerdes, 2007). In our parameterization, the highest Mn concentrations (and relatively younger ice) are found along the outer edges of the Beaufort Gyre in the Canada Basin, while older ice transported to the interior of the Gyre by convergence has lower Mn concentrations (Fig. 9a). Sea ice formed over the Beaufort Shelf is transported towards Siberia and does not directly impact the Mn concentrations in the Canada Basin.

Mn sources from the land-ocean interface, such as rivers and sediments, were more important in the CAA than in the Canada Basin, and dynamical differences between the western and eastern CAA translated into distinctive Mn concentrations and component contribution patterns. This separation in dynamics is bounded by the ≈ 120 m deep Barrow Sill and has been noted in several studies (Hughes et al., 2017; Colombo et al., 2020). In the western CAA, surface concentrations range from 2-6 nM (Fig. 9) and Mn component contributions share characteristics with the Canada Basin: similar overall river contributions, significant influence from sediments in sea ice, and weaker contributions from sediment resuspension (Table 3). In contrast, in the eastern CAA, Mn concentrations are higher (4-8 nM; Fig. 9), sediment resuspension associated with strong tidal speeds

dominates, and river discharge plays a more important role. The estimate of the component contributions is most sensitive in the eastern CAA: the importance of rivers ranges from 6.5% to 42% depending on the treatment of particulate matter. Rivers are prevalent in the eastern CAA and many of these drain glaciated regions associated with high suspended particulate matter and dissolved Mn. As a result, rivers have the potential to play an important role in the eastern CAA. However, the available information for river input and estuarine removal, limits our ability to constrain the most likely river contribution. Based on the surface concentration comparisons (Fig. 7), the upper bound river experiment alters the mean representation slightly; it is inconclusive on the most realistic representation. The uncertainties associated with these estimates highlight the need for studies on the strength of estuarine removal in the CAA.

Eurasian and North American river runoff contribute freshwater to the Arctic Ocean (Proshutinsky et al., 2019; Krishfield et al., 2014) and could contribute Mn to the surface maximum. The central Canada Basin contains significant amounts of meteoric water and sea ice melt (Guay et al., 2009) which feed its freshening (Yamamoto-Kawai et al., 2009). Several studies have looked into the composition of this water. Fichot et al. (2013) did not identify much river runoff in the central basin and Kelly et al. (2019) found that the freshwater contribution from Siberian rivers has decreased since 1997 as a result of the mainly anticyclonic atmospheric circulation pattern over the Canada Basin. Similarly, model trajectories of floats released from Siberian rivers since 1985 do not generally reach the Canada Basin by 2007 (Proshutinsky et al., 2019). In our reference and upper bound river simulations, rivers contribute only 2.2-8.5% to the total budget of Mn in the Canada Basin and 5.0-34% in the CAA (Table 2). However, freshwater sources such as the Mackenzie River on the Beaufort shelf and glacial melt off the coast of Greenland (Fig. 9a) are dominant near coastlines. Inflow from the central Arctic Ocean including Eurasian runoff enters our study domain through the northern model boundary (Fig. 1). A sensitivity experiment with the northern boundary condition (described in Text S1, boundary condition shown in Fig. S3) indicates weak impact of central Arctic Ocean inflow on dMn concentrations in the central Canada Basin (Fig. S4). Thus, North American river runoff and inflow of Eurasian runoff from the central Arctic Ocean are unlikely to significantly contribute to the freshwater-associated surface Mn maximum in the central Canada Basin.

Nutrient-rich and relatively fresh Pacific water inflow from the Bering Strait is another potential source of Mn to the freshwater surface maximum. Pacific Water is transported by the Alaskan Coastal Current along the North American continental shelf. In our domain, the Alaskan Coastal Current enters through the western boundary. An experiment with enhanced Mn concentrations in the western boundary condition (Text S1, Fig. S1) indicates that the Pacific Water surface influence is restricted to the Beaufort Shelf and does not affect the Canada Basin interior (Fig. S2). The supply of Pacific Water from Bering Strait to the Canada Basin is affected by the atmospheric circulation in the Canada Basin (Kelly et al., 2019) and floats released from Bering Strait since 2000 also did not enter the central Canada Basin by 2012 (Proshutinsky et al., 2019). It is important to note that our simulated profiles (Fig. 5) do not capture the subtle increase in Mn concentrations associated with the winter Bering Sea Water around 100-200 m depth in the Canada Basin and on the Beaufort Shelf. This limitation is likely because our western boundary condition does not fully capture the higher concentrations of Mn found in the Alaskan Coastal Current and in waters from the Chukchi Shelf. However, the deeper winter Bering Sea Water layer is isolated from the surface through stratification and does not impact surface Mn concentrations in the Canada Basin (Colombo et al., 2020).

In order to assess whether we overestimated the sediment content of sea ice, we performed an experiment with “clean” sea ice. In the “clean” ice experiment, the surface Mn concentrations are underestimated by 4 nmol L^{-1} relative to observations (Fig. 7a). If we assume that all of the missing Mn comes from sediment and that Mn added at the surface mixes down to the turbocline, we miss a source that supplies 13-213 grams of sediment per squared meter to the surface ocean across the Canada Basin (range based on model turbocline depths in 2015). The magnitude of this component is similar to the average sediment load measured in sea ice cores (Reimnitz et al., 1993; Stierle & Eicken, 2002; Eicken et al., 2005). Rivers would be unable to contribute the total amount missing since it must occur over a large area and since the upper bound river experiment shows that additional contributions from rivers do not significantly affect the Canada Basin or the overall surface representation (Fig. 7b, Table 2). In the “clean” sea ice experiment, the freshwater endmember of Mn is also underestimated (Fig. S13). The modelled Mn-salinity relationship is most similar to observations in the experiment with sediment contained in sea ice and is comparable with other central Arctic Ocean observations (Middag

et al., 2011b). The reference experiment also better reproduces regional differences in the Mn-salinity relationship between the Canada Basin and the CAA.

Our results demonstrate that the long range transport of sediments by sea ice from the Siberian shelves is an important source of Mn in the Canada Basin and the Canadian Arctic Archipelago. These findings provide support for the sea ice trace metal transport mechanism proposed by Measures (1999). Measures (1999) found that the highest Al and Fe concentrations in the central Arctic Ocean coincided with areas with high concentrations of ice-rafted sediments, instead of river input, and so they hypothesized that transport of ice rafted sediments and the subsequent seasonal melt supplies reactive elements to the surface Arctic Ocean. However, their data set did not allow the quantification of annual fluxes of material to the central Arctic Ocean and so they were unable to quantify the exact contribution of this component to the observed trace metal concentrations.

4.2 Declining Long Range Sea Ice Transport Could Reduce the Canada Basin and Canadian Arctic Archipelago Nutrient Supply

Based on the importance of non-local sediments transported by sea ice (particularly from the Siberian shelves), the distributions of trace metals, nutrients, and their biogeochemical cycles in the Arctic basins are likely to be significantly impacted by climate change associated reductions in sea ice. Rising oceanic and atmospheric temperatures delay the freeze-up period and induce earlier melt of sea ice (Stroeve et al., 2012; Stroeve & Notz, 2018). In addition, in the relatively “quiet” dynamics of the Arctic Ocean, increased mixing may bring warmer Atlantic water (or Pacific Water; Kodaira et al., 2020) to the surface and further increase sea ice melt (D’Asaro & Morison, 1992; Liang & Losch, 2018). These factors may significantly reduce the amount of first-year ice that survives in the Kara Sea, East Siberian sea, and western Laptev Sea (Krumpal et al., 2019).

Studies of the transpolar ice drift indicate an increase in drift speed associated with a thinning ice cover and as a result, an increase in exchange of ice-rafted material between regions (Spren et al., 2011; Kwok et al., 2013; Newton et al., 2017; Kipp et al., 2018). However, in recent years, summer ice extents have been small enough in the marginal ice zones, that most of the ice exported from shelves melts before it enters the transpo-

lar drift (Krumpen et al., 2019). These findings suggest a reduction in the transport of matter towards the central Arctic Ocean and Fram Strait by the transpolar ice drift.

In our study, we saw a steady increase in the Mn content of the Canada Basin polar mixed layer from 2002-2019 (Fig. 10), and the primary source of this Mn is sea ice melt (correlation R-squared of 0.97). Note that our experiments do not account for interannual changes in sea ice supply regions. The addition of Mn by melt in our model mirrors satellite observations of sea ice loss in the Beaufort Sea (Fig. 10; correlation R-squared of 0.54). Whereas in the short term, there may be an increase in nutrients supplied by sea ice into the Canada Basin through increased sea ice exchange and melt volume, in the long run, we expect a decrease in supply of sediment rich sea ice from the Siberian shelves via the transpolar drift and a subsequent decline in the surface maximum of Mn in the Canada Basin. Confounding this is the likely increase in transport of riverine and shelf-derived trace elements in the ocean by the transpolar drift as a result of an intensification of the Arctic hydrological cycle and permafrost degradation (Charette et al., 2020).

A reduction in micronutrient supply to the Canada Basin may also have an impact downstream in Baffin Bay. With our experiments, we calculated the transport of Mn through Parry Channel and the contribution of sediment released by sea ice melt to this transport (see Text S4 for details). About 87% of the net Mn transported into Parry Channel from the Canada Basin is contributed by sediments from sea ice and the rest is associated with other sources such as resuspension and runoff (Fig. S17 and S18). Sea ice contributes around 34% of net Mn transported from Parry Channel into Baffin Bay. The reduction in the contribution of these components does not indicate loss in the CAA; it reflects the additional contributions from other sources (mainly sediment resuspension) in the CAA. The sea ice contribution in the water column is significant downstream. However, it is important to note that the sea ice transport in the CAA in the ocean-ice model is stronger than observed due to the lack of a land-fast ice parameterization (Grivault et al., 2018). As a result, we may overestimate the sea ice transport and thus melt in Parry Channel, particularly for the outflow from Parry Channel into Baffin Bay. There are also further factors contributing Mn within the CAA which confound this finding. The acceleration of the hydrological cycle and permafrost thaw may increase the contributions of riverine Mn to the CAA; our experiments do not take these changes into account. On the other hand, sea ice melt is associated with an increase in stratification

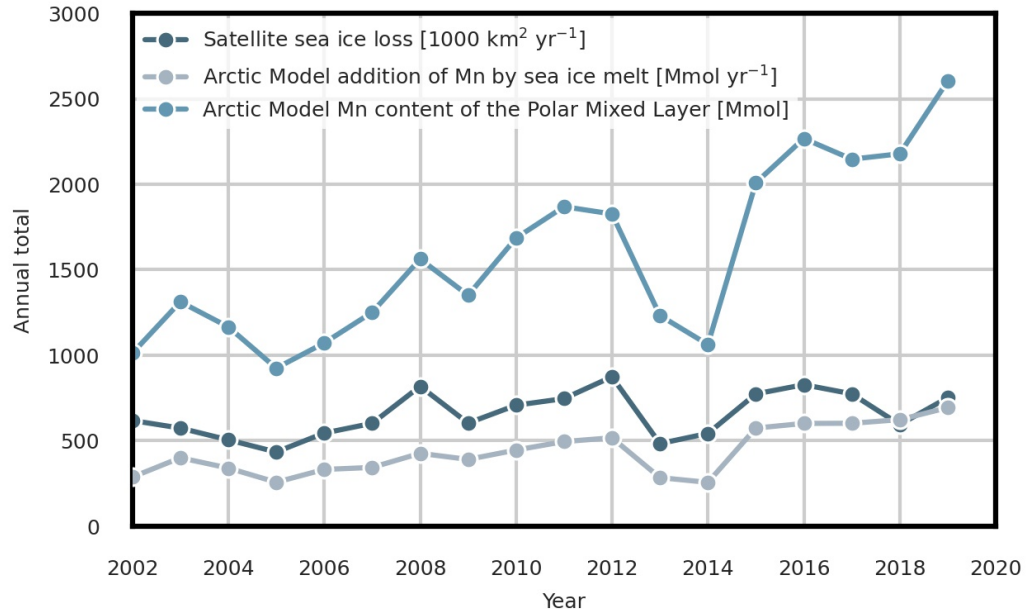


Figure 10. Interannual variations in sea ice melt contribute strongly to Mn supply to the Canada Basin. Conversely, surface Mn concentration changes in the Canada Basin are an indicator of the volume of sediments released by sea ice melt. Sea ice loss is calculated from regional monthly sea ice area changes in the Beaufort Sea measured by the Defense Meteorological Satellite Program series of passive microwave remote sensing instruments (Fetterer et al., 2017). The regional Mn model presented in this study is used to calculate Mn added by sea ice melt and the total Mn content of the Canada Basin.

which may reduce the depth up to which resuspended sediment can mix, reducing the Mn supplied into the upper water column (and productive areas) by sediment resuspension in the CAA. However, reduced sea ice cover is also associated with increased wind-driven mixing.

Our findings for Mn in the Arctic have implications for nutrients which share similar sources. In the Arctic Ocean, iron (Fe) behaves similarly to Mn, although Fe is less soluble than Mn and oxidizes more rapidly (Landing & Bruland, 1987; Colombo et al., 2020; Jensen et al., 2020, for a comprehensive discussion). Fe is an essential micronutrient and it limits primary productivity in some regions of the ocean, such as the Southern Ocean, parts of the North Atlantic, and the Pacific Northwest (J. H. Martin & Gordon, 1988; Hawkings et al., 2014; Tagliabue et al., 2017). Generally, iron is not growth limiting in the Arctic (S. Wang et al., 2014), but there is evidence that Fe is limited in specific regions: on the outer shelf and shelf break in the Bering Sea (Aguilar-Islas et al., 2008), as well as in the Barents Sea and Nansen Basin (Rijkenberg et al., 2018). Past studies have indicated that sea ice contributes to the flux of Fe into the ocean (Measures, 1999; Lannuzel et al., 2007; Aguilar-Islas et al., 2008; Kanna et al., 2020). Based on the expected changes to the Mn cycle and supply with sea ice melt over the next decades, the supply of Fe to the Canada Basin may be reduced as well. Meanwhile, the increase in simulated Mn content in the Canada Basin from 2002-2019 due to sea ice melt may also have supplied micronutrients such as Fe and have driven some of the observed increased Arctic Ocean primary production (Lewis et al., 2020). Changes to Fe availability impact the community composition and the timing of the spring phytoplankton bloom (Aguilar-Islas et al., 2008), which in turn has consequences for biological productivity, Arctic ecosystems, and the carbon cycle.

4.3 Limitations of Results

4.3.1 Mn model evaluation

The upper 100 m of the water column are most important to the key findings of this study. In this zone, the Mn representation is impacted by local sources, photo-enhanced reduction, and the physical model's salinity representation and associated mixing. Below, we discuss differences between the model and observations and identify the impacts on our findings.

In the CAA, the model underestimates Mn in the subsurface (upper 50 m) resulting in a strong vertical gradient of Mn, particularly in the central sills region. The physical model represents salinity well within the CAA, however the upper 20 m are slightly too fresh, possibly because of an overestimate in the freshwater transport due to too-mobile sea ice without a land-fast sea ice parameterization (Grivault et al., 2018). Despite this, the Mn-salinity relationship matches observations closely in the reference experiment (Fig. S13a). Increased photo-enhanced reduction could increase subsurface Mn. However, trials with a non-linear coupling between light penetration and sea ice concentration did not significantly affect the subsurface Mn concentrations. Further, while Mn oxides (oMn) are only modelled for their impact on dMn, oMn concentrations are fairly well-represented within the upper water column in the CAA (Fig. S12). Remineralization of Mn taken up by phytoplankton may also counteract some of the subsurface underestimation. However, we estimated that uptake and remineralization altered dissolved Mn profiles by only up to 0.3 nM (Fig. S19 and Text S3). Hence, we suggest that the subsurface Mn underestimation is most likely caused by improper distribution of materials in the upper water column from weaker mixing. Replicating the effect of stronger mixing by redistributing the Mn, the average Mn concentrations are underestimated by 1 nM in the upper 50 m, while in the subsurface alone they are underestimated by 3 nM. A similar argument can be made for the near-bottom overestimation of Mn at CAA9; a region known to have strong tidal mixing. If we redistribute the Mn throughout the water column, the modelled concentration is overestimated by 2 nM, compared to 5 nM for the lower water column alone.

In the Canada Basin, the physical model captures the depth of isohalines reasonably well, however the amount of freshwater in the upper water column is underestimated (Hu et al., 2019). This underestimation may be due to a lower freshwater state in the initial conditions derived from the GLORYS2v3 product, but can more likely be attributed to overestimated sea ice concentration and thickness (and underestimated melt in the model). Despite this, the model represents the overall circulation and characteristics of the Canada Basin. For Mn, this shortcoming complicates the evaluation of the Mn-salinity relationship in the Canada Basin (Fig. S13) and instead, we focused our evaluation on Mn with depth (Fig. 5). The underestimation of sea ice melt does not change the actual component contributions estimated by the Mn model: the net effect of the sea ice component is a combination of ice melt and sediment content. An increase in ice melt would

be counterbalanced by a decrease in sediment richness. The exact spatial variability and content of sediment in sea ice of the forcing field is a rough first order estimate, nevertheless it is able to provide us with an estimate of the magnitude of the sediment in sea ice component.

4.3.2 *Parameterizations*

The findings in this study are limited by the parameterizations for scavenging, sediment in sea ice, sediment resuspension, and river runoff. Overall, the model is best constrained for summer months, the southern CAA, and the Canada Basin due to the availability of observations. Scavenging rates are important throughout the water column and are most likely to affect our results in coastal regions. We assumed steady state to estimate the adsorption and desorption rates from observations; this assumption is least likely to hold in coastal regions and near the surface where scavenging rates are both important and variable. The oxidation rate was derived from observations specific to the Arctic Ocean environment and is faster than the rate used in Van Hulst et al. (2017). The comparison of the modelled and observed oMn profiles (Fig. S12) suggests that the scavenging rates used in this study are representative. However, the scavenging rates are expected to vary spatially and vertically due to variations in Mn oxidizing microbial communities and environmental conditions. No data are currently available to represent these effects. For the sediment released by sea ice, we did not account for variations in transport of sediment (and its origin) across the Arctic Ocean over the course of the time series. Sea ice drift patterns vary interannually, and so could the source regions for sediment transported to the Canada Basin by sea ice. The sediment content would more accurately be represented as a time dependent variable. The total Mn content in the Canada Basin would increase (decrease) with a higher (lower) sediment content in sea ice, while sediment in sea ice would be more (less) important overall. However, observed sediment sea ice loads range several orders of magnitude by location sampled and properties of the ice, and these fluctuations make it challenging to quantify annual changes in overall sediment content and path travelled. Similarly, sediment resuspension varies interannually and seasonally and may be better represented as a time dependent variable.

We do not take into account the contributions from breaking of internal waves, storm generated currents, and surface waves on sediment resuspension and coastal erosion. As a result, we likely underestimate sediment resuspension contributions in some areas, par-

ticularly during the summer ice-free period. Our treatment of rivers was simplistic and did not account for the complexity of transformations that occur in the estuarine zone. Our results indicate a lower and upper bound of the river contributions, however we are unable to indicate what the actual contribution is. The upper bound river experiment also indicates the effect of higher characteristic riverine Mn concentrations, such as if we had used Eurasian river Mn content within our domain instead of river observations from the CAA. We did not account for the projected seasonal ranges in riverine Mn concentrations with discharge (Colombo et al., 2019); the river discharge varies seasonally, but we hold the characteristic Mn concentrations of the rivers constant. This approximation could underestimate the riverine contributions during the spring freshet in coastal areas and is most likely to impact the northern CAA and Greenland coast, where glacial rivers are most important. Recent work has suggested ligand stabilization of riverine dissolved Fe in the Arctic Ocean, increasing its extent of influence (Charette et al., 2020). However, the cycling of dMn in the Arctic Ocean is largely shaped by its redox cycling instead of organic ligand complexation (Colombo et al., 2020; Jensen et al., 2020).

While the numbers presented here should be taken as an estimate of magnitude rather than as exact values, the key results are robust to the uncertainties described above. The only way we were able to close the Mn budget (particularly in the Canada Basin) was by incorporating the sediment in sea ice component. Similarly, the only way to represent the higher concentrations of Mn found in the lower water column at some stations in the CAA was through the sediment resuspension term. While the Mn model presented here is limited in its representation of these processes, it provides a platform to ask questions about the drivers of Mn variability and to perform larger scale estimates of the processes that contribute Mn to the Arctic Ocean. Satellite-based estimates of the distribution and quantity of sediment-laden sea ice such as explored in Waga et al. (2022) could strengthen future predictions. The Mn model accuracy would be improved by more comprehensive estimates of the scavenging and sediment resuspension rates. Observations of Mn along a transect from an estuary into the ocean would help constrain the riverine contributions.

5 Conclusions

New trace metal datasets collected in the Arctic Ocean as part of the Canadian GEO-TRACES program have provided an essential base for studying biogeochemical cycling

in this unique region. Using in situ observations from Colombo et al. (2020), we developed the first model of Mn in the Canadian Arctic Archipelago and the Canada Basin. With three model experiments using the reference period 2002-2019, we looked at (1) the drivers of Mn distributions in the CAA and the Canada Basin and (2) implications of future sea ice transport changes on the biogeochemical cycles of nutrients in the Arctic Ocean.

(1) While sediment transport by sea ice is identified as important in the Arctic Ocean (Measures, 1999; Eicken et al., 2005), this mechanism is commonly considered less significant for Mn than riverine input. However, without the contribution from sediment in sea ice to Mn, we were unable to accurately represent the Mn concentrations in the Canada Basin with our model. Sediments transported in sea ice by the transpolar drift account for up to 93% of the total annual Mn added in the Canada Basin and up to 37% in the CAA, driving Mn surface maxima. These results support the hypothesis that “ice-rafted sediment may be an important transport mechanism for supplying reactive trace elements,” proposed by Measures (1999). Rivers are certainly locally important, but contribute only 2.2-8.5% annually in the Canada Basin. Within the CAA, our estimates for river contributions ranged from 5.0% up to 34% in the upper bound river experiment. This broad range is the result of the limited information available regarding estuarine cycling in the Arctic. A clear divide is present in the CAA: west of Barrow Sill, the mean concentrations are lower and the behaviour of Mn is more similar to the Canada Basin, while in the eastern CAA, sediments resuspended by high tidal speeds, as well as many glacial rivers drive higher Mn concentrations.

(2) Sea ice transport via the transpolar drift is interrupted by Arctic warming (Krumpen et al., 2019) and the decline in this long range transport could reduce the Canada Basin and the CAA nutrient supply. These changes not only impact the Arctic, but also sub-arctic seas, with up to 34% of the Mn transported from Parry Channel into Baffin Bay added by sea ice melt. Mn behaves similarly to Fe in the Arctic Ocean and both of these micronutrients support phytoplankton growth. The importance of sea ice for nutrient supply to the photic zone in the Canada Basin, as well as downstream, is concerning given the recent changes in the Arctic Ocean sea ice regime (reduced summer minimum ice extent, ice thinning, reduction in multi-year ice extent, and altered drift paths). There are many competing factors that will contribute to changes in the biogeochemical cycles; com-

977 bined model-observation studies are highly valuable to understand the individual con-
 978 tribution of these factors.

979 Acronyms

980 **CAA** Canadian Arctic Archipelago

981 **NEMO** Nucleus for European Modelling of the Ocean

982 **ANHA12** Arctic and Northern Hemispheric Atlantic 1/12 degree

983 **LIM2** Louvain-la-Neuve version 2

984 **TOP** Tracers in the Ocean Paradigm

985 **TVD** Total Variance Dissipation scheme

986 **CESM** Community Earth System Model

987 **CAM-Chem** Community Atmosphere Model with Chemistry

988 Acknowledgments

989 We thank Marco van Hulten for openly sharing his model code and results, Jacqui-Lee
 990 Epstein for extracting the tidal speeds for the sediment resuspension parameterization,
 991 Nadja Steiner and Hakase Hayashida for sharing CanOE model results, and Genevieve
 992 Parton for helpful discussions regarding sediment resuspension. We'd also like to thank
 993 the two reviewers for their helpful comments. This work was funded by the Natural Sci-
 994 ences and Engineering Council (NSERC) Climate Change and Atmospheric Research Grant:
 995 GEOTRACES (RGPCC 433848-12) and VITALS (RGPCC 433898), an NSERC Discov-
 996 ery Grant (RGPIN-2016-03865) to SEA, and by the University of British Columbia through
 997 a four year fellowship to BR. Computing resources were provided by Compute Canada
 998 (RRG 2648 RAC 2019, RRG 2969 RAC 2020, RRG 1541 RAC 2021). The model con-
 999 figuration, code, results, and analysis code are archived on FRDR at
 1000 <https://doi.org/10.20383/102.0388>. Analysis code is also available via Github at
 1001 <https://github.com/brogalla/Mn-sea-ice-paper>.

1002 References

1003 Aguilar-Islas, A. M., Rember, R. D., Mordy, C. W., & Wu, J. (2008). Sea
 1004 ice-derived dissolved iron and its potential influence on the spring algal
 1005 bloom in the Bering Sea. *Geophysical Research Letters*, 35(24). doi:

1006 10.1029/2008GL035736

1007 Bacon, S., Marshall, A., Holliday, N. P., Aksenov, Y., & Dye, S. R. (2014). Seasonal
1008 variability of the East Greenland Coastal Current. *Journal of Geophysical Re-*
1009 *search: Oceans*, 119(6), 3967-3987. doi: 10.1002/2013JC009279

1010 Balzer, W. (1982). On the distribution of iron and manganese at the sediment/water
1011 interface: Thermodynamic versus kinetic control. *Geochimica et Cosmochimica*
1012 *Acta*, 46(7), 1153-1161. doi: 10.1016/0016-7037(82)90001-1

1013 Bamber, J., Van Den Broeke, M., Ettema, J., Lenaerts, J., & Rignot, E. (2012).
1014 Recent large increases in freshwater fluxes from Greenland into the North
1015 Atlantic. *Geophysical Research Letters*, 39(19). doi: 10.1029/2012GL052552

1016 Bhatia, M. P., Waterman, S., Burgess, D. O., Williams, P. L., Bundy, R. M., Mel-
1017 lett, T., ... Bertrand, E. M. (2021). Glaciers and Nutrients in the Cana-
1018 dian Arctic Archipelago Marine System. *Global Biogeochemical Cycles*, 35,
1019 e2021GB006976. doi: 10.1029/2021GB006976

1020 Bouillon, S., Morales Maqueda, M. A., Legat, V., & Fichefet, T. (2009). An elastic-
1021 viscous-plastic sea ice model formulated on Arakawa B and C grids. *Ocean*
1022 *Modelling*, 27(3-4), 174-184. doi: 10.1016/j.ocemod.2009.01.004

1023 Brand, L. E., Sunda, W. G., & Guillard, R. R. L. (1983). Limitation of marine
1024 phytoplankton reproductive rates by zinc, manganese, and iron. *Limnology and*
1025 *Oceanography*, 28(6), 1182-1198. doi: 10.4319/lo.1983.28.6.1182

1026 Brown, K. A., Williams, W. J., Carmack, E. C., Fiske, G., François, R., McLennan,
1027 D., & Peucker-Ehrenbrink, B. (2020). Geochemistry of small Canadian Arctic
1028 rivers with diverse geological and hydrological settings. *Journal of Geophysical*
1029 *Research: Biogeosciences*, 125(1). doi: 10.1029/2019JG005414

1030 Bruland, K. W., Donat, J. R., & Hutchins, D. A. (1991). Interactive influences
1031 of bioactive trace metals on biological production in oceanic waters. *Limnology*
1032 *and Oceanography*, 36(8), 1555-1577. doi: 10.4319/lo.1991.36.8.1555

1033 Bruland, K. W., Orians, K. J., & Cowen, J. P. (1994). Reactive trace metals in
1034 the stratified central North Pacific. *Geochimica et Cosmochimica Acta*, 58(15),
1035 3171-3182. doi: 10.1016/0016-7037(94)90044-2

1036 Campbell, J. A., & Yeats, P. A. (1982). The distribution of manganese, iron, nickel,
1037 copper and cadmium in the waters of Baffin Bay and the Canadian Arctic
1038 Archipelago. *Oceanologica Acta*, 5(2), 161-168.

- 1039 Carrère, L., & Lyard, F. (2003). Modeling the barotropic response of the global
1040 ocean to atmospheric wind and pressure forcing-comparisons with observa-
1041 tions. *Geophysical Research Letters*, 30(6). doi: 10.1029/2002GL016473
- 1042 Charette, M. A., Kipp, L. E., Jensen, L. T., Dabrowski, J. S., Whitmore, L. M.,
1043 Fitzsimmons, J. N., ... others (2020). The Transpolar Drift as a source of
1044 riverine and shelf-derived trace elements to the central Arctic Ocean. *Journal*
1045 *of Geophysical Research: Oceans*, 125(5). doi: 10.1029/2019jc015920
- 1046 Charette, M. A., Lam, P. J., Lohan, M. C., Kwon, E. Y., Hatje, V., Jeandel, C.,
1047 ... Garcia-Orellana, J. (2016). Coastal ocean and shelf-sea biogeochemical
1048 cycling of trace elements and isotopes: lessons learned from GEOTRACES.
1049 *Philosophical Transactions of the Royal Society A: Mathematical, Physical and*
1050 *Engineering Sciences*, 374(2081), 20160076. doi: 10.1098/rsta.2016.0076
- 1051 Chelton, D. B., de Szoeke, R. A., Schlax, M. G., El Naggar, K., & Siwertz, N.
1052 (1998). Geographical variability of the first baroclinic Rossby radius of
1053 deformation. *Journal of Physical Oceanography*, 28(3), 433-460. doi:
1054 10.1175/1520-0485(1998)028%3C0433:GVOTFB%3E2.0.CO;2
- 1055 Cid, A. P., Nakatsuka, S., & Sohrin, Y. (2012). Stoichiometry among bioactive trace
1056 metals in the Chukchi and Beaufort Seas. *Journal of Oceanography*, 68(6),
1057 985-1001. doi: 10.1007/s10872-012-0150-8
- 1058 Colombo, M., Brown, K. A., De Vera, J., Bergquist, B. A., & Orians, K. J. (2019).
1059 Trace metal geochemistry of remote rivers in the Canadian Arctic Archipelago.
1060 *Chemical Geology*, 525, 479-491. doi: 10.1016/j.chemgeo.2019.08.006
- 1061 Colombo, M., Jackson, S. L., Cullen, J. T., & Orians, K. J. (2020). Dissolved iron
1062 and manganese in the Canadian Arctic Ocean: on the biogeochemical pro-
1063 cesses controlling their distributions. *Geochimica et Cosmochimica Acta*, 277,
1064 150-174. doi: 10.1016/j.gca.2020.03.012
- 1065 Colombo, M., Li, J., Rogalla, B., Allen, S. E., & Maldonado, M. T. (2022). Par-
1066 ticulate trace element distributions along the Canadian Arctic GEOTRACES
1067 section: shelf-water interactions, advective transport and contrasting biological
1068 production. *Geochimica et Cosmochimica Acta*, 323, 183-201.
- 1069 Colombo, M., Rogalla, B., Li, J., Allen, S. E., Orians, K. J., & Maldonado, M. T.
1070 (2021). Canadian Arctic Archipelago Shelf-Ocean Interactions: A Major Iron
1071 Source to Pacific Derived Waters Transiting to the Atlantic. *Global Biogeo-*

- 1072 *chemical Cycles*, 35(10), e2021GB007058. doi: 10.1029/2021GB007058
- 1073 Dai, A., Qian, T., Trenberth, K. E., & Milliman, J. D. (2009). Changes in continen-
1074 tal freshwater discharge from 1948 to 2004. *Journal of Climate*, 22(10), 2773-
1075 2792. doi: 10.1175/2008JCLI2592.1
- 1076 Damm, E., Bauch, D., Krumpen, T., Rabe, B., Korhonen, M., Vinogradova, E., &
1077 Uhlig, C. (2018). The Transpolar Drift conveys methane from the Siberian
1078 Shelf to the central Arctic Ocean. *Scientific Reports*, 8(1), 1-10. doi:
1079 10.1038/s41598-018-22801-z
- 1080 Darby, D. A. (2003). Sources of sediment found in sea ice from the western Arctic
1081 Ocean, new insights into processes of entrainment and drift patterns. *Journal*
1082 *of Geophysical Research: Oceans*, 108(C8). doi: 10.1029/2002JC001350
- 1083 Darby, D. A., Myers, W. B., Jakobsson, M., & Rigor, I. (2011). Modern dirty sea ice
1084 characteristics and sources: The role of anchor ice. *Journal of Geophysical Re-*
1085 *search: Oceans*, 116(9). doi: 10.1029/2010JC006675
- 1086 D'Asaro, E. A., & Morison, J. H. (1992). Internal waves and mixing in the Arc-
1087 tic Ocean. *Deep Sea Research Part I: Oceanographic Research Papers*, 39(2),
1088 S459-S484. doi: 10.1016/S0198-0149(06)80016-6
- 1089 Dethleff, D., & Kuhlmann, G. (2009). Entrainment of fine-grained surface deposits
1090 into new ice in the southwestern Kara Sea, Siberian Arctic. *Continental Shelf*
1091 *Research*, 29(4), 691-701. doi: 10.1016/j.csr.2008.11.009
- 1092 Dethleff, D., & Kuhlmann, G. (2010). Fram Strait sea-ice sediment provinces based
1093 on silt and clay compositions identify Siberian Kara and Laptev seas as main
1094 source regions. *Polar Science*, 29(3). doi: 10.3402/polar.v29i3.6070
- 1095 Dethleff, D., Rachold, V., Tintelnot, M., & Antonow, M. (2000). Sea-ice transport
1096 of riverine particles from the Laptev Sea to Fram Strait based on clay min-
1097 eral studies. *International Journal of Earth Sciences*, 89(3), 496-502. doi:
1098 10.1007/s005310000109
- 1099 Domena, V. (2017). *Trace metals in Arctic fast ice* (Master's thesis, Univer-
1100 sity of Alaska Fairbanks). Retrieved from [https://www.proquest.com/](https://www.proquest.com/dissertations-theses/trace-metals-arctic-fast-ice/docview/1990622990/se-2?accountid=14656)
1101 [dissertations-theses/trace-metals-arctic-fast-ice/docview/](https://www.proquest.com/dissertations-theses/trace-metals-arctic-fast-ice/docview/1990622990/se-2?accountid=14656)
1102 [1990622990/se-2?accountid=14656](https://www.proquest.com/dissertations-theses/trace-metals-arctic-fast-ice/docview/1990622990/se-2?accountid=14656)
- 1103 Drinkwater, K. F., & Harding, G. C. (2001). Effects of the Hudson Strait outflow on
1104 the biology of the Labrador Shelf. *Canadian Journal of Fisheries and Aquatic*

- 1105 *Sciences*, 58(1), 171-184. doi: 10.1139/f00-210
- 1106 Eicken, H., Gradinger, R., Gaylord, A., Mahoney, A., Rigor, I., & Melling, H.
- 1107 (2005). Sediment transport by sea ice in the Chukchi and Beaufort Seas:
- 1108 Increasing importance due to changing ice conditions? *Deep Sea Re-*
- 1109 *search Part II: Topical Studies in Oceanography*, 52, 3281-3302. doi:
- 1110 10.1016/j.dsr2.2005.10.006
- 1111 Eicken, H., Kolatschek, J., Freitag, J., Lindemann, F., Kassens, H., & Dmitrenko,
- 1112 I. (2000). A key source area and constraints on entrainment for basin-scale
- 1113 sediment transport by Arctic sea ice. *Geophysical Research Letters*, 27(13),
- 1114 1919-1922. doi: 10.1029/1999GL011132
- 1115 Eicken, H., Reimnitz, E., Alexandrov, V., Martin, T., Kassens, H., & Viehoff,
- 1116 T. (1997). Sea-ice processes in the Laptev Sea and their importance
- 1117 for sediment export. *Continental Shelf Research*, 17(2), 205-233. doi:
- 1118 10.1016/S0278-4343(96)00024-6
- 1119 Epstein, J.-L. (2018). *The impact of internal tide mixing parameterizations in*
- 1120 *an eddy-permitting model of the Arctic Ocean* (Master's thesis, University of
- 1121 British Columbia). doi: 10.14288/1.0365809
- 1122 Evans, L. K., & Nishioka, J. (2018). Quantitative analysis of Fe, Mn and Cd from
- 1123 sea ice and seawater in the Chukchi Sea, Arctic Ocean. *Polar Science*, 17, 50-
- 1124 58. doi: 10.1016/j.polar.2018.07.002
- 1125 Fetterer, F., Knowles, K., Meier, W. N., Savoie, M., & Windnagel, A. K. (2017).
- 1126 Updated daily: Sea ice index, version 3. Boulder, Colorado USA. *NSIDC:*
- 1127 *National Snow and Ice Data Center*. doi: 10.7265/N5K072F8
- 1128 Fichefet, T., & Maqueda, M. A. M. (1997). Sensitivity of a global sea ice model
- 1129 to the treatment of ice thermodynamics and dynamics. *Journal of Geophysical*
- 1130 *Research: Oceans*, 102(C6), 12609-12646. doi: 10.1029/97JC00480
- 1131 Fichot, C. G., Kaiser, K., Hooker, S. B., Amon, R. M., Babin, M., Bélanger, S., ...
- 1132 Benner, R. (2013). Pan-Arctic distributions of continental runoff in the Arctic
- 1133 Ocean. *Scientific Reports*, 3(1), 1-6. doi: 10.1038/srep01053
- 1134 Fishwick, M. P., Ussher, S. J., Sedwick, P. N., Lohan, M. C., Worsfold, P. J.,
- 1135 Buck, K. N., & Church, T. M. (2018). Impact of surface ocean con-
- 1136 ditions and aerosol provenance on the dissolution of aerosol manganese,
- 1137 cobalt, nickel and lead in seawater. *Marine Chemistry*, 198, 28-43. doi:

1138 10.1016/J.MARCHEM.2017.11.003

1139 Gent, P. R., Willebrand, J., McDougall, T. J., & McWilliams, J. C. (1995). Param-
 1140 eterizing eddy-induced tracer transport in ocean circulation models. *Journal*
 1141 *of Physical Oceanography*, 25(4), 463-474. doi: 10.1175/1520-0485(1995)025%
 1142 3C0463:PEITTI%3E2.0.CO;2

1143 GEOTRACES Intermediate Data Product Group. (2021). The GEOTRACES Inter-
 1144 mediate Data Product 2021 (IDP2021) [Dataset].
 1145 doi: 10.5285/cf2d9ba9-d51d-3b7c-e053-8486abc0f5fd

1146 Granskog, M. A., Kaartokallio, H., & Shirasawa, K. (2003). Nutrient status of
 1147 Baltic Sea ice: Evidence for control by snow-ice formation, ice permeabil-
 1148 ity, and ice algae. *Journal of Geophysical Research: Oceans*, 108(C8). doi:
 1149 10.1029/2002jc001386

1150 Greene, C. H., & Pershing, A. J. (2007). Climate drives sea change. *Science*,
 1151 315(5815), 1084-1085. doi: 10.1126/science.1136495

1152 Grivault, N., Hu, X., & Myers, P. G. (2018). Impact of the surface stress on the
 1153 volume and freshwater transport through the Canadian Arctic Archipelago
 1154 from a high-resolution numerical simulation. *Journal of Geophysical Research:*
 1155 *Oceans*, 123(12), 9038-9060. doi: 10.1029/2018JC013984

1156 Guay, C. K. H., McLaughlin, F. A., & Yamamoto-Kawai, M. (2009). Differen-
 1157 tiating fluvial components of upper Canada Basin waters on the basis of
 1158 measurements of dissolved barium combined with other physical and chem-
 1159 ical tracers. *Journal of Geophysical Research: Oceans*, 114(C1). doi:
 1160 10.1029/2008JC005099

1161 Hawkings, J. R., Wadham, J. L., Tranter, M., Raiswell, R., Benning, L. G.,
 1162 Statham, P. J., ... Telling, J. (2014). Ice sheets as a significant source of
 1163 highly reactive nanoparticulate iron to the oceans. *Nature Communications*,
 1164 5(1), 1-8. doi: 10.1038/ncomms4929

1165 Hayashida, H., Christian, J. R., Holdsworth, A. M., Hu, X., Monahan, A. H.,
 1166 Mortenson, E., ... Steiner, N. S. (2019). CSIB v1 (Canadian Sea-ice Biogeo-
 1167 chemistry): a sea-ice biogeochemical model for the NEMO community ocean
 1168 modelling framework. *Geoscientific Model Development*, 12(5), 1965-1990. doi:
 1169 10.5194/gmd-12-1965-2019

- 1170 Hölemann, J., Wegener, A., & Schirmacher, M. (1999). Dissolved and particulate
1171 major and trace elements in newly formed ice from the Laptev Sea (Transdrift
1172 III, October 1995). In *Land-ocean systems in the Siberian Arctic* (p. 101-111).
1173 Springer Berlin Heidelberg. doi: 10.1007/978-3-642-60134-7_11
- 1174 Holland, M. M., Bailey, D. A., Briegleb, B. P., Light, B., & Hunke, E. (2012). Im-
1175 proved sea ice shortwave radiation physics in CCSM4: The impact of melt
1176 ponds and aerosols on Arctic sea ice. *Journal of Climate*, 25(5), 1413-1430.
1177 doi: 10.1175/JCLI-D-11-00078.1
- 1178 Hu, X., Myers, P. G., & Lu, Y. (2019). Pacific water pathway in the Arctic
1179 Ocean and Beaufort Gyre in two simulations with different horizontal reso-
1180 lutions. *Journal of Geophysical Research: Oceans*, 124(8), 6414-6432. doi:
1181 10.1029/2019JC015111
- 1182 Hu, X., Sun, J., Chan, T. O., & Myers, P. G. (2018). Thermodynamic and dy-
1183 namic ice thickness contributions in the Canadian Arctic Archipelago in
1184 NEMO-LIM2 numerical simulations. *The Cryosphere*, 12, 1233-1247. doi:
1185 10.5194/tc-12-1233-2018
- 1186 Hughes, K. G., Klymak, J. M., Hu, X., & Myers, P. G. (2017). Water mass
1187 modification and mixing rates in a 1/12 simulation of the Canadian Arctic
1188 Archipelago. *Journal of Geophysical Research: Oceans*, 122, 803-820. doi:
1189 10.1002/2016JC012235
- 1190 Hughes, K. G., Klymak, J. M., Williams, W. J., & Melling, H. (2018). Tidally mod-
1191 ulated internal hydraulic flow and energetics in the central Canadian Arctic
1192 Archipelago. *Journal of Geophysical Research: Oceans*, 123(8), 5210-5229. doi:
1193 10.1029/2018JC013770
- 1194 Hunter, J. D. (2007). Matplotlib: A 2D graphics environment. *Computing in science
1195 & engineering*, 9(3), 90-95.
- 1196 Jakobsson, M. (2002). Hypsometry and volume of the Arctic Ocean and its con-
1197 stituent seas. *Geochemistry, Geophysics, Geosystems*, 3(5), 1-18. doi: 10.1029/
1198 2001GC000302
- 1199 Jensen, L. T., Morton, P., Twining, B. S., Heller, M. I., Hattala, M., Measures, C. I.,
1200 ... Fitzsimmons, J. N. (2020). A comparison of marine Fe and Mn cycling:
1201 U.S. GEOTRACES GN01 Western Arctic case study. *Geochimica et Cos-
1202 mochimica Acta*. doi: 10.1016/j.gca.2020.08.006

- 1203 Johnson, K. S., Coale, K. H., Berelson, W. M., & Michael Gordon, R. (1996). On
1204 the formation of the manganese maximum in the oxygen minimum. *Geochim-*
1205 *ica et Cosmochimica Acta*, 60(8), 1291-1299. doi: 10.1016/0016-7037(96)00005
1206 -1
- 1207 Kanna, N., Lannuzel, D., van der Merwe, P., & Nishioka, J. (2020). Size frac-
1208 tionation and bioavailability of iron released from melting sea ice in a
1209 subpolar marginal sea. *Marine Chemistry*, 221, 103774. doi: 10.1016/
1210 j.marchem.2020.103774
- 1211 Kay, J. E., Deser, C., Phillips, A., Mai, A., Hannay, C., Strand, G., ... Vertenstein,
1212 M. (2015). The community earth system model (CESM) large ensemble
1213 project : A community resource for studying climate change in the presence of
1214 internal climate variability. *Bulletin of the American Meteorological Society*,
1215 96(8), 1333-1349. doi: 10.1175/BAMS-D-13-00255.1
- 1216 Kelly, S. J., Proshutinsky, A., Popova, E. K., Aksenov, Y. K., & Yool, A. (2019). On
1217 the origin of water masses in the Beaufort Gyre. *Journal of Geophysical Re-*
1218 *search: Oceans*, 124(7), 4696-4709. doi: 10.1029/2019JC015022
- 1219 Kempema, E. W., Reimnitz, E., & Barnes, P. (1989). Sea ice sediment entrain-
1220 ment and rafting in the Arctic. *Journal of Sedimentary Petrology*, 59(2), 308-
1221 317. doi: 10.1306/212F8F80-2B24-11D7-8648000102C1865D
- 1222 Kipp, L. E., Charette, M. A., Moore, W. S., Henderson, P. B., & Rigor, I. G.
1223 (2018). Increased fluxes of shelf-derived materials to the central Arctic Ocean.
1224 *Science Advances*, 4(1). doi: 10.1126/sciadv.aao1302
- 1225 Klinkhammer, G. P., & Bender, M. L. (1980). The distribution of manganese in the
1226 Pacific Ocean. *Earth and Planetary Science Letters*, 46(3), 361-384. doi: 10
1227 .1016/0012-821X(80)90051-5
- 1228 Kluyver, T., Ragan-Kelley, B., Pérez, F., Granger, B., Bussonnier, M., Frederic, J.,
1229 ... others (2016). *Jupyter Notebooks – a publishing format for reproducible*
1230 *computational workflows* (F. Loizides & B. Schmidt, Eds.). IOS Press.
- 1231 Kodaira, T., Waseda, T., Nose, T., & Inoue, J. (2020). Record high Pacific
1232 Arctic seawater temperatures and delayed sea ice advance in response
1233 to episodic atmospheric blocking. *Scientific Reports*, 10(1), 1-12. doi:
1234 10.1038/s41598-020-77488-y

- 1235 Kondo, Y., Obata, H., Hioki, N., Ooki, A., Nishino, S., Kikuchi, T., & Kuma, K.
 1236 (2016). Transport of trace metals (Mn, Fe, Ni, Zn and Cd) in the western
 1237 Arctic Ocean (Chukchi Sea and Canada Basin) in late summer 2012. *Deep*
 1238 *Sea Research Part I: Oceanographic Research Papers*, 116, 236-252. doi:
 1239 10.1016/J.DSR.2016.08.010
- 1240 Krachler, M., Zheng, J., Fisher, D., & Shotyk, W. (2005). Analytical proce-
 1241 dures for improved trace element detection limits in polar ice from Arctic
 1242 Canada using ICP-SMS. *Analytica Chimica Acta*, 530(2), 291-298. doi:
 1243 10.1016/j.aca.2004.09.024
- 1244 Krishfield, R. A., Proshutinsky, A., Tateyama, K., Williams, W. J., Carmack, E. C.,
 1245 McLaughlin, F. A., & Timmermans, M. L. (2014). Deterioration of perennial
 1246 sea ice in the Beaufort Gyre from 2003 to 2012 and its impact on the oceanic
 1247 freshwater cycle. *Journal of Geophysical Research: Oceans*, 119(2), 1271-1305.
 1248 doi: 10.1002/2013JC008999
- 1249 Krumpen, T., Belter, H. J., Boetius, A., Damm, E., Haas, C., Hendricks, S., ...
 1250 Stein, R. (2019). Arctic warming interrupts the Transpolar Drift and affects
 1251 long-range transport of sea ice and ice-rafted matter. *Scientific Reports*, 9(1),
 1252 1-9. doi: 10.1038/s41598-019-41456-y
- 1253 Kuss, J., & Kremling, K. (1999). Spatial variability of particle associated trace
 1254 elements in near-surface waters of the North Atlantic (30 N/60 W to 60 N/2
 1255 W), derived by large volume sampling. *Marine Chemistry*, 68(1-2), 71-86. doi:
 1256 10.1016/S0304-4203(99)00066-3
- 1257 Kwok, R., Spreen, G., & Pang, S. (2013). Arctic sea ice circulation and drift speed:
 1258 Decadal trends and ocean currents. *Journal of Geophysical Research: Oceans*,
 1259 118(5), 2408-2425. doi: 10.1002/jgrc.20191
- 1260 Landing, W. M., & Bruland, K. W. (1987). The contrasting biogeochemistry of
 1261 iron and manganese in the Pacific Ocean. *Geochimica et Cosmochimica Acta*,
 1262 51(1), 29-43. doi: 10.1016/0016-7037(87)90004-4
- 1263 Laney, S. R., Krishfield, R. A., & Toole, J. M. (2017, 9). The euphotic zone un-
 1264 der Arctic Ocean sea ice: Vertical extents and seasonal trends. *Limnology and*
 1265 *Oceanography*, 62, 1910-1934. doi: 10.1002/LNO.10543
- 1266 Lange, M., & Van Sebille, E. (2017). Parcels v0.9: Prototyping a Lagrangian ocean
 1267 analysis framework for the petascale age. *Geoscientific Model Development*,

- 1268 10(11), 4175-4186. doi: 10.5194/gmd-10-4175-2017
- 1269 Lannuzel, D., Schoemann, V., de Jong, J., & Tison, J.-L. (2007). Distribution and
1270 biogeochemical behaviour of iron in the East Antarctic sea ice. *Marine Chem-*
1271 *istry*, 106(1-2), 18-32. doi: 10.1016/J.MARCHEM.2006.06.010
- 1272 Lavelle, J. W., Cowen, J. P., & Massoth, G. J. (1992). A model for the deposition
1273 of hydrothermal manganese near ridge crests. *Journal of Geophysical Research*,
1274 97(C5), 7413. doi: 10.1029/92JC00406
- 1275 Lehmann, N., Kienast, M., Granger, J., & Tremblay, J.-É.. (2022). Physical
1276 and Biogeochemical Influences on Nutrients Through the Canadian Arctic
1277 Archipelago: Insights From Nitrate Isotope Ratios. *Journal of Geophysical*
1278 *Research: Oceans*, 127(3), e2021JC018179. doi: 10.1029/2021JC018179
- 1279 Lévy, M., Estublier, A., & Madec, G. (2001). Choice of an advection scheme for bio-
1280 geochemical models. *Geophysical Research Letters*, 28(19), 3725-3728. doi: 10
1281 .1029/2001GL012947
- 1282 Lewis, K. M., van Dijken, G. L., & Arrigo, K. R. (2020). Changes in phytoplankton
1283 concentration now drive increased Arctic Ocean primary production. *Science*,
1284 369(6500), 198-202. doi: 10.1126/science.aay8380
- 1285 Liang, X., & Losch, M. (2018). On the effects of increased vertical mixing on the
1286 Arctic Ocean and sea ice. *Journal of Geophysical Research: Oceans*, 123(12).
1287 doi: 10.1029/2018JC014303
- 1288 Macdonald, R. W., & Gobeil, C. (2012). Manganese sources and sinks in the Arctic
1289 Ocean with reference to periodic enrichments in basin sediments. *Aquatic Geo-*
1290 *chemistry*, 18(6), 565-591. doi: 10.1007/s10498-011-9149-9
- 1291 Madec, G. (2008). NEMO ocean engine. *Note du Pôle de modélisation, Insti-*
1292 *tut Pierre-Simon Laplace*, 27(1288-1619). Retrieved from [https://www.nemo-](https://www.nemo-ocean.eu/wp-content/uploads/NEMO_book.pdf)
1293 [ocean.eu/wp-content/uploads/NEMO_book.pdf](https://www.nemo-ocean.eu/wp-content/uploads/NEMO_book.pdf)
- 1294 Mann, P. J., Spencer, R. G. M., Hernes, P. J., Six, J., Aiken, G. R., Tank, S. E.,
1295 ... Holmes, R. M. (2016). Pan-Arctic trends in terrestrial dissolved organic
1296 matter from optical measurements. *Frontiers in Earth Science*, 4, 25. doi:
1297 10.3389/feart.2016.00025
- 1298 Martin, J. H., & Gordon, R. M. (1988). Northeast Pacific iron distributions in re-
1299 lation to phytoplankton productivity. *Deep Sea Research Part I: Oceanographic*
1300 *Research Papers*, 35(2), 177-196. doi: 10.1016/0198-0149(88)90035-0

- 1301 Martin, T., & Gerdes, R. (2007). Sea ice drift variability in Arctic Ocean Model
 1302 Intercomparison Project models and observations. *Journal of Geophysical Re-*
 1303 *search: Oceans*, 112(C4). doi: 10.1029/2006JC003617
- 1304 Masina, S., Storto, A., Ferry, N., Valdivieso, M., Haines, K., Balmaseda, M., ...
 1305 Parent, L. (2017). An ensemble of eddy-permitting global ocean reanal-
 1306 yses from the MyOcean project. *Climate Dynamics*, 49(3), 813-841. doi:
 1307 10.1007/s00382-015-2728-5
- 1308 Measures, C. I. (1999). The role of entrained sediments in sea ice in the distribu-
 1309 tion of aluminium and iron in the surface waters of the Arctic Ocean. *Marine*
 1310 *Chemistry*, 68, 59-70. doi: 10.1016/S0304-4203(99)00065-1
- 1311 Michel, C., Ingram, R. G., & Harris, L. R. (2006, 10). Variability in oceano-
 1312 graphic and ecological processes in the canadian arctic archipelago. *Progress in*
 1313 *Oceanography*, 71, 379-401. doi: 10.1016/J.POCEAN.2006.09.006
- 1314 Middag, R., de Baar, H. J. W., Laan, P., Cai, P. H., & van Ooijen, J. C. (2011a).
 1315 Dissolved manganese in the Atlantic sector of the Southern Ocean. *Deep Sea*
 1316 *Research Part II: Topical Studies in Oceanography*, 58(25-26), 2661-2677. doi:
 1317 10.1016/J.DSR2.2010.10.043
- 1318 Middag, R., de Baar, H. J. W., Laan, P., & Klunder, M. B. (2011b). Fluvial and
 1319 hydrothermal input of manganese into the Arctic Ocean. *Geochimica et Cos-*
 1320 *mochimica Acta*, 75(9), 2393-2408. doi: 10.1016/J.GCA.2011.02.011
- 1321 Newton, R., Pfirman, S., Tremblay, B., & DeRepentigny, P. (2017). Increasing
 1322 transnational sea-ice exchange in a changing Arctic Ocean. *Earth's Future*,
 1323 5(6), 633-647. doi: 10.1002/2016EF000500
- 1324 Nürnberg, D., Wollenburg, I., Dethleff, D., Eicken, H., Kassens, H., Letzig, T.,
 1325 & Reimnitz, E. (1994). Sediments in Arctic sea ice: Implications for en-
 1326 trainment, transport and release. *Marine Geology*, 119, 185-214. doi:
 1327 10.1016/0025-3227(94)90181-3
- 1328 O'Brien, M. C., Macdonald, R. W., Melling, H., & Iseki, K. (2006). Particle fluxes
 1329 and geochemistry on the Canadian Beaufort Shelf: Implications for sediment
 1330 transport and deposition. *Continental Shelf Research*, 26(1), 41-81. doi:
 1331 10.1016/J.CSR.2005.09.007
- 1332 Oliphant, T. E. (2006). *A guide to NumPy* (Vol. 1). Trelgol Publishing USA.

- 1333 Pedregosa, F., Varoquaux, G., Gramfort, A., Michel, V., Thirion, B., Grisel, O., ...
1334 Duchesnay, E. (2011). Scikit-learn: Machine learning in Python. *Journal of*
1335 *Machine Learning Research*, 12, 2825-2830.
- 1336 Peeken, I., Primpke, S., Beyer, B., Gütermann, J., Katlein, C., Krumpen, T., ...
1337 Gerdt, G. (2018). Arctic sea ice is an important temporal sink and means
1338 of transport for microplastic. *Nature Communications*, 9(1), 1-12. doi:
1339 10.1038/s41467-018-03825-5
- 1340 Pfirman, S. L., Eicken, H., Bauch, D., & Weeks, W. (1995). The potential trans-
1341 port of pollutants by Arctic sea ice. *Science of The Total Environment*, 159(2-
1342 3), 129-146. doi: 10.1016/0048-9697(95)04174-Y
- 1343 Proshutinsky, A., Krishfield, R., Toole, J. M., Timmermans, M. L., Williams, W.,
1344 Zimmermann, S., ... Zhao, J. (2019). Analysis of the Beaufort Gyre freshwa-
1345 ter content in 2003–2018. *Journal of Geophysical Research: Oceans*, 124(12),
1346 9658-9689. doi: 10.1029/2019JC015281
- 1347 Reimnitz, E., McCormick, M., McDougall, K., & Brouwers, E. (1993). Sediment ex-
1348 port by ice rafting from a coastal polynya. *Arctic, Antarctic, and Alpine Re-*
1349 *search*, 25(2), 83-98. doi: 10.1080/00040851.1993.12002988
- 1350 Rijkenberg, M. J. A., Slagter, H. A., van der Loeff, M., van Ooijen, J., & Gerringa,
1351 L. J. A. (2018). Dissolved Fe in the deep and upper Arctic Ocean with a focus
1352 on Fe limitation in the Nansen Basin. *Frontiers in Marine Science*, 5, 88. doi:
1353 10.3389/fmars.2018.00088
- 1354 Roy-Barman, M. (2009). Modelling the effect of boundary scavenging on Thorium
1355 and Protactinium profiles in the ocean. *Biogeosciences*, 6, 3091-3107. doi: 10
1356 .5194/bg-6-3091-2009
- 1357 Sim, N. (2018). *Biogeochemical cycling of dissolved and particulate manganese*
1358 *in the northeast Pacific and Canadian western Arctic* (Doctoral dissertation,
1359 University of British Columbia). doi: 10.14288/1.0374222
- 1360 Smith, G. C., Roy, F., Mann, P., Dupont, F., Brasnett, B., Lemieux, J.-F., ...
1361 Bélair, S. (2014). A new atmospheric dataset for forcing ice-ocean models:
1362 Evaluation of reforecasts using the Canadian global deterministic prediction
1363 system. *Quarterly Journal of the Royal Meteorological Society*, 140(680),
1364 881-894. doi: 10.1002/qj.2194

- 1365 Spreen, G., Kwok, R., & Menemenlis, D. (2011). Trends in Arctic sea ice drift and
1366 role of wind forcing: 1992-2009. *Geophysical Research Letters*, *38*(19). doi: 10
1367 .1029/2011GL048970
- 1368 Stierle, A. P., & Eicken, H. (2002). Sediment inclusions in Alaskan coastal
1369 sea ice: Spatial distribution, interannual variability, and entrainment re-
1370 quirements. *Arctic, Antarctic, and Alpine Research*, *34*(4), 465-476. doi:
1371 10.1080/15230430.2002.12003518
- 1372 Stroeve, J. C., & Notz, D. (2018). Changing state of Arctic sea ice across all sea-
1373 sons. *Environmental Research Letters*, *13*(10). doi: 10.1088/1748-9326/
1374 aade56
- 1375 Stroeve, J. C., Serreze, M. C., Holland, M. M., Kay, J. E., Malanik, J., & Barrett,
1376 A. P. (2012). The Arctic's rapidly shrinking sea ice cover: A research synthe-
1377 sis. *Climatic Change*, *110*(3-4), 1005-1027. doi: 10.1007/s10584-011-0101-1
- 1378 Sunda, W. G., & Huntsman, S. A. (1994). Photoreduction of manganese oxides in
1379 seawater. *Marine Chemistry*, *46*(1-2), 133-152. doi: 10.1016/0304-4203(94)
1380 90051-5
- 1381 Tagliabue, A., Bowie, A. R., Boyd, P. W., Buck, K. N., Johnson, K. S., & Saito,
1382 M. A. (2017). The integral role of iron in ocean biogeochemistry. *Nature*,
1383 *543*(7643), 51-59. doi: 10.1038/nature21058
- 1384 The Pandas development team. (2020). Pandas-dev/pandas: Pandas. *Zenodo*, *21*, 1-
1385 9.
- 1386 Thyng, K. M., Greene, C. A., Hetland, R. D., Zimmerle, H. M., & DiMarco, S. F.
1387 (2016). True colors of oceanography: Guidelines for effective and accurate
1388 colormap selection. *Oceanography*, *29*(3), 9-13.
- 1389 Tilmes, S., Lamarque, J. F., Emmons, L. K., Kinnison, D. E., Marsh, D., Gar-
1390 cia, R. R., ... Blake, N. (2016). Representation of the Community Earth
1391 System Model (CESM1) CAM4-chem within the Chemistry-Climate Model
1392 Initiative (CCMI). *Geoscientific Model Development*, *9*(5), 1853-1890. doi:
1393 10.5194/gmd-9-1853-2016
- 1394 Tovar-Sánchez, A., Duarte, C. M., Alonso, J. C., Lacorte, S., Tauler, R., & Galbán-
1395 Malagón, C. (2010). Impacts of metals and nutrients released from melting
1396 multiyear Arctic sea ice. *Journal of Geophysical Research*, *115*(C7), C07003.
1397 doi: 10.1029/2009JC005685

- 1398 Tucker, W. B., Gow, A. J., Meese, D. A., Bosworth, H. W., & Reimnitz, E. (1999).
1399 Physical characteristics of summer sea ice across the Arctic Ocean. *Journal of*
1400 *Geophysical Research: Oceans*, 104(C1), 1489-1504. doi: 10.1029/98jc02607
- 1401 Van Hulten, M., Middag, R., Dutay, J.-C., De Baar, H., Roy-Barman, M., Gehlen,
1402 M., ... Sterl, A. (2017). Manganese in the west Atlantic Ocean in the context
1403 of the first global ocean circulation model of manganese. *Biogeosciences*, 14,
1404 1123-1152. doi: 10.5194/bg-14-1123-2017
- 1405 Vieira, L. H., Achterberg, E. P., Scholten, J., Beck, A. J., Liebetrau, V., Mills,
1406 M. M., & Arrigo, K. R. (2019). Benthic fluxes of trace metals in the Chukchi
1407 Sea and their transport into the Arctic Ocean. *Marine Chemistry*, 208, 43-55.
1408 doi: 10.1016/j.marchem.2018.11.001
- 1409 Virtanen, P., Gommers, R., Oliphant, T. E., Haberland, M., Reddy, T., Cour-
1410 napeau, D., ... others (2020). SciPy 1.0: fundamental algorithms for
1411 scientific computing in Python. *Nature methods*, 17(3), 261-272. doi:
1412 10.1038/s41592-019-0686-2
- 1413 Waga, H., Eicken, H., Light, B., & Fukamachi, Y. (2022). A neural network-based
1414 method for satellite-based mapping of sediment-laden sea ice in the Arctic. *Re-*
1415 *mote Sensing of Environment*, 270, 112861. doi: 10.1016/j.rse.2021.112861
- 1416 Wang, Q., Myers, P. G., Hu, X., & Bush, A. B. G. (2012). Flow constraints on
1417 pathways through the Canadian Arctic Archipelago. *Atmosphere-Ocean*, 50(3),
1418 373-385. doi: 10.1080/07055900.2012.704348
- 1419 Wang, S., Bailey, D., Lindsay, K., Moore, J. K., & Holland, M. (2014). Impact of sea
1420 ice on the marine iron cycle and phytoplankton productivity. *Biogeosciences*,
1421 11(17), 4713-4731. doi: 10.5194/bg-11-4713-2014
- 1422 Waskom, M., & the Seaborn development team. (2020). *Seaborn*. Zenodo. doi: 10
1423 .5281/zenodo.592845
- 1424 Wedepohl, H. K. (1995). The composition of the continental crust. *Geochimica et*
1425 *Cosmochimica Acta*, 59(7), 1217-1232. doi: 10.1016/0016-7037(95)00038-2
- 1426 Yamamoto-Kawai, M., Carmack, E. C., & McLaughlin, F. (2006). Nitrogen balance
1427 and Arctic throughflow. *Nature*, 443(7107), 43-43. doi: 10.1038/443043a
- 1428 Yamamoto-Kawai, M., McLaughlin, F. A., Carmack, E. C., Nishino, S., Shimada,
1429 K., & Kurita, N. (2009). Surface freshening of the Canada Basin, 2003–2007:
1430 River runoff versus sea ice meltwater. *Journal of Geophysical Research*,

- 1431 114(C1), C00A05. doi: 10.1029/2008JC005000
- 1432 Yeats, P. A., & Westerlund, S. (1991). Trace metal distributions at an Arctic Ocean
- 1433 ice island. *Marine Chemistry*, 33(3), 261-277. doi: 10.1016/0304-4203(91)
- 1434 90071-4
- 1435 Zalesak, S. T. (1979). Fully multidimensional flux-corrected transport algorithms for
- 1436 fluids. *Journal of Computational Physics*, 31(3), 335-362. doi: 10.1016/0021
- 1437 -9991(79)90051-2

Supporting Information for “Sediments in sea ice drive the Canada Basin surface Mn maximum: insights from an Arctic Mn ocean model”

B. Rogalla¹, S. E. Allen¹, M. Colombo¹, P. G. Myers², K. J. Orians¹

¹Department of Earth, Ocean, and Atmospheric Sciences, University of British Columbia, Vancouver, British Columbia V6T1Z4,

Canada

²Department of Earth and Atmospheric Sciences, University of Alberta, 1-26 ESB, Edmonton, Alberta T6G2E3, Canada

Contents of this file

1. Text S1 to S4
2. Figures S1 to S19
3. Table S1 to S2

Corresponding author: B. Rogalla, Department of Earth, Ocean, and Atmospheric Sciences, University of British Columbia, Earth Sciences Building, Vancouver BC V6T1Z4, Canada. (bro-galla@eoas.ubc.ca)

Text S1. Model boundary condition sensitivity experiments.

The Arctic Mn model domain has three boundaries: the western boundary extends along the Beaufort shelf and the western Canada Basin, the northern boundary extends along northern Canada Basin to Greenland, and the eastern boundary crosses Baffin Bay (Fig. 1). We conducted sensitivity experiments for the western and northern boundary condition, as these regions are most important to the key findings of this study. These sensitivity experiments were spun-up for three years, as for the other experiments, and then run from 2002-2005. By 2005, the year-to-year variations in the the extent of influence of the altered boundary concentrations is small and differences are related to specific flow conditions for that year.

Pacific water enters the Arctic Ocean through Bering Strait and is transported eastward along the North American continent by the Alaskan Coastal current. In the context of our Mn model domain, the Pacific water inflow occurs along the western model boundary. We conducted an experiment with artificially enhanced concentrations along the Beaufort Shelf in the western boundary condition to identify the extent of influence of the Pacific water (Fig. S1); the “Pacific water” experiment. Polar mixed layer dissolved Mn concentrations in September, 2005 are higher over the Beaufort shelf in the Pacific water experiment (Fig. S2). The influence of the increased western boundary dMn contribution is primarily restricted to the Beaufort shelf and minimally impacts the central Canada Basin. A weak increase in concentrations extends along the Chukchi borderland from the northern section of the western boundary condition.

The model northern boundary extends across northern Canada Basin to Greenland. In the context of our Mn model domain, the central Arctic Ocean or transpolar drift inflow

occurs along the northern model boundary. In order to assess the impact of the transpolar drift content on the interior of the Canada Basin, we conducted an experiment with concentrations artificially enhanced along the the northern boundary condition (Fig. S3), in particular towards Ellesmere Island where southward flow occurs; the “transpolar drift” experiment. An increase in dissolved Mn of 2-3 nM at the northern boundary results in an increase of around 0.4 nM near the boundary and less than 0.1 nM in the interior of the Canada Basin by September, 2005 (Fig. S4). Nares Strait sees an increase in dMn concentrations of 0.3-0.5 nM; indicative of the direct transport of waters from the central Arctic Ocean through Nares Strait.

Text S2. Reversible Scavenging parameterization details.

Dissolved Mn adsorbs to particle surfaces (pMn) and oxidises to oMn forming larger aggregates which sink. dMn is regenerated through the release of Mn from particles through desorption and by the reduction of oMn. These processes constitute the reversible scavenging of Mn and can be represented as follows (expanded from Van Hulten et al., 2017):

$$\frac{\partial[dMn]}{\partial t} = -k_{ox} \cdot [dMn] + k_{re} \cdot [oMn] - k_{ad} \cdot [dMn] + k_{de} \cdot [pMn] + \text{physics} + S \quad (1)$$

$$\frac{\partial[pMn]}{\partial t} = k_{ad} \cdot [dMn] - k_{de} \cdot [pMn] - s_p \frac{\partial[pMn]}{\partial z} + \text{physics} + S \quad (2)$$

$$\frac{\partial[oMn]}{\partial t} = k_{ox} \cdot [dMn] - k_{re} \cdot [oMn] - s_{ox} \frac{\partial[oMn]}{\partial z} + \text{physics} \quad (3)$$

where s_p and s_{ox} are the pMn and oMn sinking rates, respectively, and k_{ad} , k_{ox} , k_{de} , and k_{re} are the rate constants for adsorption, oxidation, desorption, and reduction. In our model, we trace dMn and oMn explicitly, while we only take the indirect effect of particle-bound Mn on dissolved Mn concentrations into account.

The physics term represents mixing and advection processes, and S represents the contribution from sources and sinks. Away from sources and sinks, assuming steady state, negligible impact of mixing and advection, and a weak vertical gradient in Mn concentrations, the equations are decoupled and we can estimate the scavenging rates from Eqn. 2 and 3:

$$[dMn] = \frac{k_{re}}{k_{ox}} \cdot [oMn] \quad (4)$$

$$[dMn] = \frac{k_{de}}{k_{ad}} \cdot [pMn] \quad (5)$$

Using the ratio of observed dissolved and oxidized (Eqn. 4) or particulate Mn (Eqn. 5) concentrations in the Canadian Arctic (Colombo et al., 2020, 2022), we can estimate

the background scavenging rates for oxidation or adsorption, $k_p = k_{ox}$ or k_{ad} , and for reduction or desorption, $k_d = k_{de}$ or k_{re} , respectively. We consider only observations in regions far away from coastal processes and the ocean surface where the assumptions hold. This condition reduces the available observations to those from stations in deeper areas of Baffin Bay and Canada Basin (Fig. S8) which have relatively small particle fluxes and are far away from sources. We match observations of dissolved and oxidized or particulate Mn at equal depths and fit a linear regression through the origin (Fig. S9). Using this method, the ratio of scavenging rates, k_p/k_d , is estimated to be 1.47 ± 0.25 (uncertainty estimate is the root-mean-square error) and with a k_d of $4.7 \cdot 10^{-7} \text{ s}^{-1}$ (Bruland et al., 1994), k_p is estimated as $7.0 \cdot 10^{-7} \text{ s}^{-1}$.

Since we model dMn and oMn, the final reversible scavenging equations in our Mn model are:

$$\frac{\partial[dMn]}{\partial t} = -k_p \cdot [dMn] + k_d \cdot [oMn] + \text{physics} + S \quad (6)$$

$$\frac{\partial[oMn]}{\partial t} = k_p \cdot [dMn] - k_d \cdot [oMn] - s_{ox} \frac{\partial[oMn]}{\partial z} + \text{physics} \quad (7)$$

These equations do not incorporate a dependence on the dissolved oxygen concentration since Arctic waters are generally well oxygenated.

Text S3. Comparison of estimate of magnitude of biological uptake.

We estimate that uptake can account for a difference in Mn concentrations of up to about 0.3 nM (Fig. S19). In order to assess our estimate, we can compare the nitrogen uptake from our model forcing with that estimated from observed primary production in the CAA.

Michel, Ingram, and Harris (2006) estimate primary production in the CAA as 53-57 MtC yr⁻¹. Using the average, 55 MtC yr⁻¹, and an area of 2.5·10⁶ km² for the CAA, this primary production corresponds to 22 gC m⁻² yr⁻¹. Taking into account the molecular weight of carbon (12 g mol⁻¹) and the Redfield ratio (106C : 16N), primary production accounts for an uptake of 0.28 moles of N m⁻² yr⁻¹. Our estimate of uptake from the CanOE model is on the order of 5 mmol N m⁻³, and with a euphotic zone depth of 100 m, this is roughly 0.5 moles of N m⁻² yr⁻¹. This nitrogen uptake, and thus the derived Mn uptake, is similar in magnitude to that estimated based on the primary production from Michel et al. (2006).

Text S4. Calculation of Net Mn transport through Parry Channel.

In this study, we calculated net Mn transport from Canada Basin into Parry Channel and from Parry Channel into Baffin Bay via Lancaster Sound. The boundaries are defined along lines of constant i or j indices (Fig. S14). The Mn flux across each of the boundaries, ϕ_{bdy} , is the sum of the dissolved Mn concentration at the boundary grid points with indices i, j, k , multiplied by the volume flux:

$$\phi_{bdy}(t) = \sum_{i,j,k} [dMn]_{i,j,k}(t) \cdot u_{i,j,k}(t) \cdot A_{i,j,k} \quad (8)$$

where u is the velocity perpendicular to the boundary at time, t , and A is the grid cell area. These time series were calculated from 5-day modelled velocity and tracer fields, interpolated onto the U grid.

Mn transport into and out of Parry Channel fluctuates seasonally, with a peak in the late summer (Fig. S17). The flux of Mn in the “clean” sea ice experiment is consistently smaller than for the experiment with sediment in sea ice. To compare the experiments, we calculate the percent contribution of the sea ice component to the net transport:

$$p = \left(1 - \frac{\phi_{off}}{\phi_{on}}\right) \cdot 100\% \quad (9)$$

where ϕ_{off} is the Mn transport from an experiment with the component “off”, i.e. the “clean” sea ice experiment, and ϕ_{on} is the Mn transport from an experiment with the component on, i.e. the reference experiment with dirty sea ice. Based on these calculations, the sediment released by sea ice contributes about 87% to the Mn transported from Canada Basin into Parry Channel and about 34% for the Mn transported from Parry Channel into Baffin Bay (Fig. S18). The sea ice contribution to Mn flux does not vary significantly between 2002-2019.

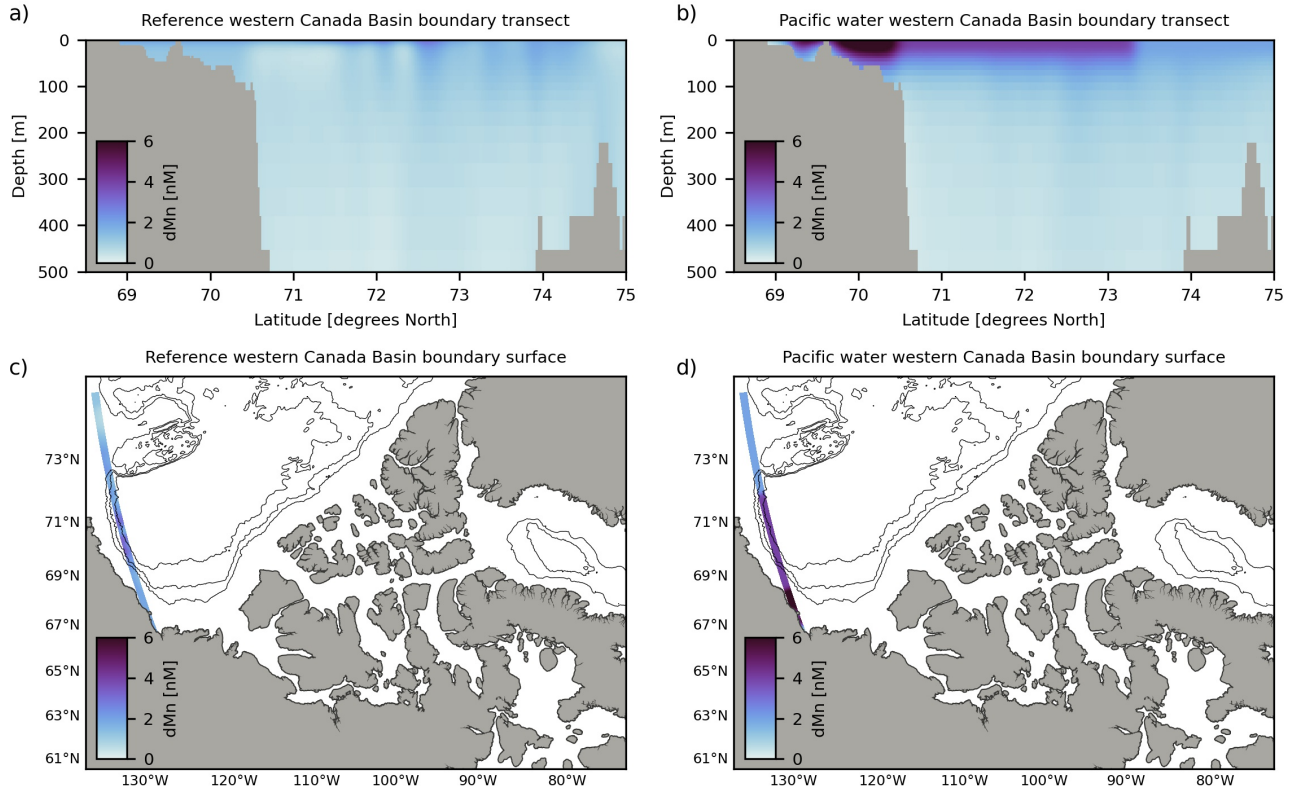


Figure S1. Western boundary conditions for dissolved Mn concentrations in the reference experiment (a, c) and Pacific water experiment (b, d). Panels (a) and (b) are vertical cross-sections of dMn concentrations along the boundary and (c) and (d) are plan views of surface dMn concentrations. The western boundary in our model domain extends from the Beaufort Sea along the shelf towards the central Arctic Ocean (Fig. 1). Pacific origin water is transported by the Alaskan Coastal Current along this shelf and enters our domain through the western boundary. The reference experiment boundary conditions (a, c) are based on the Mn model from Van Hulten et al. (2017) and are lower than observations in this region. In the Pacific water experiment (b, d), we artificially enhanced Mn concentrations along the shelf in the western boundary.

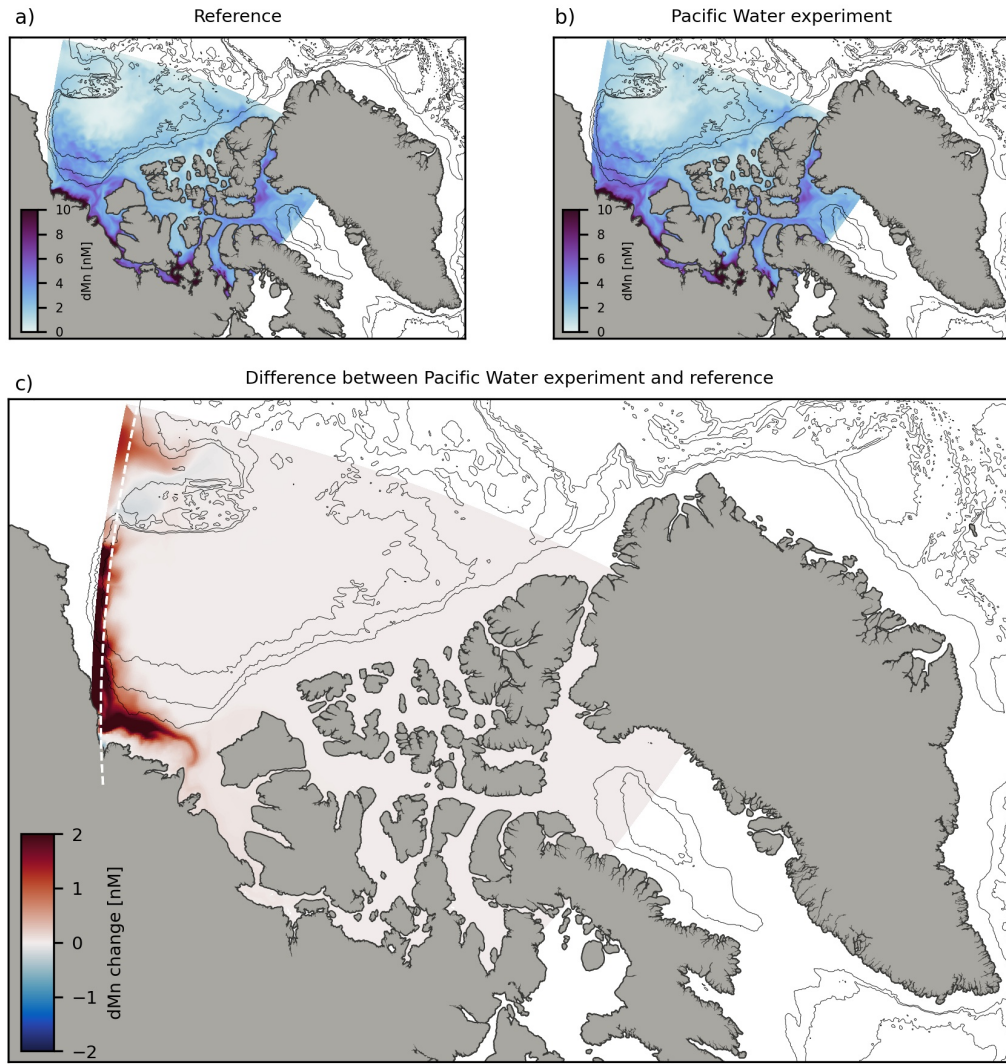


Figure S2. Depth-weighted mean dissolved Mn concentrations in the polar mixed layer in September, 2005 for the reference experiment (a), the Pacific water experiment (b), and the difference between them (c). In the reference experiment, the western boundary condition concentrations are based on the Mn model from Van Hulten et al. (2017), while we artificially enhanced concentrations along the shelf in the Pacific water experiment (Text S1, Fig. S1). Pacific origin water is transported by the Alaskan Coastal Current and its impact on dissolved Mn concentrations in the polar mixed layer is constrained to the Beaufort Shelf and does not significantly extend into the interior of the Canada Basin. The white dashed line indicates the inner-edge of the boundary condition and thin black lines correspond to bathymetry contours of 1000, 2000, and 3000 m depth.

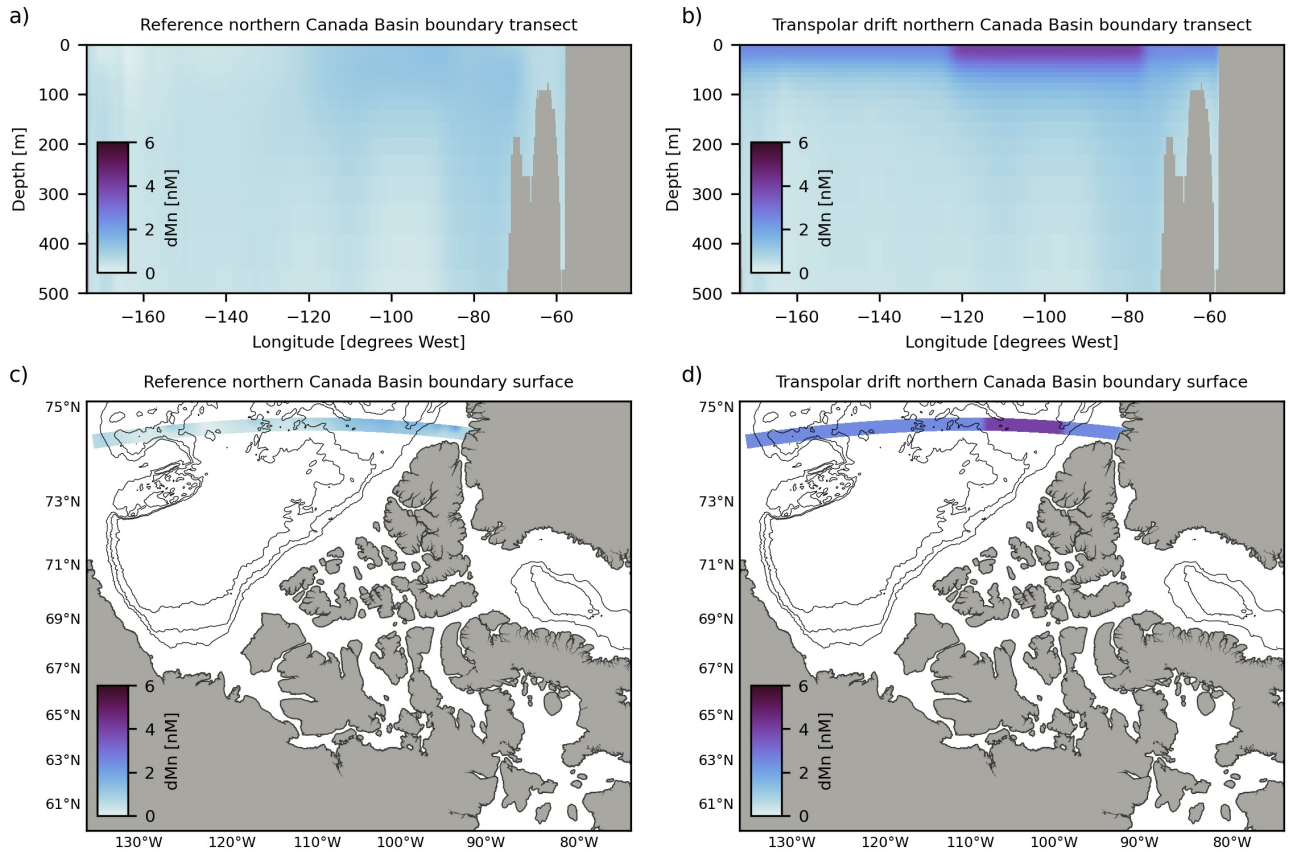


Figure S3. Northern boundary conditions for dissolved Mn concentrations in the reference experiment (a, c) and the transpolar drift experiment (b, d). Panels (a) and (b) are vertical cross-sections of dMn concentrations along the boundary and (c) and (d) are plan views of surface dMn concentrations. The northern boundary in our model domain extends across the central Arctic Ocean to Greenland (Fig. 1). The reference experiment boundary conditions (a, c) are based on the Mn model from Van Hulten et al. (2017) and are lower than observations in this region. In the transpolar drift experiment (b, d), we artificially enhanced concentrations along the northern boundary, in particular in the region of inflow from the transpolar drift.

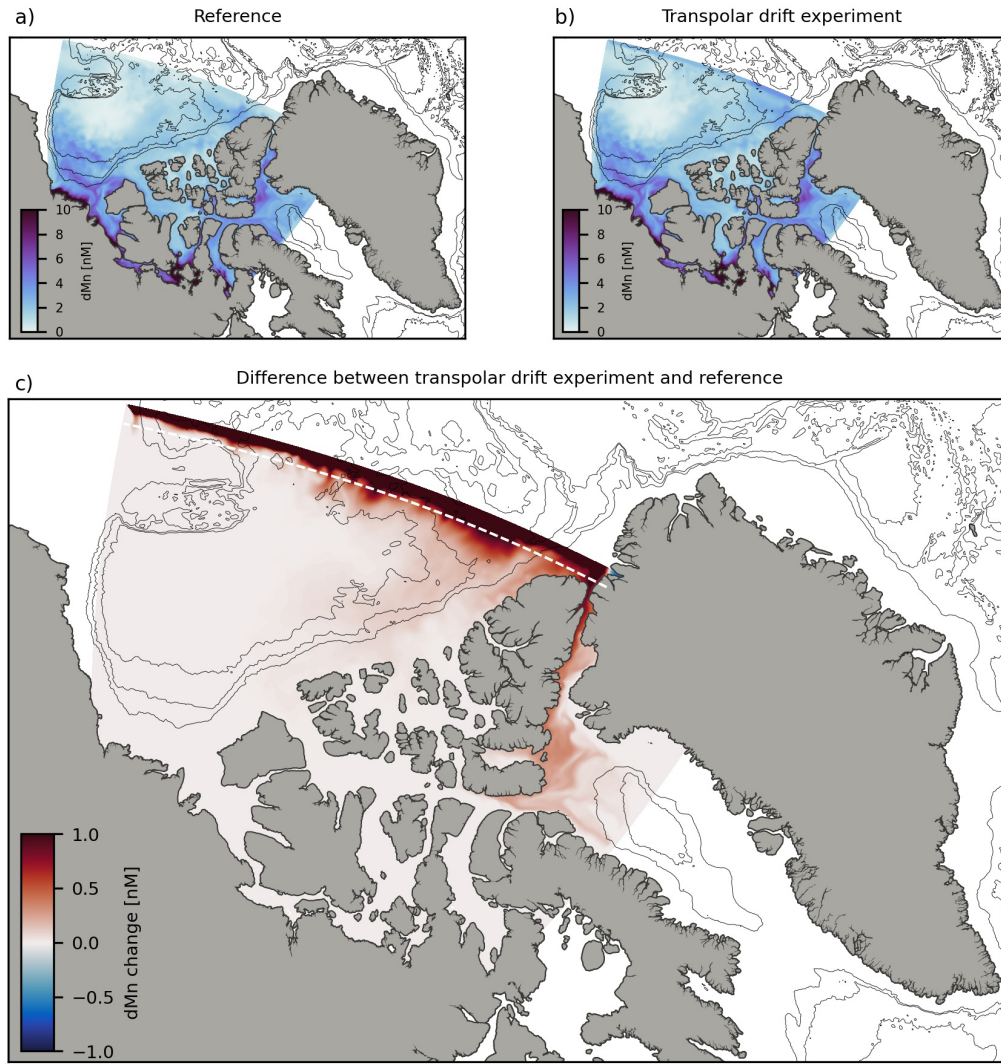


Figure S4. Depth-weighted mean dissolved Mn concentrations in the polar mixed layer in September, 2005 for the reference experiment (a), the transpolar drift experiment (b), and the difference between them (c). In the reference experiment, the northern boundary condition concentrations are based on the Mn model from Van Hulten et al. (2017), while we artificially enhanced concentrations by 2-3 nM in the transpolar drift experiment (Text S1, Fig. S3). Water from the central Arctic Ocean, including the transpolar drift, enters the Canada Basin through the northern model boundary. Near the northern boundary, dMn concentrations increased by around 0.4 nM, while concentrations increased by less than 0.1 nM in the interior of the Canada Basin. The white dashed line indicates the inner-edge of the boundary and thin black lines correspond to bathymetry contours of 1000, 2000, and 3000 m depth.

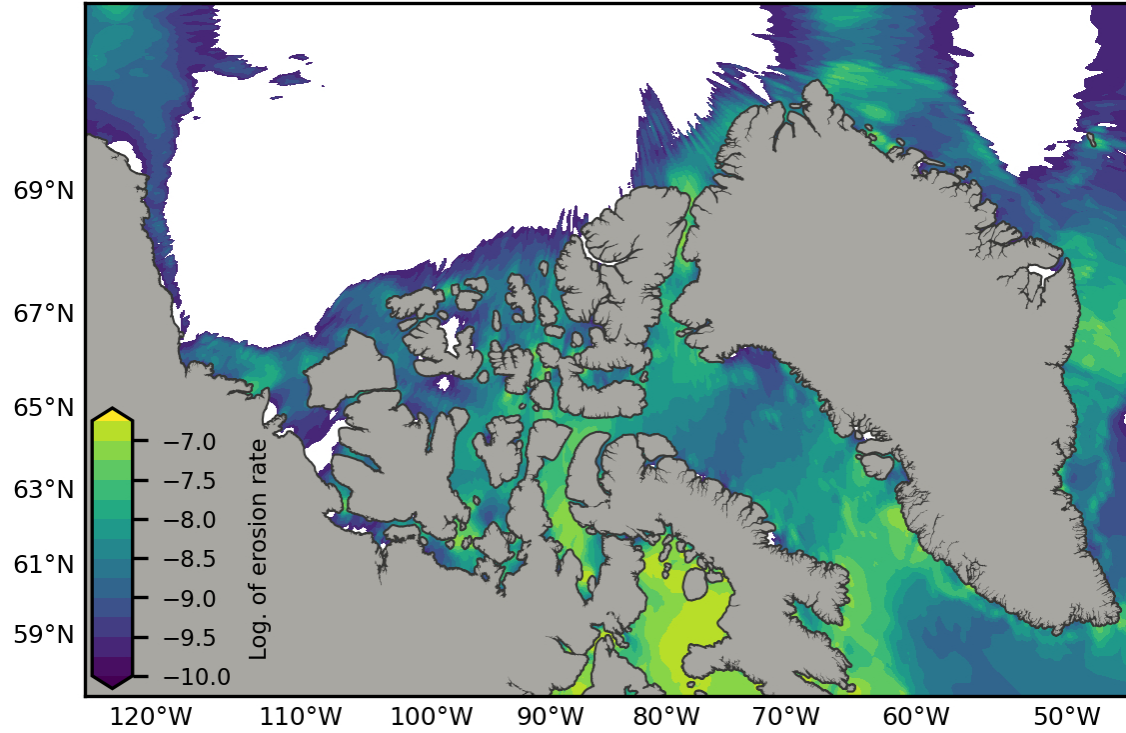


Figure S5. Erosion rates (units of $\text{kg m}^{-2} \text{s}^{-1}$) are heterogeneous across the Canadian Arctic. Regions west of Barrow Sill in central Parry Channel have lower erosion rates than eastern Parry Channel, as seen in observations (Colombo et al., 2020). We use tidal stress to estimate the spatially variable erosion rate for the sediment resuspension parameterization of our Mn model (Eqn. 6). Tidal stress is calculated as the squared barotropic tidal speeds derived from the MOG2D-G model (Carrère & Lyard, 2003). Erosion rate is zero (white) in regions where tidal speeds are below 1 cm s^{-1} . Note that the colorbar scale is logarithmic.

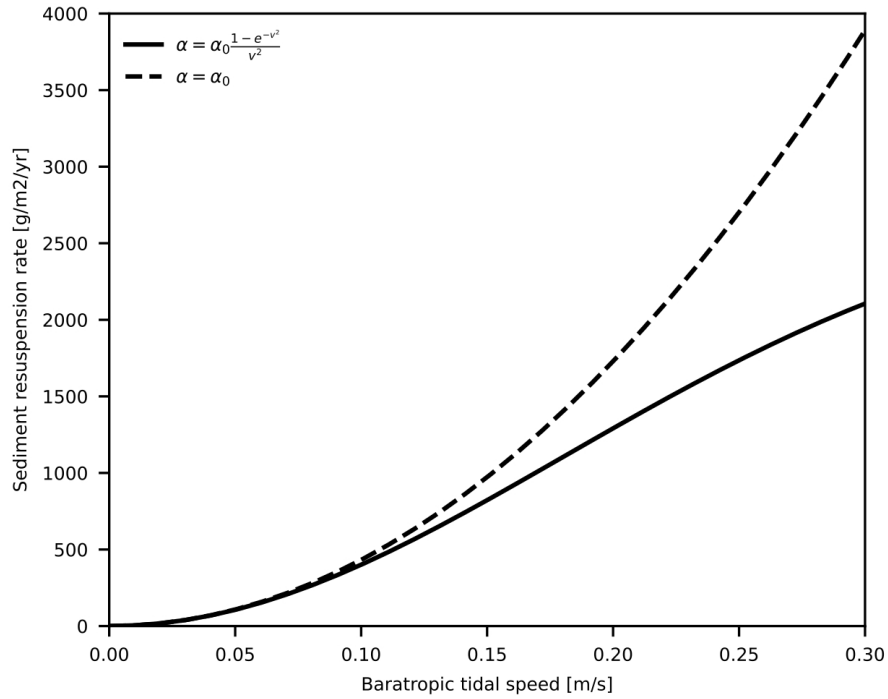


Figure S6. Sediment resuspension is modelled proportional to tidal stress (barotropic tidal speed, U_{tidal} , squared; Eqn. 5 and 6). In regions with strong tidal speeds, the readily available Mn has been dissolved from particles, and the fractional solubility is effectively reduced. We modulate the sediment resuspension rate by the fractional solubility, α , which decreases as tidal speed increases (Eqn. 7). The resulting sediment resuspension rate levels off at a maximum value at high tidal speeds (solid line), while with a constant fractional solubility, sediment resuspension increases indefinitely (dashed line).

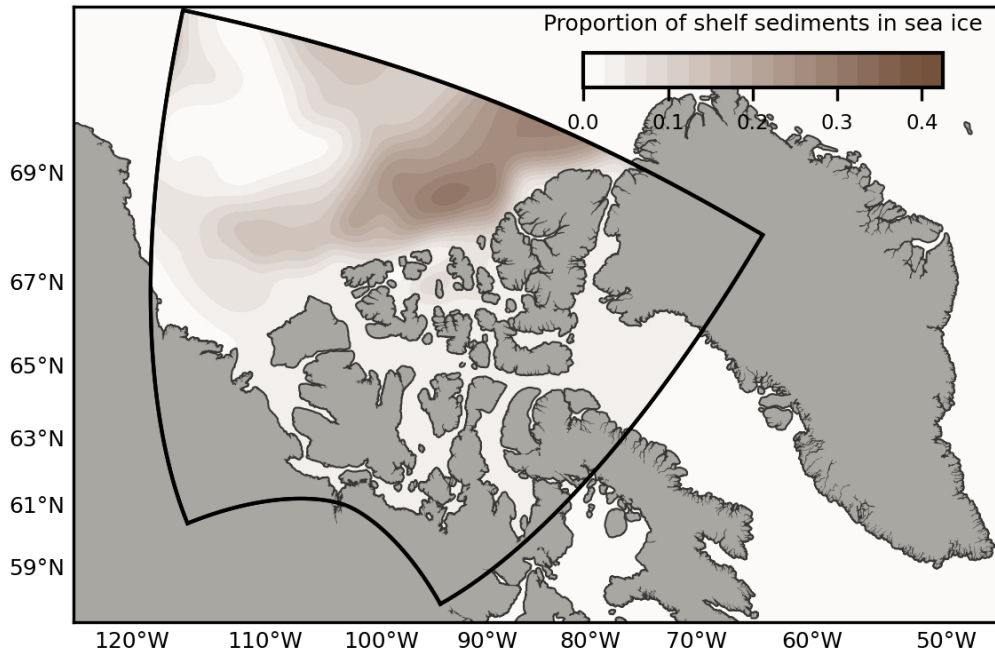


Figure S7. The sediment content of sea ice is highest along the outer edges of the Canada Basin, while the older sea ice at the core of the Beaufort Gyre is relatively “clean” in our model forcing field. The parameterization for sediment content in sea ice consists of a constant characteristic shelf sediment density, multiplied by the proportion of Siberian shelf-origin sediments in sea ice (colored contours in figure), estimated with backwards particle tracking. Within the CAA, we assume a constant, low background content.

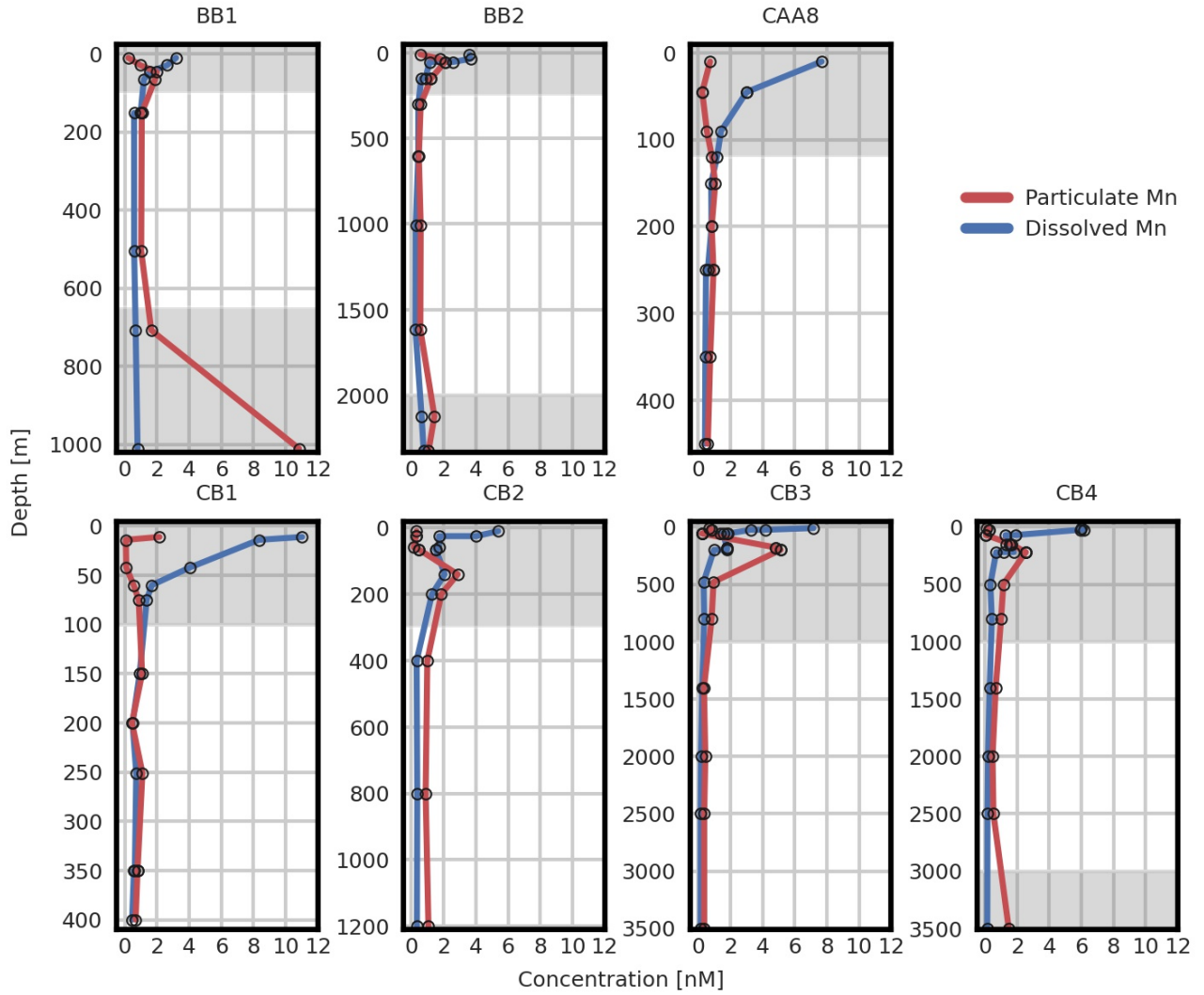


Figure S8. Scavenging rates are estimated using dissolved and particulate Mn observations far away from sources and sinks, and at depths with a negligible vertical gradient in particulate concentrations. Here, we show profiles of dissolved Mn (blue) and particulate Mn (red) from 2015 at stations in Baffin Bay, the Canadian Arctic Archipelago, and Canada Basin, that match these criteria. The depths at which external sources affect the Mn concentrations are highlighted in gray and are excluded from the scavenging rate estimate. Note that the depth scale varies between plots.

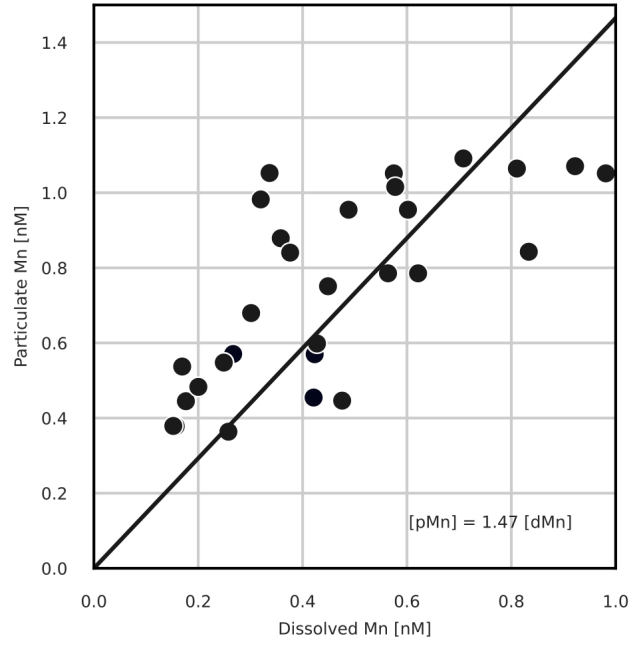


Figure S9. Far away from sources and sinks, dissolved and particulate Mn occur at ratios set by the scavenging rates. We estimate the scavenging rates from 2015 Canadian GEOTRACES observations that satisfy these criteria (profiles shown in Fig. S8) by applying a linear fit with a zero intercept (solid black line); the slope is $1.47 \pm 0.25 [dMn] [pMn]^{-1} = k_{de} (k_{ad})^{-1}$ (Eqn. S5).

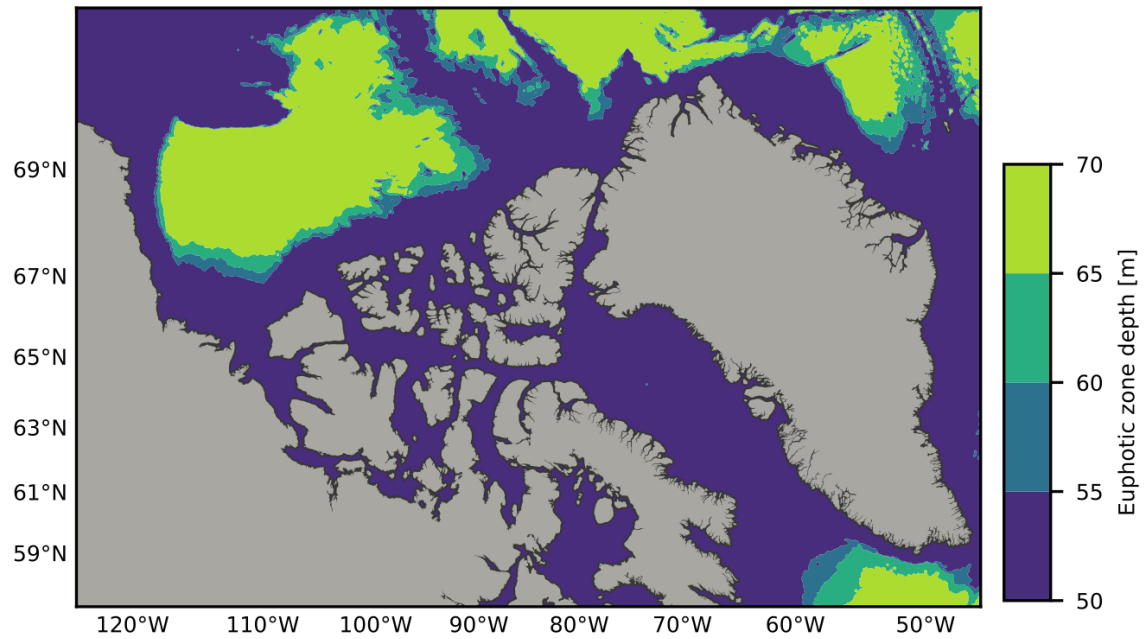


Figure S10. The euphotic zone forcing in our model gradually transitions from 70 m in the Canada Basin (shallow limit observed by Laney et al., 2017) to 50 m in the CAA based on bathymetry depth (euphotic depth from Bhatia et al., 2021). Photo-enhanced reduction is applied within the euphotic zone.

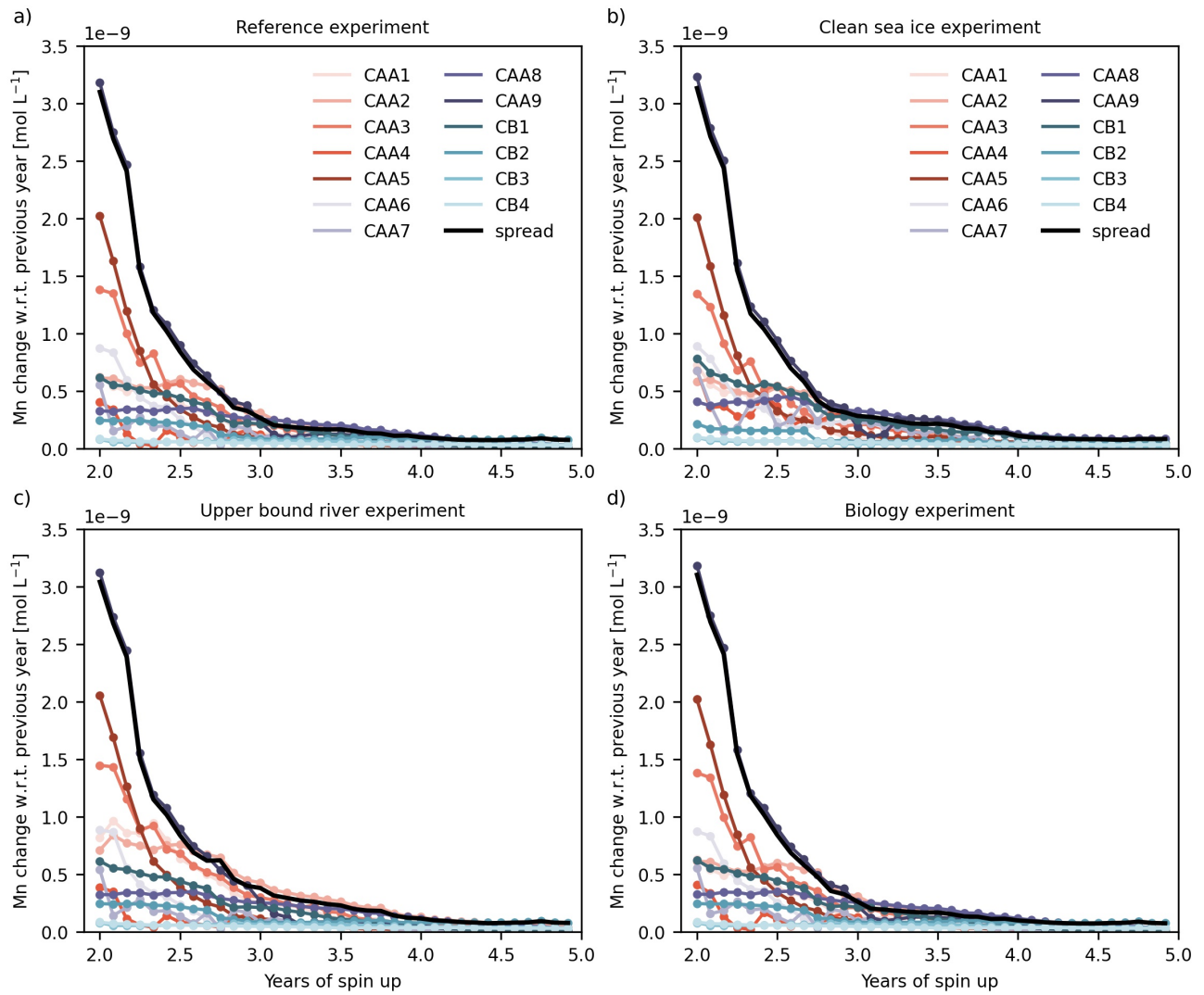


Figure S11. For each simulation: (a) reference, (b) “clean” sea ice, (c) upper bound river, and (d) biology, the Mn model is spun up by repeating the year 2002 until the year-to-year change in profile shape, estimated as the average Mn difference in the water column, at evaluation stations from 2015 Canadian GEOTRACES cruises (names in legend) is minimal. It takes about three years to achieve spin-up, after which the full experiments from 2002 to 2019 start. The “spread” is the difference between the maximum and minimum change at each month (solid black line).

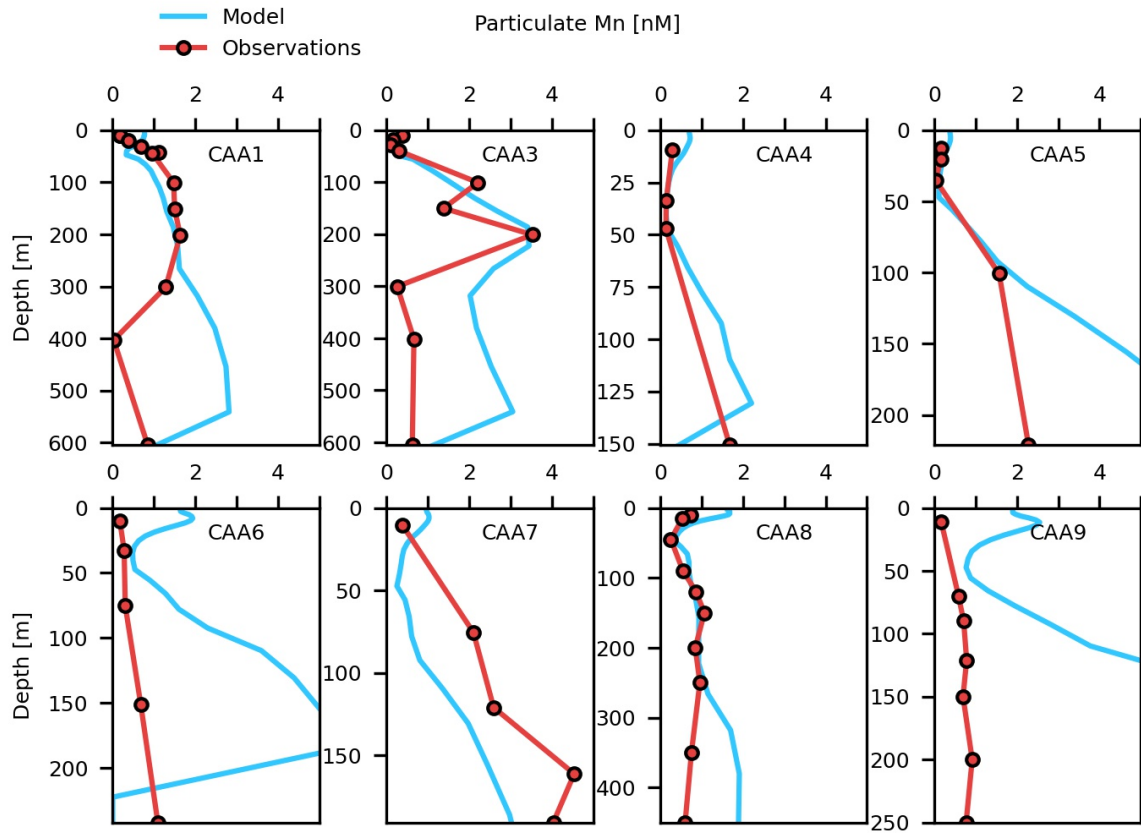


Figure S12. Modelled oxidised Mn (blue) and observed particulate Mn (red) profiles in the Canadian Arctic Archipelago for 2015 Canadian GEOTRACES stations. Observed pMn data are from Colombo et al. (2021). Particulate Mn sources are not directly incorporated into the model; instead, we modelled oMn through the coupling of scavenging with dMn. The model captures a range of behaviour within the upper 100 m of stations CAA1, CAA3, CAA4, CAA5, and CAA8, while it typically overestimates oMn in the lower water column in locations with strong sediment resuspension.

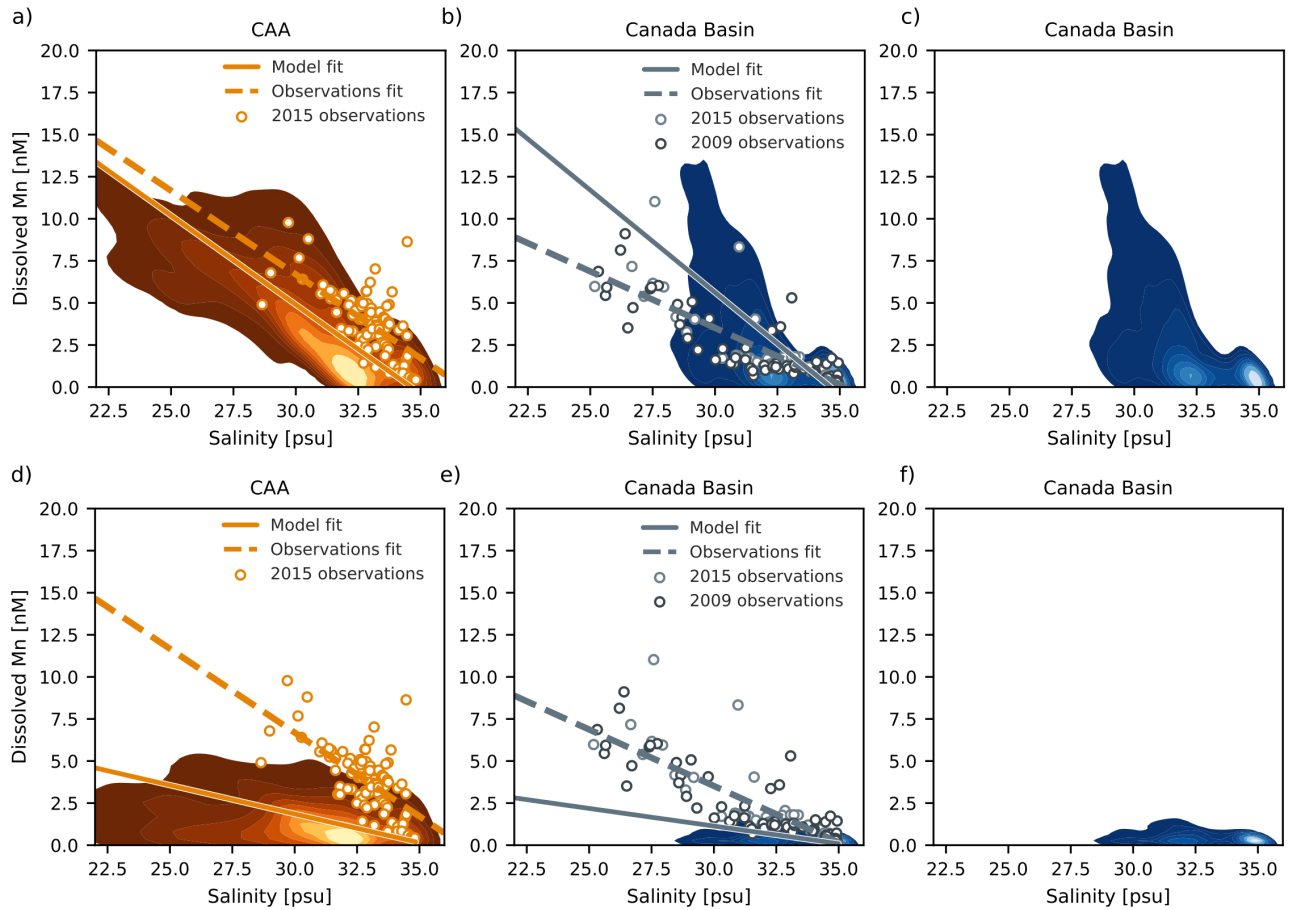


Figure S13. Modelled Mn-salinity relationship for one in five grid points at all depths (contour levels correspond to iso-proportions of the density of points) averaged over August-September, 2015, in the Canada Basin and the Canadian Arctic Archipelago (CAA) alongside observations from 2009 and 2015 (scatter points). The reference experiment (panels a-c) represents the low-salinity endmember more accurately than the experiment without sediment in sea ice (panels d-f). The solid lines are linear regression fits for the model estimates. The dashed lines are fits from observations collected in 2009 and 2015 (Sim, 2018; Colombo et al., 2020). Panels (c) and (f) show the Canada Basin contour levels alone for clarity. Note that the evaluation of the Canada Basin Mn-salinity relationship is complicated by an underestimation of surface freshwater in the model (see section 4.3.1 for a discussion of this limitation).

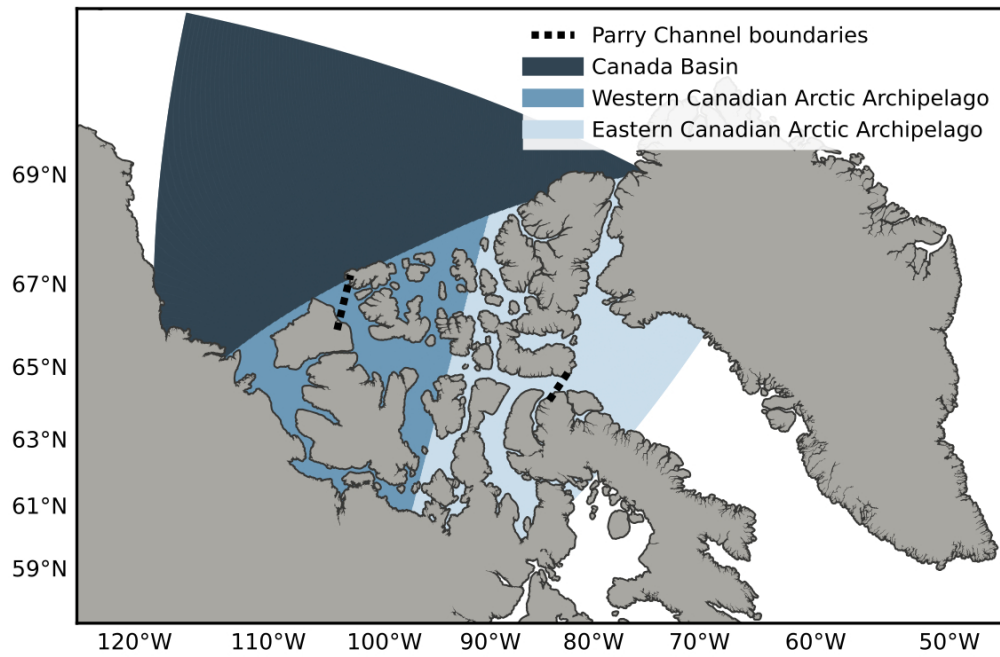


Figure S14. Region definitions for the component contribution calculations in Tables 2, 3, and S2. The CAA is divided into west and east approximately along 100°W. The boundaries indicated by black dashed lines were used for the calculations of net Mn transport into and of Parry Channel in Fig. S17 and S18.

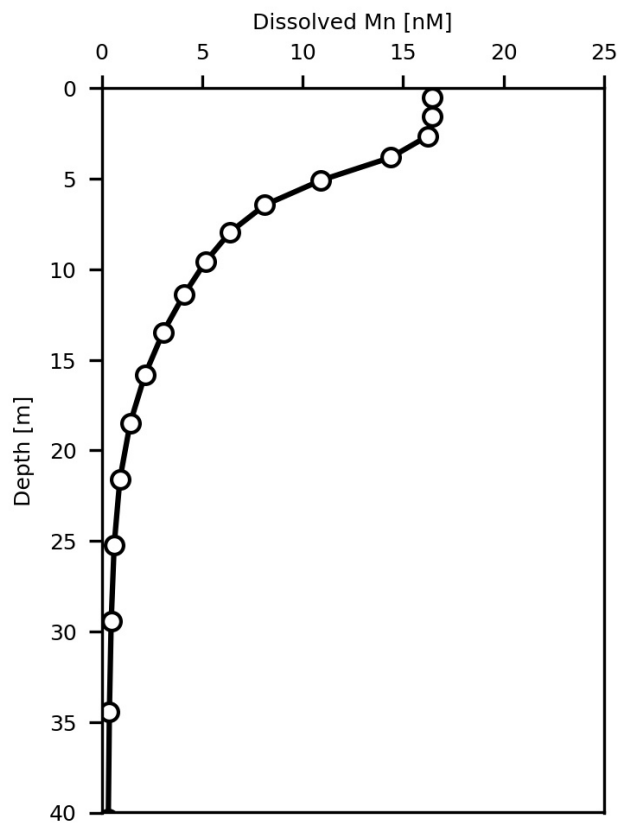
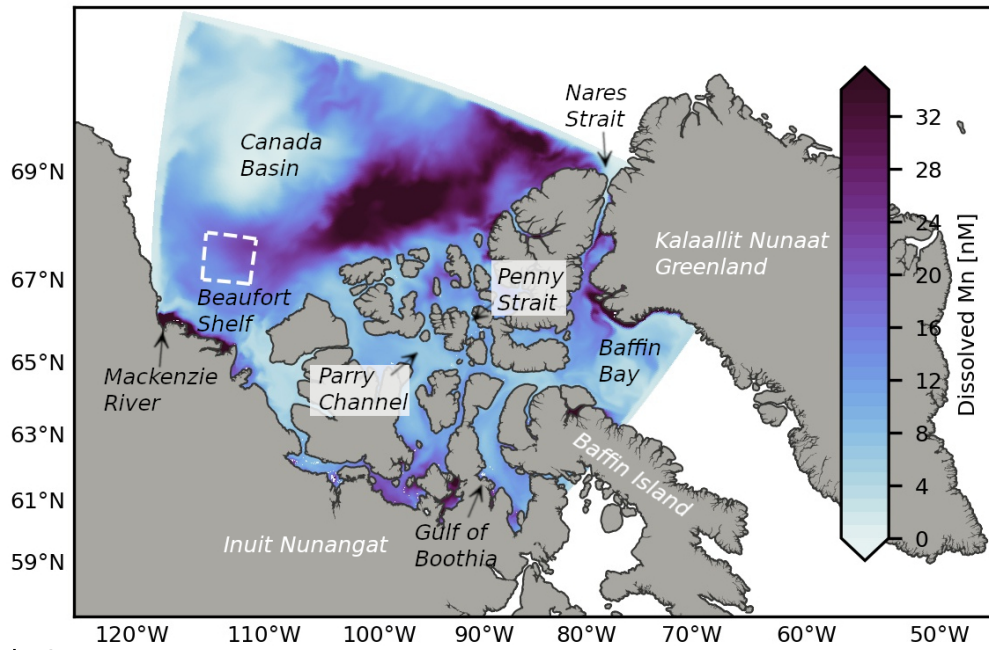


Figure S15. Dissolved Mn concentrations are highest at the surface and decrease strongly within the upper 5 m. These gradients are most visible during periods of strong surface source input, i.e. during sea ice melt. This mean profile was calculated over a sub-region of the Canada Basin (dashed white line in Fig. S16) for July, 2015. The markers indicate the model depth levels.

a) August



b) January

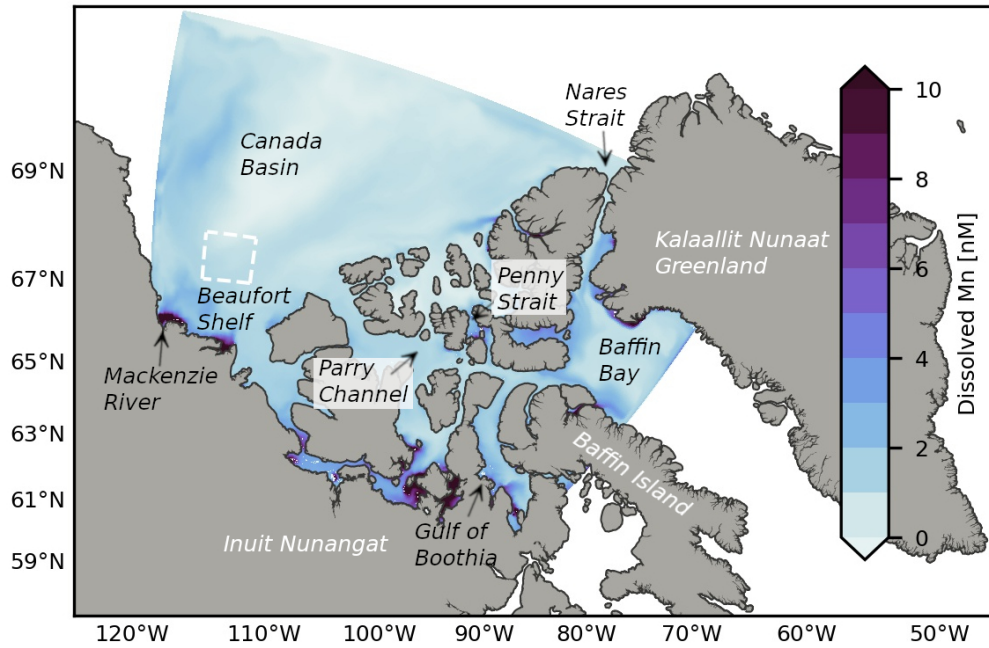


Figure S16. Simulated Mn concentrations in the ocean surface (top 1 m) in (a) August, 2015 and (b) January, 2015. The region outlined by a white dashed line is used to calculate a mean Mn profile with depth (Fig. S15). Note that the surface concentrations are much higher than for the polar mixed layer fields presented in Fig. 9, since there is a strong surface Mn gradient (as shown in Fig. S15). Panel (a) and (b) have different colorbar scale ranges.

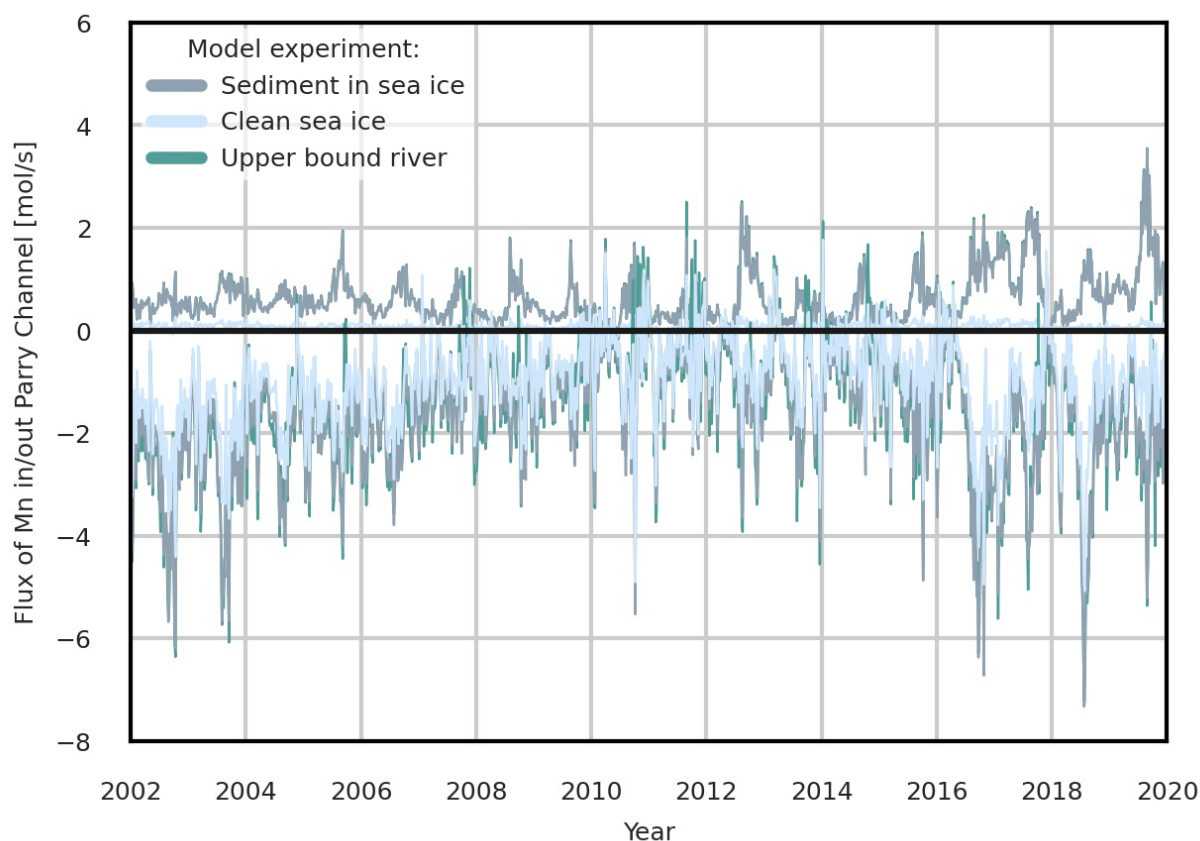


Figure S17. Mn flux into and out of Parry Channel along the boundaries defined in Fig. S14 for each of the main model experiments (calculation described in Text S4). The experiment with sediment in sea ice is the “reference” and uses a lower bound river estimate which incorporates only the direct dissolved Mn contribution. The clean sea ice experiment does not include sediment in ice. The upper bound river experiment has sediment in ice and incorporates the additional contribution of suspended matter from rivers. A positive flux represents transport into Parry Channel (typically from the Canada Basin) while a negative flux is transport out of Parry Channel (towards Baffin Bay). Mn transport into and out of Parry Channel fluctuates seasonally, with a peak in the late summer.

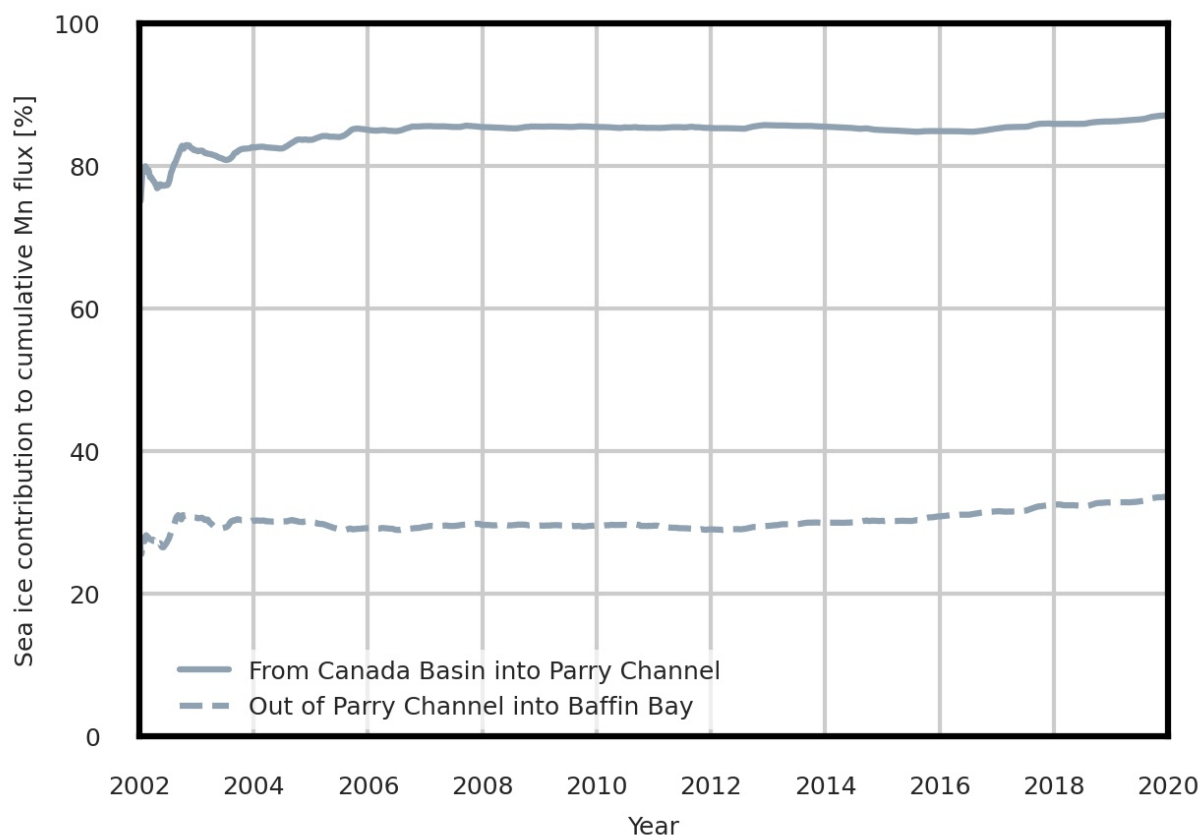


Figure S18. The percent contribution of sea ice melt to cumulative transport of Mn into and out of Parry Channel (boundaries shown in Fig. S14), estimated from the relative difference in transport between the clean sea ice and reference experiments (calculation described in Text S4). Almost 87% of Mn flowing into Parry Channel comes from sea ice melt, while it comprises about 34% of the outflow.

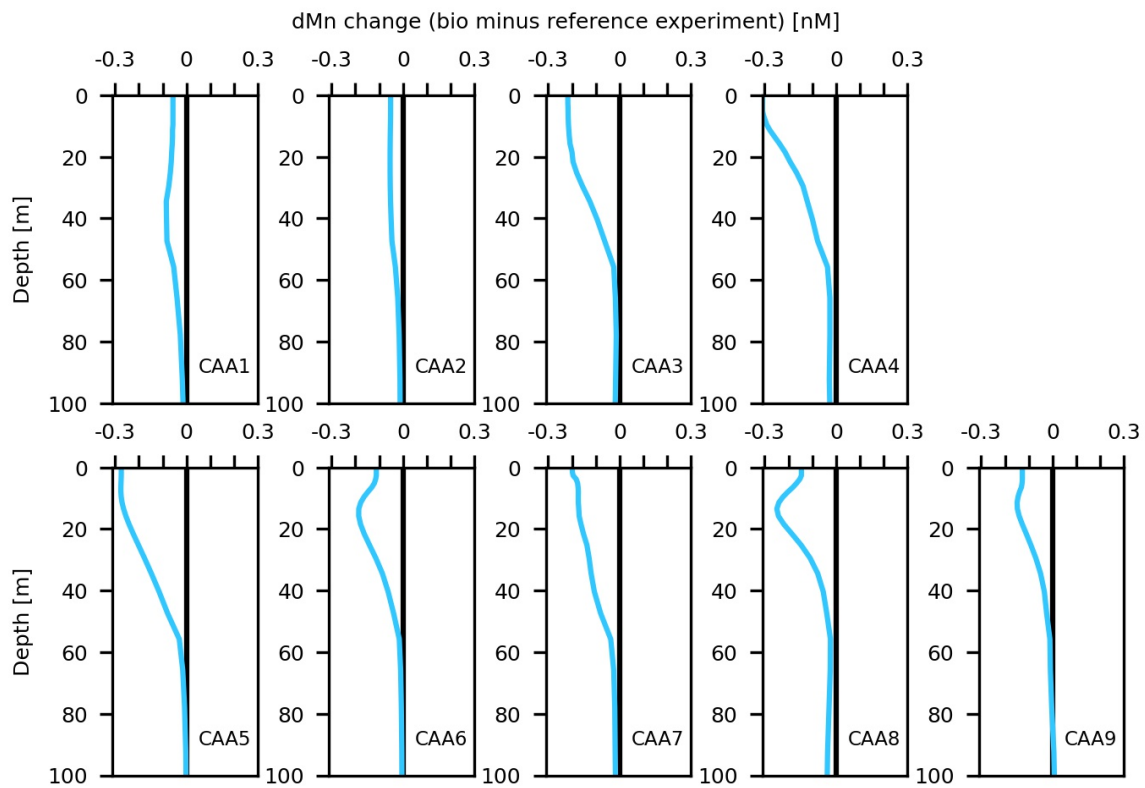


Figure S19. Difference in dissolved Mn from August-September 2015 in the upper 100 m of the water column between the experiment with uptake and remineralization of Mn (“bio” experiment) and the reference experiment for stations in the Canadian Arctic Archipelago. Uptake within the euphotic zone accounts for a reduction of up to 0.3 nM in dissolved Mn concentrations. Remineralization does not clearly appear in this figure because it occurs deeper and over a broad range of depths, and because of our coarse method of estimation using nitrate. The estimate of the magnitude of nitrate uptake is comparable to an estimate based on primary production from Michel et al. (2006) (Text S3).

Table S1. A summary of average sediment loads and suspended particulate matter (SPM) concentrations measured in sea ice cores in the Arctic Ocean. The range of measured values are in parentheses. Observed sediment content in sea ice is highly heterogeneous and can span multiple orders of magnitude. Where two estimates are given for the average content, the lower number is from “clean” ice cores and the higher number from turbid ice.

Sediment load (g m ⁻²)	SPM (g m ⁻³)	Location	Source
179 (0-972)	142 (24-192)	Laptev Sea	Eicken et al. (2000)
-	149 (5-500+)	Lena delta	Hölemann, Wegener, and Schirmacher (1999)
16 (9-46)	70 (8-600+)	Laptev sea	Eicken et al. (1997)
-	45, 349 (0-964)	Laptev Sea	Nürnberg et al. (1994)
(0-7000+)	-	NW of Alaska	Darby, Myers, Jakobsson, and Rigor (2011)
128 (69-203)	342 (91-508)	Chukchi Sea	Eicken et al. (2005)
232 (2-384)	564 (24-1474)	Alaska coast	Stierle and Eicken (2002)
289	157 (31-593)	Beaufort Sea	Reimnitz, McCormick, McDougall, and Brouwers (1993)
1400	-	Central Arctic	Darby et al. (2011)
32 (8-84)	360 (7-2228)	Central Arctic	Tucker, Gow, Meese, Bosworth, and Reimnitz (1999)
-	68, 6800 (1-31013)	Central Arctic	Nürnberg et al. (1994)
-	24 (0-725)	Fram Strait	Dethleff and Kuhlmann (2010)
-	11 (2-137)	Kara Sea	Dethleff and Kuhlmann (2009)

Table S2. The spatial average annual dissolved Mn contributed by external model source components for the full water column ($\mu\text{mol m}^{-2} \text{yr}^{-1}$) in the reference experiment, averaged over the years 2002-2019, separated by region (Fig. S14). Sediment release by sea ice is the only component that varies significantly year-to-year. Estimates from the upper bound river experiment are indicated in parentheses.

Component contribution	Canada Basin		Canadian Arctic Archipelago	
	$\mu\text{mol m}^{-2} \text{yr}^{-1}$	%	$\mu\text{mol m}^{-2} \text{yr}^{-1}$	%
River discharge	5.3 (22)	2.1 (7.8)	19 (178)	2.3 (18)
Sediment resuspension	34	13 (12)	662	81 (68)
Sediment from sea ice	221	85 (80)	138	17 (14)
Dust released by sea ice	0.2	0.1	0.3	0.0
Direct dust deposition	0.0	0.0	0.0	0.0
Total	261 (277)	100	819 (978)	100

References

- Bhatia, M. P., Waterman, S., Burgess, D. O., Williams, P. L., Bundy, R. M., Mellett, T., ... Bertrand, E. M. (2021). Glaciers and Nutrients in the Canadian Arctic Archipelago Marine System. *Global Biogeochemical Cycles*, 35, e2021GB006976. doi: 10.1029/2021GB006976
- Carrère, L., & Lyard, F. (2003). Modeling the barotropic response of the global ocean to atmospheric wind and pressure forcing-comparisons with observations. *Geophysical Research Letters*, 30(6). doi: 10.1029/2002GL016473
- Colombo, M., Jackson, S. L., Cullen, J. T., & Orians, K. J. (2020). Dissolved iron and manganese in the Canadian Arctic Ocean: on the biogeochemical processes controlling their distributions. *Geochimica et Cosmochimica Acta*, 277, 150–174. doi: 10.1016/j.gca.2020.03.012
- Colombo, M., Li, J., Rogalla, B., Allen, S. E., & Maldonado, M. T. (2022). Particulate trace element distributions along the Canadian Arctic GEOTRACES section: shelf-water interactions, advective transport and contrasting biological production. *Geochimica et Cosmochimica Acta*, 323, 183-201.
- Colombo, M., Rogalla, B., Li, J., Allen, S. E., Orians, K. J., & Maldonado, M. T. (2021). Canadian Arctic Archipelago Shelf-Ocean Interactions: A Major Iron Source to Pacific Derived Waters Transiting to the Atlantic. *Global Biogeochemical Cycles*, 35(10), e2021GB007058. doi: 10.1029/2021GB007058
- Darby, D. A., Myers, W. B., Jakobsson, M., & Rigor, I. (2011). Modern dirty sea ice characteristics and sources: The role of anchor ice. *Journal of Geophysical Research: Oceans*, 116(9). doi: 10.1029/2010JC006675
- Dethleff, D., & Kuhlmann, G. (2009). Entrainment of fine-grained surface deposits into new ice in the southwestern Kara Sea, Siberian Arctic. *Continental Shelf Research*, 29(4), 691–701.

doi: 10.1016/j.csr.2008.11.009

- Dethleff, D., & Kuhlmann, G. (2010). Fram Strait sea-ice sediment provinces based on silt and clay compositions identify Siberian Kara and Laptev seas as main source regions. *Polar Science*, 29(3). doi: 10.3402/polar.v29i3.6070
- Eicken, H., Gradinger, R., Gaylord, A., Mahoney, A., Rigor, I., & Melling, H. (2005). Sediment transport by sea ice in the Chukchi and Beaufort Seas: Increasing importance due to changing ice conditions? *Deep Sea Research Part II: Topical Studies in Oceanography*, 52, 3281–3302. doi: 10.1016/j.dsr2.2005.10.006
- Eicken, H., Kolatschek, J., Freitag, J., Lindemann, F., Kassens, H., & Dmitrenko, I. (2000). A key source area and constraints on entrainment for basin-scale sediment transport by Arctic sea ice. *Geophysical Research Letters*, 27(13), 1919–1922. doi: 10.1029/1999GL011132
- Eicken, H., Reimnitz, E., Alexandrov, V., Martin, T., Kassens, H., & Viehoff, T. (1997). Sea-ice processes in the Laptev Sea and their importance for sediment export. *Continental Shelf Research*, 17(2), 205–233. doi: 10.1016/S0278-4343(96)00024-6
- Hölemann, J., Wegener, A., & Schirmacher, M. (1999). Dissolved and particulate major and trace elements in newly formed ice from the Laptev Sea (Transdrift III, October 1995). In *Land-ocean systems in the Siberian Arctic* (pp. 101–111). Springer Berlin Heidelberg. doi: 10.1007/978-3-642-60134-7_11
- Laney, S. R., Krishfield, R. A., & Toole, J. M. (2017, 9). The euphotic zone under Arctic Ocean sea ice: Vertical extents and seasonal trends. *Limnology and Oceanography*, 62, 1910–1934. doi: 10.1002/LNO.10543
- Michel, C., Ingram, R. G., & Harris, L. R. (2006, 10). Variability in oceanographic and ecological processes in the Canadian Arctic archipelago. *Progress in Oceanography*, 71, 379–401. doi:

10.1016/J.POCEAN.2006.09.006

- Nürnberg, D., Wollenburg, I., Dethleff, D., Eicken, H., Kassens, H., Letzig, T., & Reimnitz, E. (1994). Sediments in Arctic sea ice: Implications for entrainment, transport and release. *Marine Geology*, 119, 185–214. doi: 10.1016/0025-3227(94)90181-3
- Reimnitz, E., McCormick, M., McDougall, K., & Brouwers, E. (1993). Sediment export by ice rafting from a coastal polynya. *Arctic, Antarctic, and Alpine Research*, 25(2), 83–98. doi: 10.1080/00040851.1993.12002988
- Sim, N. (2018). *Biogeochemical cycling of dissolved and particulate manganese in the north-east Pacific and Canadian western Arctic* (Doctoral dissertation, University of British Columbia). doi: 10.14288/1.0374222
- Stierle, A. P., & Eicken, H. (2002). Sediment inclusions in Alaskan coastal sea ice: Spatial distribution, interannual variability, and entrainment requirements. *Arctic, Antarctic, and Alpine Research*, 34(4), 465–476. doi: 10.1080/15230430.2002.12003518
- Tucker, W. B., Gow, A. J., Meese, D. A., Bosworth, H. W., & Reimnitz, E. (1999). Physical characteristics of summer sea ice across the Arctic Ocean. *Journal of Geophysical Research: Oceans*, 104(C1), 1489–1504. doi: 10.1029/98jc02607
- Van Hulten, M., Middag, R., Dutay, J.-C., De Baar, H., Roy-Barman, M., Gehlen, M., ... Sterl, A. (2017). Manganese in the west Atlantic Ocean in the context of the first global ocean circulation model of manganese. *Biogeosciences*, 14, 1123–1152. doi: 10.5194/bg-14-1123-2017